VIBRATIONAL SUM FREQUENCY SPECTROSCOPIC INVESTIGATIONS OF CARBOXYLIC ACID-CONTAINING POLYELECTROLYTES AT THE OIL-WATER INTERFACE

by

ELLEN JEAN ROBERTSON

A DISSERTATION

Presented to the Department of Chemistry and Biochemistry
and the Graduate School of the University of Oregon
in partial fulfillment of the requirements
for the degree of
Doctor of Philosophy

June 2014

DISSERTATION APPROVAL PAGE

Student: Ellen Jean Robertson

Title: Vibrational Sum Frequency Spectroscopic Investigations of Carboxylic Acid-Containing Polyelectrolytes at the Oil-Water Interface

This dissertation has been accepted and approved in partial fulfillment of the requirements for the Doctor of Philosophy degree in the Department of Chemistry and Biochemistry by:

Marina Guenza	Chairperson
Geraldine L. Richmond	Advisor
Mark C. Lonergan	Core Member
S. James Remington	Institutional Representative

and

Kimberly Andrews Espy	Vice President for Research and Innovation; Dean of the Graduate School

Original approval signatures are on file with the University of Oregon Graduate School.

Degree awarded June 2014

DISSERTATION ABSTRACT

Ellen Jean Robertson

Doctor of Philosophy

Department of Chemistry and Biochemistry

June 2014

Title: Vibrational Sum Frequency Spectroscopic Investigations of Carboxylic Acid-Containing Polyelectrolytes at the Oil-Water Interface

The boundary between two immiscible fluids is an important location for the adsorption and assembly of polyelectrolytes. A good description of the fundamental properties of polyelectrolytes at such interfaces is a prerequisite to understanding a multitude of important phenomena in biological, environmental, and industrial systems. This dissertation examines the molecular-level details involved in the adsorption and assembly of carboxylic acid-containing polyelectrolytes at the oil-water interface. Vibrational sum frequency spectroscopy, a surface-selective spectroscopic technique, was used to obtain vibrational spectra of oriented polyelectrolytes at the carbon tetrachloride-water interface. Studies that vary both polyelectrolyte and solution conditions are presented that identify the factors that dictate whether or not polyelectrolytes will adsorb to the oil-water interface and that describe the specifics of the adsorption process.

First, the role of the position of ionizable groups along the polyelectrolyte backbone is examined. This is accomplished through studies of syndiotactic poly(methacrylic acid) (sPMA) and isotactic poly(methacrylic acid) (iPMA). Both sPMA and iPMA rapidly adsorb to the interface as highly ordered layers, but only sPMA is able to accumulate to the interface over time.

Studies exploring the role of polyelectrolyte charging are presented next. Molecular weight studies of sPMA as a function of pH show the effect of the number of charges per polyelectrolyte chain on interfacial adsorption and assembly. Results show that charge accumulation on polymer chain segments plays a major role in polyelectrolyte behavior at the oil-water interface.

Subsequently, studies of both iPMA and sPMA with Ca^{2+} and K^{+} are presented to demonstrate the influence of the presence and identity of ions on polyelectrolyte interfacial behavior. These ions only induce the adsorption of iPMA to the oil-water water interface under solution conditions when it is not normally surface active. The identity of the cation is important to the adsorption process.

Lastly, studies of two different peptoid polymers emphasize the role of intermolecular interactions between adsorbed polymer chains in polyelectrolyte interfacial assembly. It is shown that favorable electrostatic interactions between negatively charged carboxylate and positively charged amine groups are important in ordered monolayer assembly.

This dissertation includes both published and unpublished co-authored materials.

CURRICULUM VITAE

NAME OF AUTHOR: Ellen Jean Robertson

GRADUATE AND UNDERGRADUATE SCHOOLS ATTENDED:

University of Oregon, Eugene
Kalamazoo College, Kalamazoo, MI

DEGREES AWARDED:

Doctor of Philosophy, Chemistry, 2014, University of Oregon
Master of Science, Chemistry, 2010, University of Oregon
Bachelor of Arts, Chemistry, 2008, Kalamazoo College

AREAS OF SPECIAL INTEREST:

Interfacial Chemistry, Polymer Chemistry, and Environmental Chemistry.

PROFESSIONAL EXPERIENCE:

Research Assistant in the Richmond Laboratory, Department of Chemistry and Biochemistry, University of Oregon, Eugene, OR (2008-present)

Graduate Teaching Assistant, Physical Chemistry Laboratory, Department of Chemistry and Biochemistry, University or Oregon, Eugene, OR (2008-2009)

Teaching Assistant, Physical and Organic Chemistry, Chemistry Department, Kalamazoo College, Kalamazoo, MI (2006-2008)

Research Experience for Undergraduates in the Richmond Laboratory, University of Oregon, Eugene, OR (2007)

Research Experience for Undergraduates in the Grubbs Laboratory, Dartmouth College, Hanover, NH (2006)

Supplemental Instruction Leader, Introductory Chemistry, Chemistry Department, Kalamazoo College, Kalamazoo, MI (2005)

GRANTS, AWARDS, AND HONORS:

Student Poster Presentation Award, ACS Division of Colloid and Surface Chemistry, 247th ACS National Meeting, 2014

Phi Beta Kappa Award, Kalamazoo College, 2008

Lemuel F. Smith Award, Kalamazoo College, 2007

Connable Scholarship, Kalamazoo College, 2005

Cooper Prize in Physics, Kalamazoo College, 2005

Department of Chemistry Prize, Kalamazoo College, 2005

Honors Scholarship, Kalamazoo College, 2004

PUBLICATIONS:

Robertson, E. J.; Oliver, G. K.; Qian, M.; Proulx, C.; Zuckermann, R. N.; Richmond, G. L. Assembly and Molecular Order of Two-Dimensional Peptoid Nanosheets through the Oil-Water Interface. *Submitted to Proc. Natl. Acad. U. S. A.*

Robertson, E. J.; Carpenter, A. P.; Courtney, C. M.; Richmond, G. L. Metal Ion Induced Adsorption and Ordering of Charged Macromolecules at the Aqueous/Hydrophobic Liquid Interface. *Submitted to J. Phys. Chem. C.*

Robertson, E. J.; Beaman, D. K.; Richmond, G. L. Designated Drivers: The Differing Roles of Divalent Metal Ions in Surfactant Adsorption at the Oil-Water Interface. *Langmuir* **2013**, *28*, 15511-15520.

Robertson, E. J.; Richmond, G. L. Chunks of Charge: Effects at Play in the Assembly of Macromolecules at Fluid Surfaces. *Langmuir* **2013**, *29*, 10980-10989.

Beaman, D. K.; Robertson, E. J.; Richmond, G. L. Metal Ions: Driving the Orderly Assembly of Polyelectrolytes at a Hydrophobic Surface. *Langmuir* **2012,** *28*, 14245-14253.

Beaman, D. K.; Robertson, E. J.; Richmond, G. L. Ordered Polyelectrolyte Assembly at the Oil-Water Interface. *Proc. Natl. Acad. U. S. A.* **2012,** *109*, 3226-3231.

Beaman, D. K.; Robertson, E. J.; Richmond, G. L. The Unique Assembly of Charged Polymers at the Oil-Water Interface. *Langmuir* **2011,** *27*, 2104-2106.

Beaman, D. K.; Robertson, E. J.; Richmond, G. L. From Head to Tail: Structure, Solvation, and Hydrogen Bonding of Carboxylate Surfactants at the Organic-Water Interface. *J. Phys. Chem. C* **2011,** *115*, 12508-12516.

ACKNOWLEDGMENTS

I would like to express my sincere gratitude to the people who have helped me during my time in graduate school. First and foremost, I would like to thank my advisor, Geraldine Richmond, who has been a constant source of support and motivation. She has helped shaped the way I think about science and has inspired me to achieve more than I ever thought I could.

I would also like to thank my lab members, both present and past, who have inspired or guided my research. Daniel Beaman severed as an excellent mentor to me, and the work I did with him in my first year was critical to shaping my research focus. Katy Plath, Stephanie Ota, Laura McWilliams, Nicholas Valley, Sumi Wren, and Jenny Hensel were always willing to listen to me talk about my research and offer great insight into whatever problems I was encountering. I additionally appreciate the friends I have made who have been supportive of me both in and out of the lab, especially Katy, Stephanie, and Laura. Because of them, I experienced more of Eugene than I ever would have on my own. I have also enjoyed the antics of Brandon Schabes and Jet Meitzer, who were always able to make lab interesting.

Furthermore, I would like to thank those who have collaborated with me on different projects. Dr. Fred Moore from Whitman College was always able to offer great advice concerning problems with experimental equipment. Additionally, I was fortunate enough to have the opportunity work with Ronald Zuckermann, Gloria Oliver, and Caroline Proulx from Lawrence Berkeley National Laboratory. Without them suggesting a collaboration and providing sample to study, I never would have been exposed to their

interesting research and I would not have been so lucky to be offered a more exciting postdoctoral opportunity.

Lastly, I would like to thank my friends and my family for supporting me during my graduate work. My parents, Roy and Mary Robertson, and my sister, Sarah Robertson, are all scientists at heart, and so understood my desire to stay in school for so many years to obtain my degree. Finally, I want to thank my grandfather, George Musselman, for understanding that I haven't been able to visit very often, and also for attempting to understand what I do. His weekly emails have not only served as a source of entertainment, but more importantly gave me a sense of connection to home. In one such email, he said:

"We hope that all the little nano molecules are ordering themselves so that there is some sort of surface phenomenon to be discovered and/or understood. Or do I have that all wrong. Never mind. Even if you explained it I wouldn't understand it."

I think he got it pretty close.

This research was funded by the Department of Energy.

To my family.

TABLE OF CONTENTS

Chapter Page

LIST OF FIGURES

Figure Page

Figure Page

LIST OF TABLES

CHAPTER I

INTRODUCTION

Polyelectrolytes are a ubiquitous class of molecules that occur naturally in the form of proteins, DNA, enzymes, and humic acids, and can also be synthesized to produce extensive libraries of polyelectrolytes that are used in a multitude of applications. Polyelectrolytes have particular relevance at the interface between two phases. The boundary between two immiscible fluids (i.e. a liquid-liquid interface, and most often, an oil-water interface) is an important locale for the adsorption and assembly of such charged macromolecules, having significance in biology, environmental remediation, and industry. For example, the interaction of biological polyelectrolytes with "soft" cell surfaces is crucial to a variety of life functions.[1] In the environment, the adsorption of charged humic macromolecules to the interface between oil and water has important implications for water remediation[2-8] and also plays a role in determining the fate and transport of toxic materials.[9-12] In industrial applications, the assembly of charged carboxylic acid containing-macromolecules at oil-water interfaces is essential to the stabilization of emulsions for a variety of processes[13-17] such as enhanced oil recovery, efficient drug delivery, and the manufacturing of personal care products. The behavior of polyelectrolytes at these fluid interfaces determines their degree of effectiveness in these important biological, environmental, and industrial processes.

It is especially important to understand a) the specific conditions that favor or discourage polyelectrolyte surface adsorption; b) interfacial adsorption dynamics under these various conditions; and c) the resulting polyelectrolyte surface structures. As several polyelectrolytes consist of long hydrophobic backbones with charged hydrophilic

functional groups equally spaced along the polymer chain, one might expect that the interfacial activity of a polyelectrolyte will depend upon a balance between hydrophobicity and hydrophilicity. Understanding this balance on a molecular-level is thus essential for describing fundamental processes that involve charged macromolecular assembly at the boundary between water and nonpolar fluids. A preliminary understanding of the adsorption of charged macromolecules to hydrophobic liquid-water interfaces has been achieved through interfacial tension measurements.[18-23] However, such measurements only give general information pertaining to polyelectrolyte adsorption dynamics and resulting interfacial structure, and fail to give the molecular-level details necessary to fully characterize the behavior of polyelectrolytes at the oil-water interfaces.

Vibrational sum frequency (VSF) spectroscopy has proven to be a powerful technique to probe the molecular-level details of buried oil-water interfaces that are otherwise difficult to access.[24-48] VSF spectroscopy generates vibrational spectra of oriented interfacial molecules, and can thus give specific information regarding bond strengths, interactions between chemical species, and molecular orientations of polyelectrolytes adsorbed to an oil-water interface. This technique has already been a useful tool for studying charged biological macromolecules at air-water,[49-56] solid-liquid,[49, 50, 55-64] and membrane interfaces,[55, 56, 65-71] as well as polyelectrolytes at the air-water[72-74] and solid-liquid[75-80] interfaces. While informative, these previous VSF studies do not capture the role of a unique oil-water interfacial environment on polyelectrolyte adsorption and assembly. Furthermore, the majority of the solid-liquid interface studies focused on the adsorption of a polyelectrolyte onto an oppositely charged surface.[75-79] In this case, electrostatic interactions are found to dominate polyelectrolyte adsorption behavior, which is contrary to

what is expected for polyelectrolyte adsorption to a liquid-liquid interface. Despite the fluidity of the air-water interface, the vapor phase lacks the ability to specifically interact with the hydrophobic moieties of polyelectrolytes, as is the case for the nonpolar phase of an oil-water interface.

The studies presented in this dissertation specifically utilized VSF spectroscopic and interfacial tension measurements to probe the behavior of poly(methacrylic acid) (PMA), a simple poly(carboxylic acid), and peptoid polymers, more complex carboxylic acid containing biomimetic polymers, at the carbon tetrachloride-aqueous (CCl_4-H_2O) interface. Not only is CCl_4 an ideal solvent to use in the spectroscopic studies (it is invisible to the incident and detected beams) but it also serves as an appropriate model for toxic halogenated solvents that are persistent in the environment. Poly(carboxylic acids), such as PMA, represent a class of polyelectrolytes and they serve as good models for more complex environmental[81] and biological[82] macromolecules. Because their charging behavior, and thus their degree of hydrophobicity, is tunable, they also represent ideal systems with which to probe the competing effects of hydrophobicity vs. hydrophilicity on the oil-water interfacial behavior. Here, studies of PMA as a function of both polyelectrolyte characteristics and solution conditions provide details concerning the molecular-level factors that dictate whether polyelectrolytes remain water solvated or adsorb to the oil-water interface, as well as the manner in which polyelectrolyte interfacial assembly specifically occurs. Before these studies are presented in Chapters III-VI, a brief introduction to VSF spectroscopy and additional experimental considerations are provided in Chapter II.

The specific manner in which the functional groups are positioned on the

polyelectrolyte chain can affect macromolecular hydrophobicity and thus interfacial behavior, as examined in Chapter III. PMA, in particular, is available as different isomers that behave quite differently in bulk solution. Specifically, the isotactic isomer (iPMA), in which the carboxyl groups are positioned along the same side of the polyelectrolyte chain when the monomers are in the *all anti*-conformation, is both more hydrophobic and has a greater local charge density than the syndiotactic isomer (sPMA), in which the carboxyl groups are located on both sides of the chain and alternate sides when the monomers are in the *all anti*-conformation.[83-88] VSF spectroscopic and interfacial tension studies involving the different isomers of PMA will demonstrate how the backbone configuration affects polyelectrolyte oil-water interfacial behavior. Discussions of complementary computational studies performed by Dr. Nicholas Valley will further emphasize the influence of polymer backbone configuration on interfacial behavior.

The role of polymer charging in sPMA interfacial behavior is explored in Chapter IV. sPMA is a weak polyacid that is pH tunable, such that at higher pH values the chains are highly charged, while at lower pH values they are more neutral. By altering the pH of the solution, the number of charges per polyelectrolyte chain can thus be varied. Another aspect of polymer charging behavior that can be tuned is the number of ionizable monomers that are linked together in a single chain. For polyelectrolyte solutions that consist of the same number of monomers, the molecular weight of the polyelectrolytes will dictate the total number of charges that are able to accumulate on each chain. For solutions of long polyelectrolytes, there are few chains in solution that can accumulate many charges, while for short polyelectrolytes, there are many chains in solution that can accumulate few charges. The pH-dependent molecular weight studies of sPMA presented in Chapter IV

demonstrate how collective charge accumulation on a single polyelectrolyte chain affects interfacial adsorption and assembly. This work has been previously published, with Geraldine L. Richmond as a coauthor.[40]

The extent of polymer charging, and thus hydrophobicity, can also be tuned through screening with different counterions, which is the topic of Chapter V. For instance, it is well known that multivalent cations interact much more strongly with polyanions compared to monovalent cations.[89] Carboxylic acid groups in particular are known to bind in specific manners to different types of cations. The binding of metal ions can thus drastically alter the bulk configuration and hydrophobicity of certain carboxylic acid containing-polyelectrolytes. Studies of PMA with varying concentration of different counterions will reveal how polyelectrolyte charge screening and metal ion binding play a role in polyelectrolyte interfacial behavior. Interfacial tension studies for this chapter were performed by Andrew P. Carpenter and Courtney M. Olson. This work has been submitted to *The Journal of Physical Chemistry C*, with Andrew P. Carpenter, Courtney M. Olson, and Geraldine L. Richmond as coauthors.

Chapters III-V all explore the interfacial behavior of simple, negatively charged carboxylic acid-containing polyelectrolytes. Studies of peptoid polymers, which are presented in Chapter VI, provide an opportunity to probe a more complex class of poly(carboxylic acids) at the oil-water interface that have interesting applications in self-assembled nanomaterials. Here, two specific peptoid polymers are studied: one with both negatively charged carboxylate groups and positively charged amine groups, and one with only negatively charged carboxylate groups. These studies provide a means to determine the role of intermolecular electrostatic interactions between adsorbed chains in

polyelectrolyte interfacial assembly. Samples were graciously prepared by Gloria K. Oliver and Caroline Proulx from the Zuckermann group at Lawrence Berkeley National Laboratory. This work has been submitted to *PNAS*, with Gloria K. Oliver, Menglu Quan, Caroline Proulx, Ronald N. Zuckermann, and Geraldine L. Richmond.

Chapter VII concludes with a summary of the experimental results, along with an outlook for future work. Overall, the results presented in this dissertation provide a molecular-level description of poly(carboxylic acid) adsorption to an oil-water under a variety of conditions for which the balance between polyelectrolyte hydrophobicity and hydrophilicity is altered. The fundamental findings of these model systems can be extended to further the understanding of the interfacial behavior of more complex environmental, biological, and industrial charged macromolecules.

CHAPTER II

VIBRATIONAL SUM FREQUENCY SPECTROSCOPY BACKGROUND AND EXPERIMENTAL CONSIDERATIONS

Vibrational sum frequency (VSF) spectroscopy is a well-established surface selective technique that produces vibrational spectra of oriented interfacial molecules, and several resources exist on the topic.[90-97] This chapter first provides an overview of the theory behind VSF spectroscopy, with discussions of spectral interpretation as it relates to experiments presented in this dissertation. Next, experimental considerations are discussed that were specifically utilized in obtaining the VSF spectroscopic data shown throughout this dissertation. These are followed by a description of the spectrum of the neat carbon tetrachloride-water (CCl_4-H_2O) interface in order to demonstrate the changes to this spectrum that occur when molecules adsorb to the interface. Lastly, complementary interfacial tension measurements are described.

Interaction of Light with Matter: Nonlinear Effects

When an electric field $\vec{E}$ interacts with a molecule, it induces an oscillating dipole:

$$\vec{\mu} = \mu_0 + \alpha\vec{E} \ . \tag{2.1}$$

Here, μ_0 is a molecule's permanent dipole moment, and α is the polarizability and is an intrinsic property of the molecule. In a macroscopic system, the induced dipole per unit volume is known as the induced polarization and is written as:

$$\vec{P} = \varepsilon_0 \overleftrightarrow{\chi}^{(1)} \vec{E} \ . \tag{2.2}$$

Here, $\overleftrightarrow{\chi}^{(1)}$ is the first order susceptibility of the medium and ε_0 is the permittivity in a vacuum. In eqn. 2.2, the macroscopic average of μ_0 has been ignored, as most media do not have a static dipole moment. This linear approximation works for electric fields of low intensity and describes everyday phenomena such as reflection and refraction.

In the case of high intensity electric fields, such as laser beams, incident on a medium, the linear approximation presented above is no longer accurate. In this case, higher order terms of a power series expansion of the induced polarization must be considered:

$$\vec{P} = \varepsilon_0(\overleftrightarrow{\chi}^{(1)} \cdot \vec{E} + \overleftrightarrow{\chi}^{(2)} : \vec{E}\vec{E} + \overleftrightarrow{\chi}^{(3)} \vdots \vec{E}\vec{E}\vec{E} + \cdots + \overleftrightarrow{\chi}^{(n)} \vec{E}^n) . \qquad (2.3)$$

Here, $\overleftrightarrow{\chi}^{(2)}$ and $\overleftrightarrow{\chi}^{(3)}$ are the second and third order susceptibilities, respectively. Unlike linear spectroscopy, in which the induced polarization oscillates at the same frequency as the incident electric field, the higher order terms describe phenomena in which the induced polarization oscillates at a frequency different than the incident electric field. This is the basis of VSF spectroscopy, which is attributed to a second order nonlinear optical process.

Second order processes occur when two electric fields ($\vec{E}(\omega_1)$ and $\vec{E}(\omega_2)$) are incident upon a media. When the frequencies of both electric fields are the same ($\omega_1 = \omega_2$), second harmonic generation can occur, with the frequency of the induced polarization oscillating at $2\omega_1$. When the frequencies of the electric fields are different ($\omega_1 \neq \omega_2$), processes can result in which the induced polarization oscillates at either $\omega_1 + \omega_2$ (sum frequency generation) or $\omega_1 - \omega_2$ (difference frequency generation). This dissertation specifically focuses on sum frequency generation, in which a fixed visible beam (ω_{vis}) and

a tunable infrared beam (ω_{IR}) are used to generate the sum frequency beam (ω_{SF}), as is depicted in Figure 2.1.

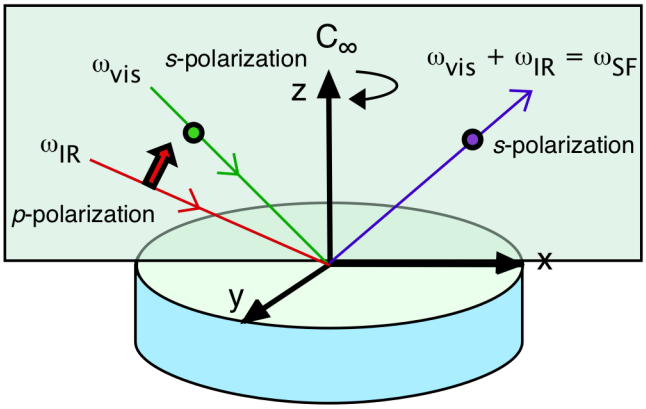

Figure 2.1. Schematic for the vibrational sum frequency generation process at a C_∞ surface, showing polarizations of the incident and generated beams.

Surface-Selectivity of VSF Spectroscopy

The second order susceptibility ($\chi^{(2)}_{ijk}$) is a third rank tensor with 27 elements. Under the dipole approximation, $\chi^{(2)}_{ijk}$ is zero in centrosymmetric media, such as most bulk media. This is due to the fact that the inversion symmetry present in centrosymmetric media requires that:

$$\chi^{(2)}_{ijk} = \chi^{(2)}_{-i-j-k} = -\chi^{(2)}_{ijk} \,. \tag{2.4}$$

The only solution that satisfies this requirement is $\chi^{(2)}_{ijk} = 0$. When there is a break in symmetry, such as where two bulk media meet, $\chi^{(2)}_{ijk} = 0$, therefore making VSF a surface-selective spectroscopic technique.

Liquid surfaces, in general, have C_∞ symmetry, and so are isotropic in the xy

interfacial plane (Fig. 2.1). Here, x=-x and y=-y, but z≠-z. This property dramatically reduces the number of non-zero tensor elements. By applying the operations that compose the C_∞ point group to each tensor element, and using the logic presented above, it can be shown that there are only 7 non-vanishing elements of $\chi^{(2)}_{ijk}$, which are shown in Table 2.1. As the x and y axes are interchangeable under C_∞ symmetry, only four of these elements are unique, and can be probed with different polarization combinations of the incident and generated beams. Here, *s*-polarized light oscillates perpendicular to the xz plane, while *p*-polarized light oscillates parallel to the xz plane (Fig. 2.1).

Table 2.1. Non-zero elements of $\chi^{(2)}_{ijk}$ for a surface with C_∞ symmetry that are probed with the corresponding polarization schemes.

Non-Zero Elements of $\chi^{(2)}_{ijk}$	Polarization Scheme (SF, vis, IR)
$\chi^{(2)}_{xxz} = \chi^{(2)}_{yyz}$	*ssp*
$\chi^{(2)}_{xzx} = \chi^{(2)}_{yzy}$	*sps*
$\chi^{(2)}_{zxx} = \chi^{(2)}_{zyy}$	*pss*
$\chi^{(2)}_{zzz}$	*ppp*

Generating Surface Vibrational Spectra with VSF Spectroscopy

In VSF spectroscopy, a fixed frequency visible laser beam and a tunable infrared laser beam are coherently overlapped at an interface. The intensity of the detected signal is proportional to the square of the effective second order susceptibility and the intensities of the incident visible and infrared beams:

$$I(\omega_{SF}) \propto \left|\chi^{(2)}_{eff}\right|^2 I(\omega_{vis}) I(\omega_{IR}) \,. \tag{2.5}$$

The effective second order susceptibility ($\chi_{eff}^{(2)}$) is related to the actual susceptibility ($\chi^{(2)}$) through the Fresnel coefficients, which describe how electric fields are reflected and transmitted at an interface, and the unit polarization vectors, which relate the molecular reference frame to the laboratory reference frame.

The second order susceptibility contains a nonresonant component ($\chi_{NR}^{(2)}$) and the sum of all resonant components ($\chi_{R_v}^{(2)}$):

$$\chi^{(2)} = \chi_{NR}^{(2)} + \sum_v \chi_{R_v}^{(2)} . \tag{2.6}$$

The nonresonant component depends on the polarizability of substrate material and is independent of the incident IR frequency. The resonant components are related to both the number of contributing surface molecules (N) and the orientationally averaged molecular hyperpolarizability ($\langle \beta_v \rangle$) through the following expression:

$$\chi_{R_v}^{(2)} = \frac{N}{\varepsilon_0} \langle \beta_v \rangle . \tag{2.7}$$

This indicates that not only does the VSF signal depend on how many molecules are at the interface, but also how the molecular dipoles are oriented such that a net orientation of molecular dipoles is required for $\chi_{R_v}^{(2)}$ to be nonzero.

Under the dipole approximation, and assuming that the visible and sum frequency beam frequencies is far from resonance with any electronic transitions, the molecular hyperpolarizability is written as:

$$\beta_v = \sum_v \frac{A_K M_{IJ}}{\omega_v - \omega_{IR} - i\Gamma_v} . \tag{2.8}$$

Here, A_K is the IR transition moment, M_{IJ} is the Raman transition probability, ω_v is the

resonant mode frequency, and Γ_v is the natural linewidth of the transition. That both A_K and M_{IJ} appear in this equation indicates that allowed sum frequency transitions must be both Raman and IR active. Additionally, it is clear that enhancement of the sum frequency signal occurs when the IR beam frequency (ω_{IR}) is resonant with the energy of an allowed vibrational transition. To summarize, VSF spectroscopy generates vibrational spectra of molecules (with allowed sum frequency transitions) at an interface that have an average net orientation. As discussed above, different polarization schemes can be used to probe the different elements of $\chi^{(2)}_{ijk}$, which in turn probe different molecular orientations.

Specifically, *ssp* probes dipole moment components normal to the plane of the interface, *sps* and *pss* probe dipole moment components in the plane of the interface, and *ppp* probes dipole moment components both in the plane and normal to the plane of the interface. All spectra shown in this dissertation were taken in the *ssp* polarization scheme, and thus probe molecular dipole moment components that are normal to the plane of the interface.

Interpreting VSF Spectra through Spectral Fitting

Since VSF spectroscopy is a coherent technique in which $\chi^{(2)}$ is generally complex, the non-resonant and each resonant component of $\chi^{(2)}$ have an associated amplitude and phase. Unlike linear spectroscopies, the nonresonant and resonant contributions are summed before squaring:

$$I(\omega_{SF}) \propto \left| A_{NR} e^{i\phi_{NR}} + A_{1R} e^{i\varphi_1} + A_{2R} e^{i\varphi_2} + A_{3R} e^{i\varphi_3} + \cdots \right|^2 . \qquad (2.9)$$

Eqn. 2.9 dictates that interferences (both constructive and destructive) will exist between the nonresonant and resonant modes, as well as between overlapping vibrational states. Unlike linear vibrational spectroscopy, in which spectra are composed of a superposition of individual vibrational modes, one cannot interpret VSF spectra visually by looking at vibrational peak frequencies, amplitudes and widths. Because of these nonlinearities, a rigorous fitting method is required to accurately interpret the line shapes that appear in VSF spectra. The spectra shown in this dissertation were fit using a routine that was first implemented by Moore and co-workers:[98]

$$\left|\chi^{(2)}(\omega_{SF})\right|^2 = \left|\chi^{(2)}_{NR} e^{i\phi_{NR}} + \sum_v \int_{-\infty}^{\infty} \frac{A_v e^{i\varphi_v} e^{-\left[(\omega_L-\omega_v)/\Gamma_v\right]^2}}{\omega_L - \omega_{IR} - i\Gamma_L} d\omega_L \right|^2 . \qquad (2.10)$$

In this equation, the first term describes the response due to the nonresonant second order susceptibility, in which ϕ_{NR} is the nonresonant phase. Each resonant feature has an associated amplitude (A_v) that is proportional to N and the orientationally averaged IR and Raman transition probabilities, a phase (φ_v), a Lorentzian width (Γ_L), a Gaussian width (Γ_v), and a frequency (ω_v). The frequencies of the IR and Lorentzian are ω_{IR} and ω_L, respectively. This line shape is a convolution of a Gaussian and Lorentzian, as first described by Bain et al,[99] and takes into account both homogenous broadening (HWHM, Γ_L) due to the inherent nature of the transition, as well as inhomogeneous broadening (FWHM, $\sqrt{2\ln 2}\Gamma_v$) due to the local environments of the molecules. For this lineshape, there are 5 unknown parameters to fit for each resonant feature, plus the nonresonant amplitude and phase.

In order to reduce the number of variables associated with the fits, and thus the

number of non-unique solutions, certain parameters were fixed at constant values, while others were allowed to vary between reasonable values. For the studies presented in this dissertation, the nonresonant component was found to be negligible, and so the nonresonant amplitude and phase were fixed at 0. Depending on the interference pattern in the spectrum, the resonant phases were fixed at either 0 or 3.14. Peak center frequencies were constrained based on known literature values. The Lorentzian line widths were fixed at values consistent with typical vibrational lifetimes,[100-103] while the Gaussian line widths were allowed to vary to account for the wide array of complex molecular environments. Peak amplitudes were also allowed to vary. To achieve more confidence in the fitting results, a global fitting routine was implemented when necessary. This routine fit a series of spectra at once while constraining peak center frequencies, phases, and Lorentzian widths for all spectra, and thus only allowing amplitudes and Gaussian widths to vary.

Spectroscopic Measurements

All spectra shown in this dissertation were taken on a commercially available sum frequency generation system that was designed and built by Ekspla (Vilnius, Lithuania). A schematic of the experimental set-up is depicted in Figure 2.2. The laser system (model PL2343A/SH) consists of a master oscillator in which 1064 nm seed pulses are generated with a flash lamp-pumped Nd-YAG rod that have pulse lengths of ~ 30 ps, repetition rates of 10 Hz, and energies of ~600 μJ per pulse. The generation of pulses that are stable in both energy and time is achieved by active and passive mode-locking via a Pockel cell, polarizer, and solid state saturable absorber. The introduction of dynamic and fixed losses

creates stabilized pulses at ~10 μJ that, after 200 roundtrips in the oscillator, are sent to the regenerative amplifier via a second Pockel cell.

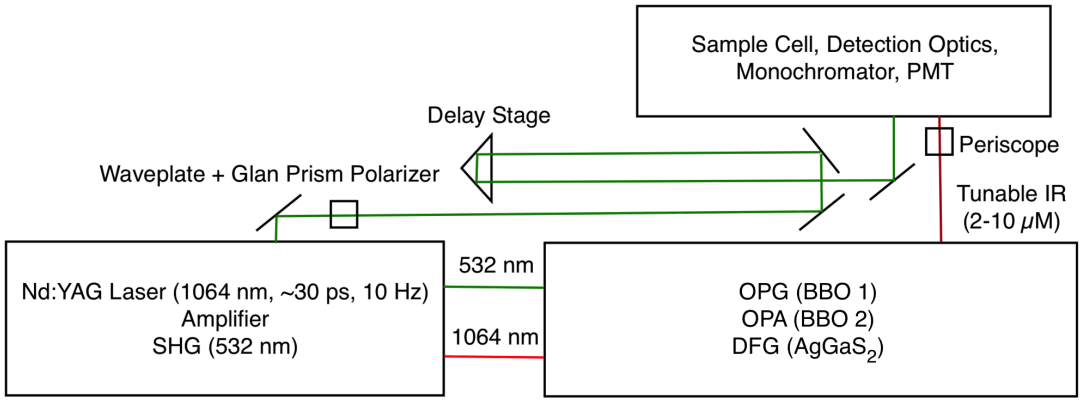

Figure 2.2. Schematic of the laser experiment used for the VSF spectroscopic studies.

In the regenerative amplifier, pulses can be amplified to ~500 μJ without damaging the solid state saturable absorber. After a fixed number of passes in the regenerative amplifier, pulses picked by a third Pockel cell are directed into the double pass power amplifier. The power amplifier consists of a second Nd:YAG rod that is pumped by two flash lamps. Amplification is achieved by changing the timing between the flashlamps, with energy outputs in the tens of mJ. After amplification, the 1064 nm beam is split, and a portion is frequency doubled in a KDP (potassium dideuteridum phosphate) crystal to generate 532 nm light. A small portion of the 532 nm beam is sent to the interface to be used as the visible beam after it is spatially filtered and collimated.

The remainder of the 532 nm line along with the 1064 nm line that was not frequency doubled, is used to generate tunable IR light via a standard optical parametric generation (OPG) / optical parametric amplification (OPA) / difference frequency

generation (DFG) setup (model PG501/DFG2-10P). The energies of the 532 nm and 1064 nm beams entering this setup were <8 mJ so as not to damage the nonlinear optical crystals. Here, the 532 nm beam is split into 2 lines. The first line is double passed through a heated BBO crystal (OPG). The generated parametric beam is reflected off of a grating to spectrally narrow the bandwidth. This generated seed beam, along with the second 532 nm line, are collinearly double passed through a second heated BBO crystal (OPA). The signal and idler for the amplified parametric beam are separated via a Glan prism polarizer. The idler (1.064-2.3 microns) is sent to a $AgGaS_2$ crystal (DFG), where it is collinearly overlapped in space and time with the 1064 nm beam. The generated IR beam is tunable from 2-10 microns. The IR and visible beams are sent to the sample area, which is depicted in Figure 2.3.

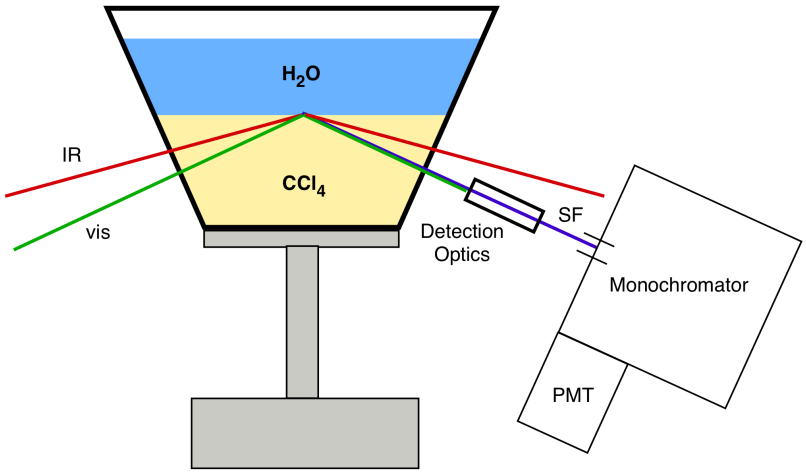

Figure 2.3. Schematic of the sample area showing the overlap of the 532 nm and tunable IR beams at the CCl_4-H_2O interface, with the generated sum frequency beam sent into a monochromator and detected with a PMT.

After focusing, the visible (80 μJ) and IR (80-250 μJ) beams are overlapped in space and time at the CCl_4-H_2O interface at their respective total internal reflection angles

relative to the interfacial plane (24.1° for the visible; 15-17° for the IR). These angles are used to maximize the generated sum frequency signal.[28, 30, 31, 35, 36, 41, 44, 46, 47, 104] CCl_4 does not absorb the fixed 532 nm beam or the tunable IR beam in the spectral regions under study. Polarization of the visible bream is selected via a wave-plate/Glan prism polarizer combination, while the polarization of the IR beam is selected using a periscope. Spatial overlap between the visible and IR beams is accomplished using a motorized gold mirror situated before the interface which, through control via a LabView program, directs the position of the IR beam at the interface. This makes it easy to track the movement of the IR beam that results from tuning the DFG crystal. Correct timing between the visible and IR beams is accomplished with a prism delay stage that is situated in the relatively long visible beam path length.

The detections line is aligned to the reflected visible beam, as the angle of the generated sum frequency beam should not vary much relative to that of the high energy 532 nm beam. The detection optics consist of a filter to remove the 532 nm beam; an anti-reflective coated BK7 lens to focus the generated sum frequency beam; and a Glan prism polarizer/half-wave plate combination that selects the polarization of the detected beam. After passing through the detection optics, the generated sum frequency beam is sent through a monochromator (model MS2001) and then detected with a photomultiplier tube (PMT, Hamamatsu R7899).

The sample cell was machined from a solid piece of Kel-F with a CaF_2 window facing the incident beams and a BK7 glass window facing the out-going beams. The windows were sealed with Dupont Kalrez® perfluoropolymer o-rings. All glassware, the sample cell, o-rings, and BK7 window were soaked in a NoChromix-sulfuric acid bath for

at least 12 h and subsequently rinsed in water (18.2 MΩ-cm resistivity) from an E-pure water filtration system for 5-20 mins, depending on the size of the glassware. The CaF_2 window was soaked in the acid bath for no more than 15 mins before rinsing in water from the E-pure system. Daily, clean layers of CCl_4-H_2O were cycled through the cell to ensure cleanliness before spectra of the sample of interest were obtained. Interfaces were prepared by first depositing the CCl_4 layer in the cell, and then the aqueous solution of interest on top of the CCl_4. Data collection began within a minute of interfacial preparation and continued until spectra were no longer observed to change significantly with time. All spectra shown are an average of at least 300 laser shots per data point, and were normalized by dividing the raw spectra by nonresonant gold spectra in the corresponding spectral regions. This accounts for changes in timing and overlap as the IR beam frequency is tuned.

The Neat CCl_4-H_2O Interface

In order to determine the effects of polyelectrolyte adsorption to the oil-water interface, it is first important to understand the characteristics of the neat CCl_4-H_2O interfacial spectrum. Figure 2.4 (top) shows a spectrum of the neat CCl_4-H_2O interface in the water OH stretching region. Here, two distinct regions can be seen. An intense sharp peak appears near 3700 cm^{-1}, and is assigned to the uncoupled OH mode of the top-most water molecules that straddle the interface and are oriented into the organic phase. The reduction of this peak in the VSF spectrum of this interface is a qualitative indicator of the presence of adsorbates at the interface and the complete absence of this peak indicative of significant adsorbate coverage.[90] Broad peaks appear between 3000-3600

cm^{-1} that are due to ordered water molecules that exist deeper into the interfacial region and have differing degrees of hydrogen bonding. In general, the interfacial depth and degree of coordination of the surface water molecules increases with decreasing frequency.[90] A cartoon of these different interfacial water environments is shown in Figure 2.4 (bottom).

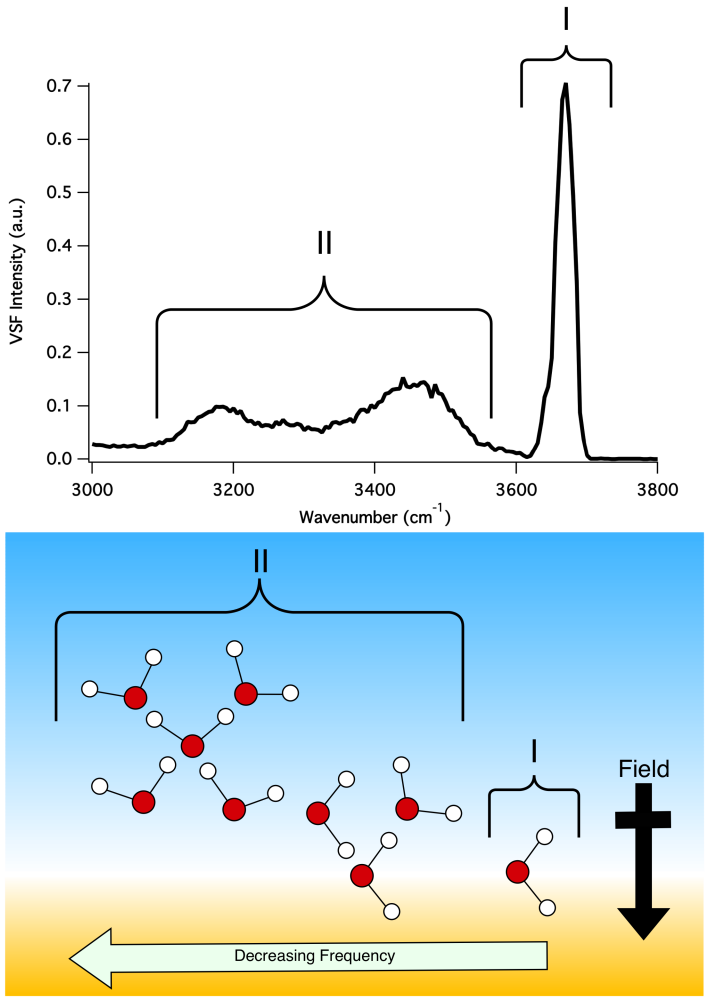

Figure 2.4. VSF spectrum (*ssp* polarization) of the neat CCl_4-H_2O interface in the water OH stretching region (top), and a cartoon of the different surface water environments and interfacial field (bottom). Region I corresponds to the free-OH oscillator from the top-most water molecules, while Region II corresponds to oriented waters deeper into the interface with differing degrees of hydrogen bonding.

The strong orientation of the interfacial water molecules provides this oil-water interface with interesting properties. Previous VSF spectroscopic and computational studies have shown that the high degree of ordering of the top-most interfacial water molecules is in part due to interactions with the organic phase.[34, 36, 105-107] Additionally, ordering of the CCl_4 is seen to occur several molecular layers into the organic phase.[108] The ordering of both the water and CCl_4 molecular dipoles acts to create an electric field across the interface, which has been shown to play a role in inducing the adsorption of both inorganic ions and charged macromolecules to the CCl_4-H_2O interface.[24, 26, 29, 36] In general, effects of adsorbates on the interfacial field are pronounced in the water OH stretching modes between 3000-3600 cm^{-1}. Specifically, screening of the interfacial field by adsorbates results in a significant depression of these modes, while the adsorption of highly charged molecules increases the field strength and results in enhancement of these modes.[32] Observing changes to both the free-OH and the coordinated surface water modes is thus important for detailing the specifics of polyelectrolyte adsorption and assembly.

Interfacial Tension Measurements

Since VSF spectral amplitudes give information about both the number density and orientation of interfacial molecules, it is difficult to determine whether spectral changes are due to a change in the number of molecules at the interface, a change in their net orientation, or both of these effects. Interfacial tension is used to decouple these effects, since this method gives information about the interfacial concentration of molecules and is

not as sensitive to orientational changes.

Interfacial tension measurements were performed using either the pendant drop (poly(methacrylic acid) studies) or the Wilhelmy plate (peptoid studies) method. A schematic for the pendant drop method is shown in Figure 2.5. Here, measurements were recorded on a pendant drop tensiometer (KSV) that consists of a camera and an LED backlight to ensure good photograph resolution. For the measurements, an aqueous drop containing the sample of interest was dispensed from a 1 mL Hamilton gas-tight syringe with a Hamilton repeating dispenser. The formed drop was suspended from a 22-gauge hooked Kel-F hub needle into a 1x1 cm^2 quartz cuvette filled with approximately 4 mL CCl_4.

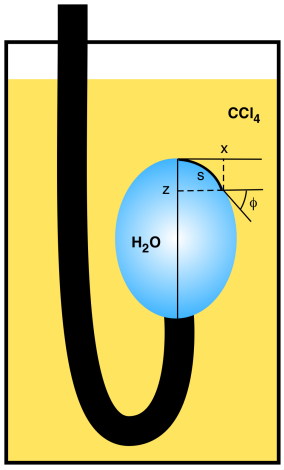

Figure 2.5. Depiction of a pendant drop interfacial tension experiment in which an aqueous drop is suspended in a cuvette of CCl_4.

Samples were measured by recording a photograph of the drop every minute until the interfacial tension no longer changed with time. Using the software provided with the instrument, the drop shape was first fit to the Laplace-Young equation:

$$\frac{dx}{ds} = \cos\phi$$
$$\frac{dz}{ds} = \sin\phi \qquad (2.11)$$
$$\frac{d\phi}{ds} = 2 + \beta z - \frac{\sin\phi}{x}$$

to determine the shape factor, β. The value of β was then used to calculate the interfacial tension, γ, according to Eqn. 2.12, in which $\Delta\rho$ is the density difference between the two liquids, g is the gravitational constant, and R_0^2 is the square of the radius of the drop curvature at the drop apex.

$$\gamma = \frac{\Delta\rho g R_0^2}{\beta}. \qquad (2.12)$$

Results of the PMA interfacial tension measurements are reported as surface pressure, which is the difference between the interfacial tension of the neat CCl_4-H_2O interface (~45 mN/m[29]) and the interfacial tension of the sample of interest. Here, a surface pressure value of ~0 mN/m indicates little to no adsorption at the interface, while a surface pressure value >>0 indicates strong adsorption to the oil-water interface.

In the Wilhelmy plate method, the interfacial tension γ is calculated based on the force (F) applied to a thin plate by a liquid surface:

$$\gamma = \frac{F}{l \cdot \cos\phi} \qquad (2.13)$$

Here, l is the perimeter of the plate edge touching the liquid and ϕ is the contact angle between the plate and the liquid. A schematic of the experimental set-up is shown in Figure 2.6.

For the peptoid studies, the interfacial tension was measured using a platinum plate

attached to a balance (KSV). The plate was first lowered to the neat CCl_4-H_2O interface until the interfacial tension was measured to be 44-46 mN/m. To the aqueous layer was added an aliquot of concentrated Tris buffer solution to obtain a bulk concentration of 10 mM (pH 8). Subsequently, an appropriate aliquot of stock 2 mM peptoid solution in a 2:1 (v/v) mixture of DMSO:water mixture was deposited to the buffer layer and the interfacial tension was measured for ~2 hours. Surface pressure values were obtained by subtracting the equilibrium interfacial tension value of the peptoid solution from the CCl_4-Tris buffer interfacial tension value (~44 mN/m).

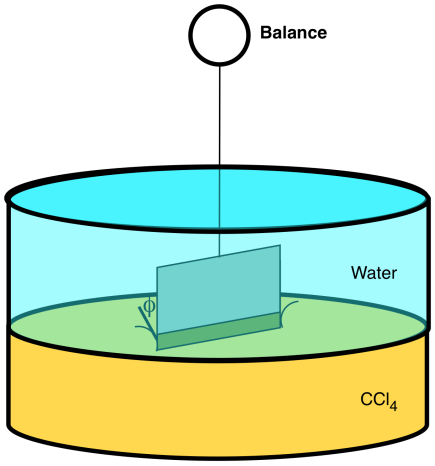

Figure 2.6. Schematic of the Wilhemly plate experimental set-up, in which a platinum plate attached to a balance is lowered to the CCl_4-H_2O interface.

The results presented in this dissertation are obtained through a combination of the techniques presented in this chapter. The VSF spectroscopic measurements provide a molecular-level picture of polyelectrolytes at the oil-water interface, while the interfacial tension measurement provide macroscopic information pertaining to the population of interfacial polyelectrolytes. These methods provide a broad description for the systems under study.

CHAPTER III

THE ROLE OF BACKBONE CONFIGURATION IN MACROMOLECULAR ADSORPTION AND ASSEMBLY AT THE OIL-WATER INTERFACE

Polyelectrolyte hydrophobicity is often dictated by the specific arrangement of functional groups along the polymer chain backbone,[83-88] and has the potential to greatly affect the adsorption and assembly behavior of charged macromolecules at fluid interfaces. In this chapter, the role of polyelectrolyte backbone configuration in the assembly of poly(methacrylic acid) at the carbon tetrachloride-water interface is explored by comparing the interfacial behavior of the isotactic and syndiotactic isomers of poly(methacrylic acid). These studies implement both vibrational sum frequency spectroscopy, which is shown to probe the structure of the initially adsorbed oriented polymer layer, and interfacial tension, which is shown to probe the accumulation of randomly oriented polymer to the interface over time. Computational studies performed by Dr. Nicholas Valley are also discussed in order to better describe the interfacial structures of the PMA isomers and to better interpret the VSF spectra. Results show that the differing backbone configurations of the two isomers greatly affect both the interfacial structure of the initially adsorbed polymer layer and the ability for more poly(methacrylic acid) to accumulate at the interface over time.

Introduction

The ability of polyelectrolytes to assemble at the boundary between water and a nonpolar fluid is essential to a wide variety of processes ranging from environmental,[2-8] to

biological,[1] to industrial.[13, 16, 109-113] For these applications, it is not only important to know if polyelectrolytes adsorb to an interface, but it is also imperative to understand the factors that dictate the assembly process and resulting macromolecular surface conformation. For example, it is important to understand polyelectrolyte characteristics that allow them to accumulate at an oil-water interface to a great extent. Such a degree of polyelectrolyte interfacial accumulation is important for applications that require a large reduction of interfacial tension, such as in enhanced oil recovery,[110, 114] water remediation,[2, 8, 115, 116] and emulsion stabilization[13] with both natural and synthetic polyelectrolytes. Also, in the environment, whether or not humic substances accumulate at fluid interfaces can dictate the transport of natural organic matter.[9-12] Additionally, it has been established that the accumulation of misfolded amyloid proteins on cellular membranes results in neurodegenerative diseases like Alzheimer's, but the mechanism for this accumulation is not well understood.[52, 117-122] It is therefore important to understand on the molecular-level the specific characteristics of polyelectrolytes that lead to the adsorption, assembly and accumulation at an oil-water interface.

This chapter explores the molecular-level details related to how the backbone configuration of a model polyelectrolyte, specifically polymethacrylic acid (PMA), affects its adsorption and accumulation at the carbon tetrachloride-aqueous (CCl_4-H_2O) interface. Here, vibrational sum frequency (VSF) spectroscopic data are shown, with complementary information obtained from interfacial tension measurements and computation studies. PMA is a good example of a polyelectrolyte whose backbone configuration greatly affects its degree of hydrophobicity. For the isotactic isomer (iPMA), the ionizable carboxylic acid groups are on the same side of the polyelectrolyte chain when it is in the *all anti-*

conformation, while for the syndiotactic isomer (sPMA) the carboxylic acid groups are located on both sides of the chain and alternate sides every monomer when it is in the *all anti*-conformation. The chemical structures of the two isomers of PMA are shown in Figure 3.1. Both experimental[83, 84, 86-88] and theoretical studies[83, 85] have shown that the different arrangement of functional groups along the polymer chains for the different PMA isomers renders iPMA more hydrophobic than sPMA. Such a difference in hydrophobicity has the potential to greatly affect polyelectrolyte interfacial adsorption and assembly.

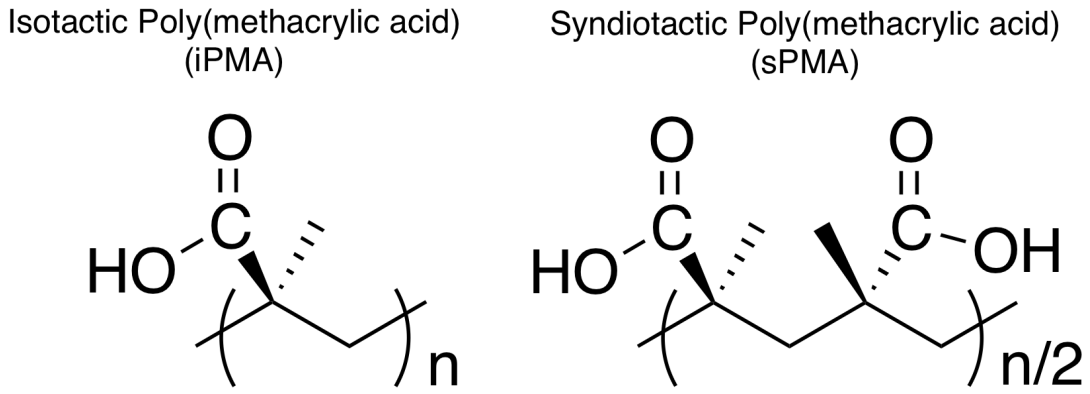

Figure 3.1. Chemical structures of isotactic poly(methacrylic acid) (iPMA, left) and syndiotactic poly(methacrylic acid) (sPMA, right). For the studies in this chapter, n=34.

For the studies presented here, both isomers of PMA (molecular weight=3 kD, n=34) were studied at pH 2, where most of the carboxylic acid groups are protonated. These solution conditions allow for determining specifically the role of the backbone configuration in the absence of any charging affects, which will be explored in depth in Chapters IV and V. Additionally, under these solution conditions, previous studies have shown the bulk conformation of iPMA and sPMA to be somewhat different. Specifically, sPMA is in a compact coil structure in which its methyl groups reside more on the interior

and its carboxylic acid groups reside more on the exterior, while iPMA is in a more extended conformation in which its methyl groups are more exposed to the aqueous phase than they are for sPMA.[83-85] The differences in these isomers allows for exploring how the polyelectrolyte bulk conformation of PMA relates to its interfacial structure. This study clearly demonstrates that the backbone configuration plays a major role in the oil-water interfacial adsorption and assembly of PMA.

Oil-Water Interfacial Behavior of sPMA and iPMA

VSF spectra obtained for both sPMA and iPMA at pH 2 in the carbonyl stretching region are shown in Figure 3.2. Given the selection rules for VSF spectroscopy, the presence of signal for each isomer indicates that both iPMA and sPMA adsorb to the CCl_4-H_2O interface and that their carbonyl functional groups are highly ordered normal to the plane of the interface. In order to reproduce the experimental line shapes, the spectra were fit to two peaks, one near 1730 cm^{-1} and one near 1790 cm^{-1}. The observation of peaks at different vibrational frequencies is attributed to the carbonyl groups being in different environments. The lower energy peak near 1730 cm^{-1} is attributed to carbonyl groups in a more water rich, hydrogen bonded environment, and is consistent with the literature frequencies.[123] The higher energy peak centered at 1790 cm^{-1} is attributed to carbonyl groups in a more oil-rich environment and is consistent with frequencies observed in FT-IR studies of simple carboxylic acids in bulk CCl_4.[124]

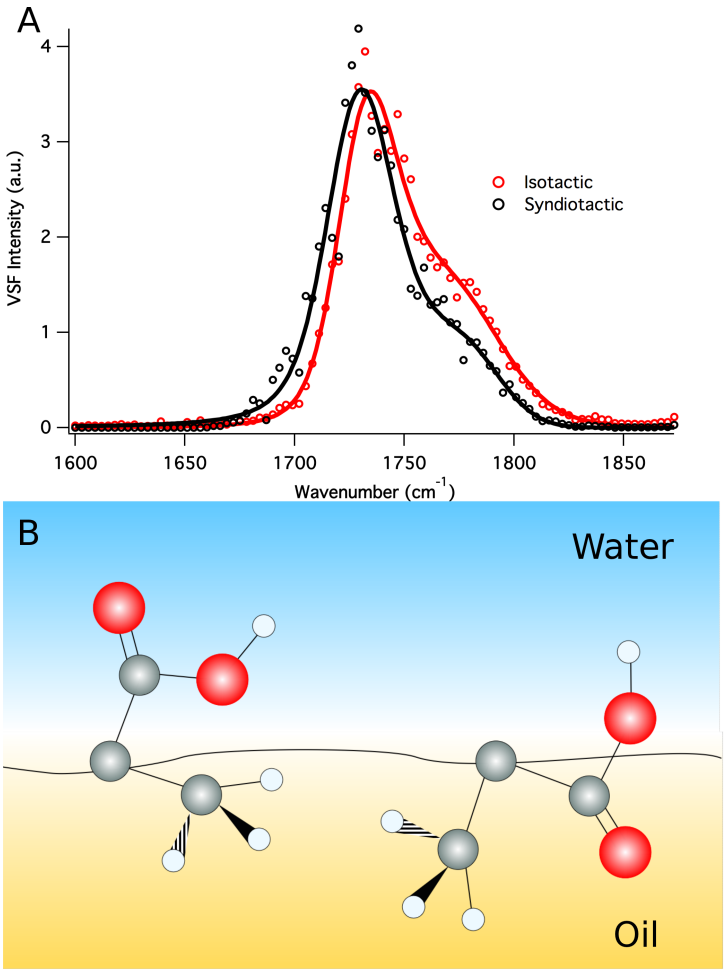

Figure 3.2. (A) VSF spectra (*ssp* polarization) of 5 ppm sPMA (black) and iPMA (red) at pH 2 in the carbonyl stretching region. The solid lines are fits to the data. (B) Cartoon depicting the two different solvation environments of the carbonyl groups corresponding to the peaks near 1730 cm^{-1} (left) and 1790 cm^{-1} (right).

Figure 3.2B shows a representation of the two different carbonyl environments. This picture is consistent with the fits, which show that the two carbonyl peaks are out of phase with each other, indicative of differing orientations of the groups. Previous studies of poly(acrylic acid) (PAA) at the oil-water interface show the absence of a high-energy peak.[24-26] It is concluded that the appearance of this higher energy peak for iPMA and sPMA is due to the more hydrophobic nature of these polymers compared to PAA, which results in a larger fraction of the carbonyl groups on PMA existing in a more oil-rich

environment compared to PAA. That the amplitude for the peak near 1790 cm^{-1} is larger for iPMA compared to sPMA suggests that there are more oriented carbonyl groups in the oil-rich environment for the adsorbed iPMA than there are for sPMA. This is consistent with bulk studies that suggest that iPMA is overall more hydrophobic than sPMA [83-88], and therefore may sit further into the oil phase than sPMA.

The spectra in the CH/OH stretching region for each PMA isomer, shown in Figure 3.3, also confirm the adsorption of highly ordered polymer layers to the oil-water interface. The data is in contrast to results expected from the more disordered coiled conformation of PMA that is expected to exist in bulk solution, which is especially true for the compact coiled conformation of sPMA.[83-85] If such disordered conformations did adsorb to the interface, they would be expected to produce little to no VSF signal. It is clear, however, that a very intense signal is present that is attributed to ordered polymers at the interface. The spectra are very complex due to the high density of modes in this region. General assignments, however, can be made. The broad peak near 2500 cm^{-1} is assigned to the OH stretching mode of the polymer carboxylic acid groups,[125] the sharp peaks between 2800-3000 are assigned to the CH stretching modes of the polymer methyl and methylene groups,[123] and the broad peaks between 3000-3400 cm^{-1} are assigned to the OH stretching modes of the coordinated surface water molecules.[34] The presence of such a strong signal appears due to the polymer carboxylic acid OH, methyl, and methylene groups for both PMA isomers is evidence of the highly ordered nature of the adsorbed iPMA and sPMA, and suggests that the adsorbed polymer chains are highly extended rather than existing in more disordered coiled conformations that are expected in bulk

solution. Additionally, the absence of the free-OH mode near 3670 cm^{-1} in the spectra of both isomers signifies that these interfaces are completely covered by polymer.[42, 90]

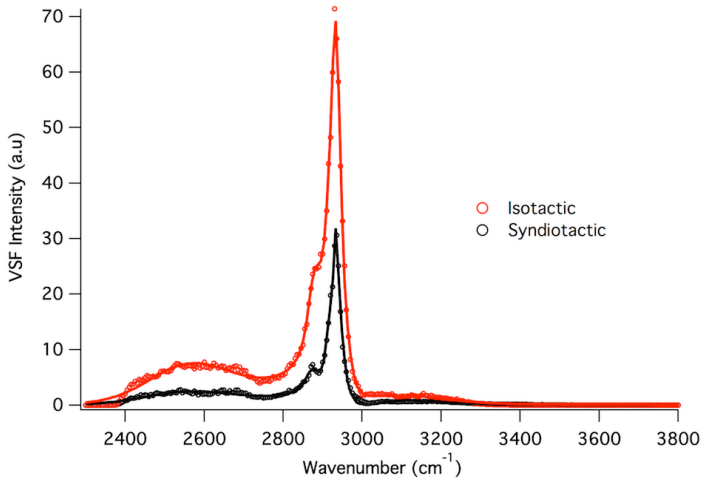

Figure 3.3. VSF spectra (*ssp* polarization) of 5 ppm sPMA (black) and iPMA (red) at pH 2 in the CH/OH stretching region. The solid lines are fits to the data.

Even though both sPMA and iPMA show a high degree of order at the oil-water interface, is clear from the spectra that differences exist between the different interfacial PMA isomers. In order to determine the significant differences between the iPMA and sPMA CH/OH stretching region spectra, the spectra were fit using a global routine in which all variables were held constant except for the peak Gaussian widths and amplitudes. Peaks due to the adsorbed polymers specifically appear near 2534 cm^{-1} for the carboxylic OH stretching mode, and near 2888, 2928, 2934, and 2980 cm^{-1} for the methyl and methylene stretching modes. The peaks are assigned to the methyl and methylene groups of the polymer end caps (2888 cm^{-1}), and the methyl (2928 and 2934 cm^{-1}) and methylene (2980 cm^{-1}) groups of the polymer backbone. These assignments are based on literature values,[123] values predicted by theory as discussed below, and the

fitting results discussed in depth in Chapter IV. The fits here specifically show that the amplitudes for the peaks near 2534, 2928, and 2934 cm^{-1} are significantly larger for iPMA, but that the peak near 2980 cm^{-1} is significantly larger for sPMA. As discussed previously, differences in VSF peak amplitudes can be due to a difference in interfacial populations, orientations, or both factors. In order to decouple these factors and better interpret the spectra in Figure 3.3, interfacial tension measurements were obtained for each isomer and are shown in Figure 3.4.

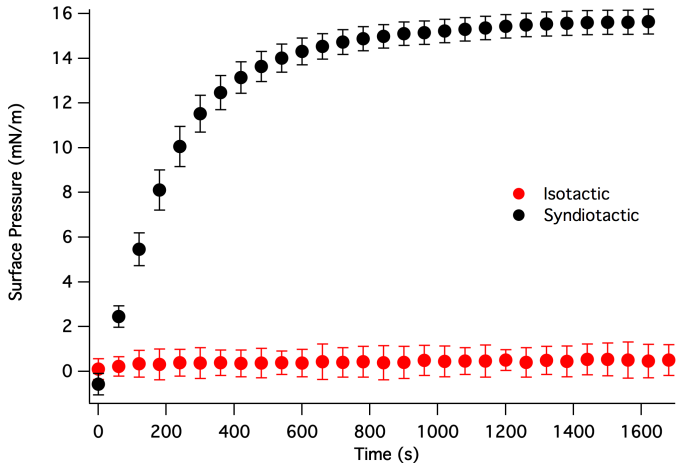

Figure 3.4. Surface pressure vs. time data for 5ppm sPMA (black) and iPMA (red) at pH 2. The error bars represent the standard error.

It is clear that the surface pressure behavior is very different for each PMA isomer. For iPMA, the surface pressure increases only slightly to ~ 0.5 mN/m in the first few seconds, and then does not noticeably change with time. For sPMA, the surface pressure increases to ~16 mN/m over ~800 s, and then does not noticeably change with time. The time dependence observed in the surface pressure data of sPMA is not reflected in the VSF spectroscopic data of either isomer. VSF signal is seen within a minute of interfacial preparation and does not significantly change with time. Because VSF

spectroscopy can only detect molecular functional groups with a net orientation, the changes that appear in the surface pressure over time for sPMA must be due to the adsorption of disordered polymer to the interface. For iPMA, where no large changes in surface pressure are seen over time, polymer does not appear to adsorb beyond the initial monolayer.

The combination of the VSF spectroscopic and interfacial tension data shows very different adsorption behavior for the two isomers of PMA. Even though sPMA has been shown to exist as a disordered compact coil in bulk solution, the data suggest an extended interfacial conformation. iPMA, whose bulk conformation has been shown to be more extended than that of sPMA, also initially adsorbs to the interface in a highly ordered manner. This is seen from the strong VSF intensities of the CH, carbonyl, and carboxylic acid OH stretching mode peaks for both PMA isomers that appear almost instantaneously and whose intensities do not significantly change with time. Because of this, the adsorption and spreading of the polymers at the interface is too fast to be observed with the spectroscopy. For sPMA, polymer in a disordered conformation, potentially similar to its bulk conformation, continues to adsorb to the interface over time. For iPMA no further accumulation occurs. This further accumulation, or lack thereof, cannot be detected with VSF spectroscopy, but can be detected with the surface pressure measurements. A cartoon depicting these differences is shown in Figure 3.5.

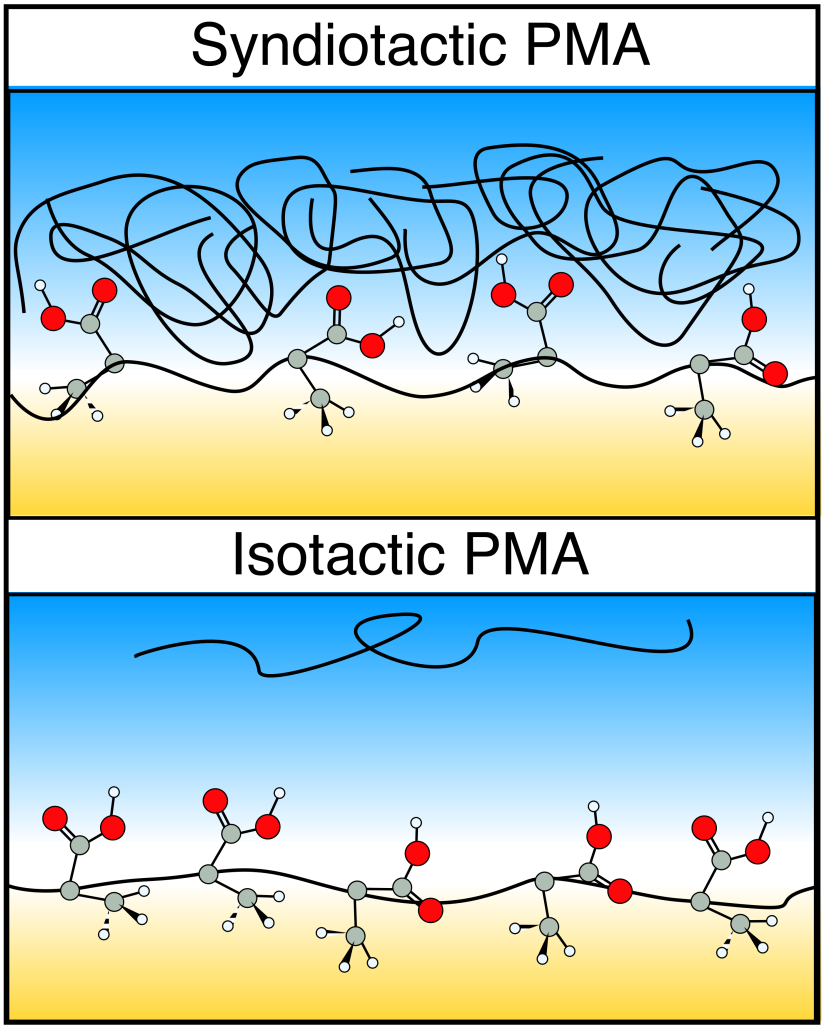

Figure 3.5. Cartoon representing the differing interfacial behavior of sPMA (top) compared to iPMA (bottom).

Multilayer formation has been observed in other polyelectrolyte systems at the oil-water interface.[24-26] In these previous studies, the initial quick adsorption of a highly ordered and extended polymer layer to the interface was attributed to the inherent CCl_4-H_2O interfacial field. It was demonstrated that this field assists in the quick adsorption of highly oriented material to the oil-water interface. This field does not penetrate deep enough into the bulk water to orient the slower adsorbing material in part due to

neutralization by the polymer that initially adsorbs to the interface, causing the slower adsorbing polymer to adsorb to the interface in a disordered manner. That the initial layer does not significantly increase the surface pressure was suggested to be due to the entropy loss associated with the restricted conformation of the extended polymer at the interface.[126] For these previous studies, and also for studies of protein adsorption to the oil-water interface,[127] the ability for macromolecules to adsorb as multilayers was attributed to favorable hydrophobic interactions between the initially adsorbed layer and the layers that subsequently adsorb to the interface. These same conclusions can be applied to the systems under study here, in which the interfacial field assists in the quick adsorption of ordered polymer layers to the interface for both PMA isomers, but that favorable hydrophobic interactions only occur between the initially adsorbed sPMA layer and the sPMA that continues to adsorb to the interface over time.

As discussed previously, bulk studies have shown that iPMA is overall more hydrophobic than sPMA.[83-88] Thus, it seems counterintuitive that sPMA continues to adsorb to the interface over time, yet iPMA does not. A likely explanation for this phenomenon is that the characteristics of the initially adsorbed layer dictates whether or not multilayer formation can occur. This is consistent with the fact that the VSF spectra in the CH/OH stretching region for sPMA and iPMA appear to be very different from each other, suggesting that the initially adsorbed polymer layers are very different. Because the surface pressure data appear to mainly give information about the amount of polymer that accumulates to the interface over time, rather than the relative number of molecules that comprise the initially adsorbed ordered layer, it is difficult to say whether

the differences that arise in the CH/OH spectra are due to a difference in the adsorbed polymer populations, orientations, or both factors.

Computational studies of iPMA and sPMA at the CCl_4-H_2O interface have recently been preformed by Dr. Nicholas Valley in the Richmond lab in order to better describe the differences in the interfacial conformations of the PMA isomers, and also to better interpret the CH spectra. These preliminary studies indicate that the backbone configuration of iPMA (Fig. 3.1, left) allows the hydrophobic methyl moieties to be completely solvated by the oil phase and the carboxylic acid OH groups to be completely solvated by the water phase. For sPMA, however, the backbone configuration causes sPMA (Fig. 3.2, right) to be more disordered at the interface such that some of the methyl groups are able to point into the aqueous phase. Figure 3.6 shows a representation of the calculated interfacial conformations of the iPMA (left) and sPMA (right) monomers.

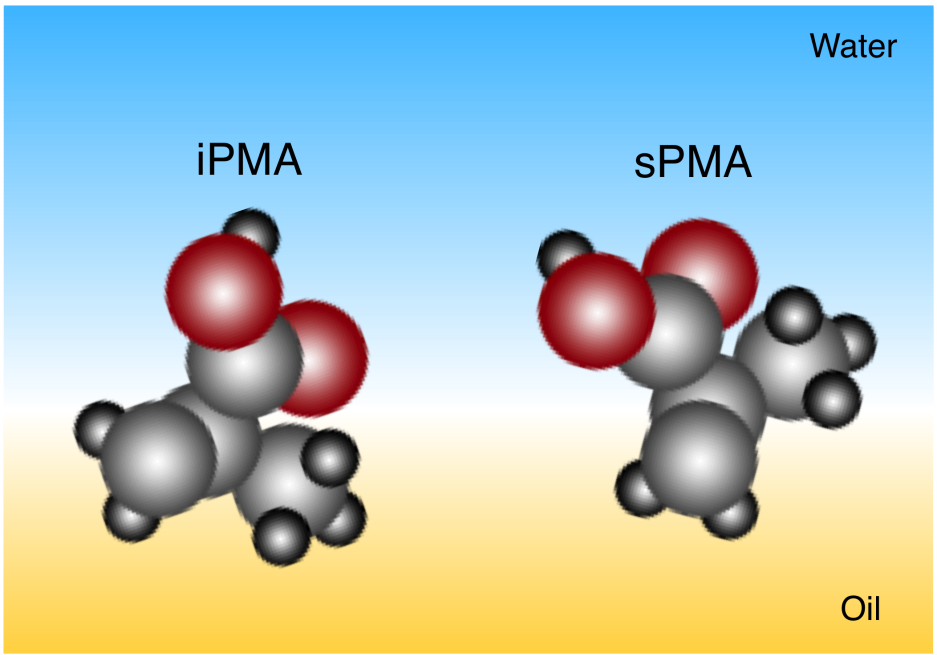

Figure 3.6. Representation of the interfacial conformations of the monomers of iPMA (left) and sPMA (right) obtained from theory.

Such different interfacial polymer conformation would produce very different spectra in the CH stretching region. VSF spectra of the CH stretching modes calculated from these interfacial conformations specifically show that iPMA has a significantly larger peak near 2916 cm^{-1} that is due to the methyl symmetric stretching mode. This intense peak is due the highly ordered methyl groups that are solvated by the oil phase. Conversely, sPMA has a significantly larger peak near 2980 cm^{-1}, which is due to the methylene symmetric stretching mode. The backbone methylene groups are more oriented into the oil phase than the methyl groups, as some of the methyl groups are oriented into the aqueous phase. These trends in peak intensities are consistent with what is seen experimentally, as shown in Table 3.1, which suggests that the conformations of the absorbed PMA isomers from experimental results are very similar to those determined computationally.

Table 3.1. Experimental and calculated CH peak frequencies and corresponding intensities for sPMA and iPMA.

Exp. Freq. (cm^{-1})	Exp. Int. (sPMA)	Exp. Int. (iPMA)	Calc. Freq. (cm^{-1})	Calc. Int. (sPMA)	Calc. Int. (iPMA)
2886	1.6	1.9	2890	0.1	0.04
2930	5.2	5.4	2916	7.7	11
2933	2.0	3.3			
2978	1.4	0.019	2977	11.8	2.7

A picture consistent with the spectroscopic, interfacial tension, and computational results is one in which iPMA initially adsorbs to the interface with its methyl groups highly solvated by the oil phase and its carboxylic acid OH groups highly solvated by the water phase. This is supported by the relatively large peak due to the carboxylic acid OH groups seen in the CH/OH spectrum of iPMA. Because such highly hydrophilic groups point into the aqueous phase, it is unlikely that favorable hydrophobic interactions to

occur between this initially adsorbed polymer layer and the polymer that remains in bulk solution. sPMA, on the other hand, initially adsorbs to the oil-water interface in a more disordered manner than iPMA, such that some of the methyl groups are able to point into the aqueous phase. That these hydrophobic moieties are exposed to remaining polymer in bulk solutions likely promotes hydrophobic interactions between the initially adsorbed sPMA and the sPMA that remains in solution, allowing sPMA to adsorb to the interface over time.

Summary and Conclusions

The studies presented in this chapter are consistent with a picture in which sPMA and iPMA initially adsorb to the oil-water interface as highly ordered polymer layers, with a net orientation of the carboxylic acid, methyl, and methylene functional groups normal to the interfacial plane. The extended nature of the polymers at the interface exists despite the fact that the bulk coiled conformations of these polymers have been shown to be more disordered, as is especially true for sPMA. The process of adsorption and spreading of these polymers at the oil-water inface occurs so quickly that it cannot be detected with the spectroscopy. This rapid adsorption of highly ordered polymer to the oil-water interface is in part attributed to the inherent interfacial field. The interfacial tension studies indicate that sPMA continues to adsorb to the interface over several minutes in a disordered manner, since the field is likely unable to penetrate deep enough into the interface to cause ordering of this later adsorbing material. iPMA, however, does not appear to accumulate at the interface over time. This is attributed to favorable hydrophobic interactions existing

between the initially adsorbed sPMA layer and the sPMA that continues to adsorb to the interface, which are not as prevalent in the iPMA system. Computational results, which are consistent with the experimental data, suggest that the conformation of the initally adsorbed sPMA allows for further polymer to adsorb to the interface over time, but that the conformation of iPMA does not.

These results have implications for research aimed at either utilizing natural polyelectrolytes or designing synthetic ones that have the ability to accumulate to oil-water interfaces, either for the purpose of stabilizing emulsions, recovering oil to be used as a fuel source, or remediating contaminated water supplies. As shown here, not only does the chemical nature of the monomer play a role in the ability of a polyelectrolyte to adsorb to the interface, but also the specific stereochemistry of monomers along the polymer chain dictates whether the adsorption is that of a signal layer or multilayers. Incorporating stereocenters into synthetic polyelectrolytes, or selecting natural polyelectrolytes with specific stereochemistries, can thus serve as a means to control the degree of polyelectrolyte accumulation to an oil water interface. As will be shown in Chapter V, stereochemistry additionally plays a role in the ability of metal ions to bind to polyelectrolytes in bulk solution, which in turn affects macromolecular interfacial behavior. Chapter IV will first explore the role of polymer charging on polyelectrolyte interfacial adsorption and assembly.

CHAPTER IV

CHUNKS OF CHARGE: EFFECTS AT PLAY IN THE ASSEMBLY OF MACROMOLECULES AT THE OIL-WATER INTERFACE

Large macromolecules with hydrophobic backbones are known to assemble at the interface between immiscible liquids. This assembly is often unpredictable because of the subtle interplay between hydrophobic interactions, hydrophilic solvation, structural constraints, and the thermodynamics of adsorption. This chapter presents vibrational sum frequency spectroscopy and interfacial tension measurements that probe the carbon tetrachloride-water interfacial assembly of the syndiotactic isomer of poly(methacrylic acid) as a function of both polyelectrolyte charge and size. By adjusting the polyelectrolyte charge through pH studies and the polymer size through molecular weight studies, it is demonstrated that charge accumulation in segments of the polymer chains is a critical factor in macromolecular interfacial adsorption and desorption. The results have implications for related charged macromolecules whose ability to assemble between two immiscible fluid media is essential for many biological processes, water remediation efforts, and enhanced oil recovery. This work has previously been published as "Chunks of Charge: Effects at Play in the Assembly of Macromolecules at Fluid Surfaces" by Ellen J. Robertson and Geraldine L. Richmond in *Langmuir*, 2013, *29*, 10980. I designed and performed all experiments, performed all analyses, and did all of the writing.

Introduction

Fluid interfaces are a platform for a variety of important processes that include interface catalyzed reactions,[128, 129] ion transfer,[130, 131] nanoparticle synthesis and assembly,[132-134] oil recovery and water remediation,[110] as well as biological processes that occur at the interface between a fluid cell membrane and water.[135, 136] These processes often depend on the adsorption and assembly of ionizable macromolecules to the interface between a nonpolar fluid and water.

Carboxylic acids are important functional groups that comprise ionizable interfacial macromolecules. For instance, carboxylic acids are present in proteins in the forms glutamic and aspartic acid, and interactions with proteins and fluid cell surfaces are often essential for biological processes.[1] Carboxylic acids also comprise much of natural organic matter in the form of humic and fulvic acids, and these materials are often utilized in oil recovery and water remediation technologies.[3-8] The fact that the carboxylic acid functional group is pH tunable allows it to be engineered into "smart" materials that are able to assemble at interfaces for a variety of technologies.[137, 138] Fatty acids are a classic example of carboxylic acid-containing macromolecules that are able to target fluid interfaces for applications ranging from emulsion stabilization to water remediation to monolayer formation.

Previously, work has been done to understand the adsorption and assembly of carboxylic acid-containing alkyl surfactants at oil-water interfaces.[139, 140] It is well known that a key feature that drives the adsorption of these surfactants to the interface is their amphiphilic nature, with highly hydrophilic headgroups preferring the aqueous phase and

highly hydrophobic tails preferring the oil phase. Previous pH studies have shown that the charge of alkyl surfactants plays a large role in their adsorption and assembly to an oil-water interface, and, specifically, the charge of the carboxylate headgroup is essential for the formation of an ordered monolayer at the oil-water interface.[29]

As alkyl surfactant interfacial behavior has become increasingly well understood, interest has shifted to discovering how the behavior of macromolecular charging dictates the adsorption and assembly of carboxylic acid containing polymers at similar oil-water interfaces. Unlike alkyl surfactants that are composed of an ionizable, hydrophilic headgroup on one end and an oily hydrocarbon tail on the opposite end, carboxylic acid containing polymers are weak polyelectrolytes in which several ionizable groups are linked together along a hydrophobic backbone. In this case, there is an even distribution of hydrophobic groups (methyl and methylene) and hydrophilic groups, (either carboxylic acid or carboxylate) along the length of the molecule. The balance between polymer chain hydrophobicity and hydrophilicity and the role of charging in interfacial behavior has the potential to be quite different for carboxylic acid containing-polymers compared to alkyl surfactants. While several experimental and theoretical studies have detailed the behavior of carboxylic acid containing-polymers in the bulk,[83-85] at planar solid[141-143] and particle[144-146] surfaces, as well as at fluid interfaces in the presence of oppositely charged surfactants,[147-149] few have focused on the molecular-level details concerning the adsorption and assembly of these polyelectrolytes to the interface between polar and nonpolar fluids.[24-26, 53]

In this chapter, both vibrational sum frequency (VSF) spectroscopic and interfacial tension data are presented to demonstrate how the charging behavior of a carboxylic acid-containing polymer, specifically the syndiotactic isomer of poly(methacrylic acid) (sPMA)

(Fig. 3.1, right), affects its adsorption to and assembly at the carbon tetrachloride-water (CCl_4-H_2O) interface. Such simple polyelectrolytes have been shown to be good models for naturally occurring poly(carboxylic acids) such as peptides[82] and humic substances,[81] whose applications at fluid interfaces are quite relevant. Through variation of the pH in the aqueous phase, the number of charges per polymer chain is varied; at low pH most of the carboxylic acid groups are neutral, and as the pH is increased the number of charges per chain increases. Also explored, herein, is the effect of the number of ionizable groups per chain on polymer interfacial behavior, using sPMA polymers with molecular weights of 3 kD (34 monomers per chain) and 28 kD (326 monomers per chain). By keeping the carboxylate group (monomer) concentrations constant for the different molecular weight samples, larger polymer samples contain fewer chains than the smaller polymer samples. At similar pHs, the larger polymer chains will accumulate more charges than the smaller polymer chains, and, as a consequence of their flexibility, can have enhanced charge cooperatively than the shorter chains. How these "chunks of charge" impact the assembly of these macromolecules is demonstrated in these studies.

Interfacial Assembly of Low Molecular Weight sPMA

To study the effects of polymer charging on the adsorption behavior of sPMA with a molecular weight of 3 kD, VSF spectra were collected over a range of pHs at the CCl_4-H_2O interface. VSF spectra in the carbonyl stretching region from 1600-1900 cm^{-1} are shown in Figure 4.1. Given the selection rules for VSF, the presence of sPMA signal is indicative that it is at the interface. At pH ≥ 5.5, no carbonyl signal is observed, indicative

of either no polymer present or completely disordered polymer at the interface. As discussed in Chapter III, the spectra in Figure 4.1 are fit to two peaks in order to reproduce the experimental line shape, with the peak near 1730 cm^{-1} representing carbonyl groups in a more water rich environment and the peak near 1790 cm^{-1} representing carbonyl groups in a more oil-rich environment (Fig. 3.2B).

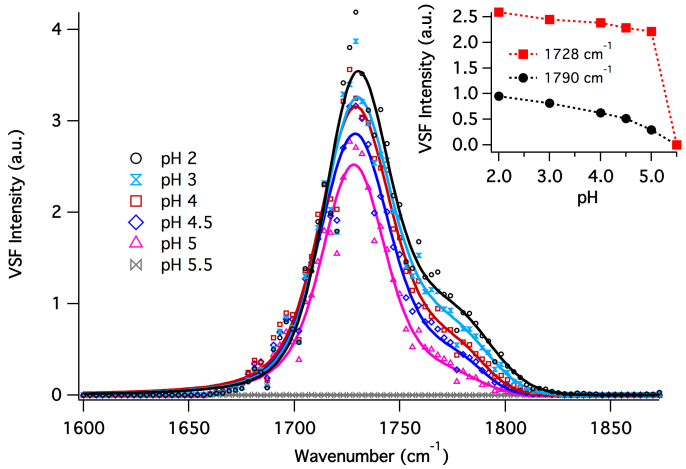

Figure 4.1. VSF spectra (*ssp* polarization) of 3 kD sPMA (5 ppm) at different pHs in the carbonyl stretching region. The solid lines are fits to peaks near 1730 cm^{-1} and 1790 cm^{-1}. The inset is a plot of the fit amplitudes for both peaks as a function of pH.

The inset in Figure 4.1 shows the fit amplitudes for both peaks as a function of pH. Signal doesn't appear until pH<5.5, and gradually the amplitude increases as the pH is further decreased. This suggests that as the pH decreases and more carboxylate groups become protonated, the population of oriented carbonyl groups increases at the interface, with functional groups pointing both into the oil and water phases.

Similar to the data in the carbonyl stretching region, VSF signal due to the polymer is only observed at pH<5.5 in the CH/OH stretching region. At pH 5.5, no peaks appear to indicate that polymer is present at the interface, or if it is, it has no net orientation. In fact, the spectrum in this region closely overlays with a spectrum of the CH/OH stretching

region in the absence of polymer (Fig. 2.4), indicating a nearly neat CCl_4-H_2O interface.[36] As shown in Figure 4.2A, at pH 5 and below, there are peaks in the region between 2800 and 3000 cm^{-1} due to the polymer methylene and methyl stretching modes. Adsorption of 3 kD sPMA to the oil-water interface at a relatively low pH is consistent with previous studies of poly(acrylic acid) (PAA).[24-26] Adsorption of sPMA to the CCl_4-H_2O interface occurs only at pH≤5 since polymer charging above this pH makes solvation in water more energetically favorable than interfacial adsorption.

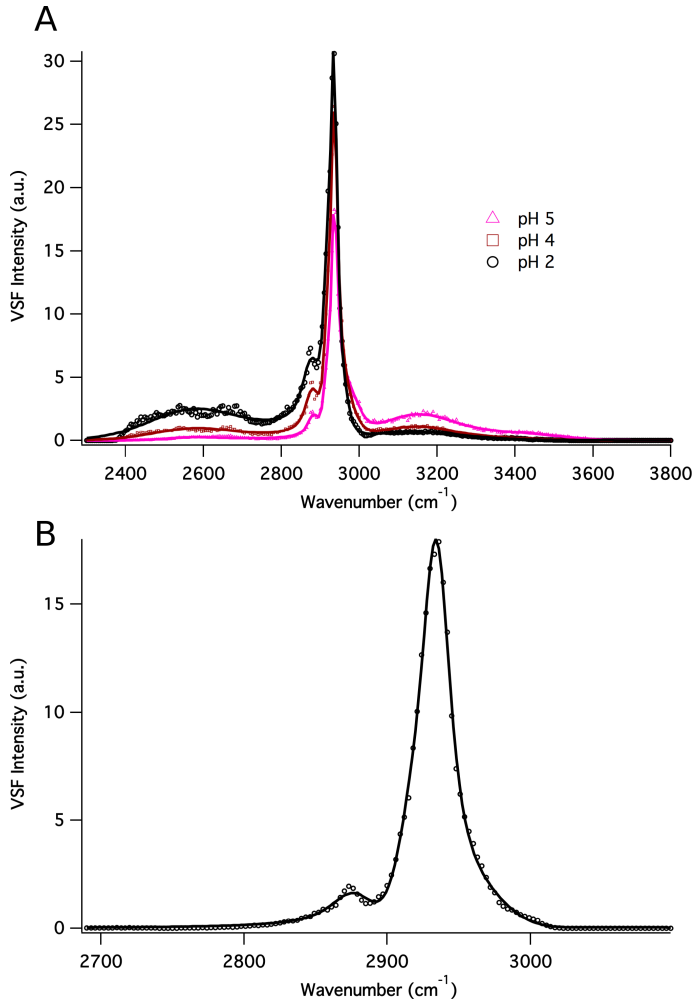

Figure 4.2. (A) VSF spectra (*ssp* polarization) of 3 kD sPMA (5 ppm) at different pHs in the CH/OH stretching region. (B) VSF spectrum of 3 kD sPMA (5 ppm) in D_2O at pD 2 in the CH stretching region. The solid lines are fits to the data.

Gradual spectral changes as the pH decreases from 5 to 2 are also observed in the CH/OH stretching region. The spectra of 3 kD sPMA in H_2O, which are shown in Figure 4.2A, are very complex. Along with the sharp CH stretching modes between 2800-3000 cm^{-1} due to both the methyl and methylene groups on the polymer, broad peaks are also present on both sides of the CH peaks due to the OH stretching modes of both water and the carboxylic acid groups on the polymer. In order to assist in the fitting and to elucidate the trend in the data, a spectrum of 3 kD sPMA in D_2O was taken at pD~2 and is shown in Figure 4.2B. The pD was adjusted using DCl to assure that most of the carboxylic acid hydrogen atoms were replaced by deuterium atoms. As can be seen, the broad peaks present in the H_2O spectrum are not present in the D_2O spectrum, indicating that the gradual pH-dependent changes in the 3 kD sPMA spectra taken in water are in part a result of changes in the peaks due to the carboxylic acid and water OH stretching modes.

The spectra of sPMA in H_2O were fit using a global routine in which all variables were held constant except for peak amplitudes and Gaussian widths. The peak frequencies assigned to the CH stretching modes used in the global routine were constrained to be within the error of those used to fit the D_2O data. Three additional broad peaks were added to account for the OH stretching modes. The peaks due to the methylene and methyl stretching modes appear near 2888 cm^{-1}, 2928 cm^{-1}, 2934 cm^{-1}, and 2980 cm^{-1}. These fitting parameters are consistent with what was observed in Chapter III (Table 3.1). The peak assigned to the carboxylic acid OH stretching mode appears near 2534 cm^{-1} and is consistent with literature values of simple aqueous carboxylic acid IR studies,[125] while the peaks assigned to the water OH stretching modes appear near 3200 cm^{-1} and 3450 cm^{-1} are consistent with literature values from previous VSF spectroscopic studies of more and less

coordinated water near charged CCl_4-H_2O surfaces, respectively.[31] The water OH signal stems from the charged interfacial carboxylate groups that create a field due to the double layer effect, which in turn acts to align water molecules at the interface over a longer interfacial distance.[150]

From the results of the spectral fits, it is clear that the decrease in pH from 5 to 2 causes an increase in amplitude of the peak assigned to the carboxylic acid OH stretching mode (2534 cm^{-1}) and a decrease in amplitude of the peaks assigned to the water OH stretching modes (3200 cm^{-1} and 3400 cm^{-1}). The amplitude increase of the 2534 cm^{-1} peak with pH decrease suggests an increase in population of oriented carboxylic acid groups at the oil-water interface, consistent with the carbonyl stretching mode data (Fig. 4.1). The decrease in amplitudes of the 3200 cm^{-1} and 3400 cm^{-1} peaks confirms this picture. The adsorption of the charged 3 kD sPMA to the CCl_4-H_2O interface creates a field that acts to orient water molecules adjacent to the interfacial polymer layer. The neutralization of interfacial charges through the protonation of carboxylate groups results in a decrease in the interfacial field strength and subsequently fewer oriented interfacial water molecules.[29] Additional small changes in peak amplitudes assigned to the CH stretching modes most likely indicate a change in interfacial packing and/or backbone orientation due to the increased degree of oriented interfacial carboxylic groups as the pH decreases from 5 to 2.

Despite the evidence for a change in charging of interfacial polymer as a function of pH seen in the carbonyl, CH, and OH stretching regions, signal was not observed near 1400 cm^{-1} due to the carboxylate stretching mode for the pHs studied. The lack of ordered interfacial polymer carboxylate groups is consistent with previous studies of PAA,[24-26] and is attributed to the carboxylate groups adopting opposite and/or random orientations on

chain sections protruding in to the water phase to minimize charge-charge repulsions and thus canceling the VSF signal.

The gradual pH induced changes observed in the VSF spectroscopic data resulting from the change in interfacial polymer charge is reflected in the interfacial tension data, shown in Figure 4.3.

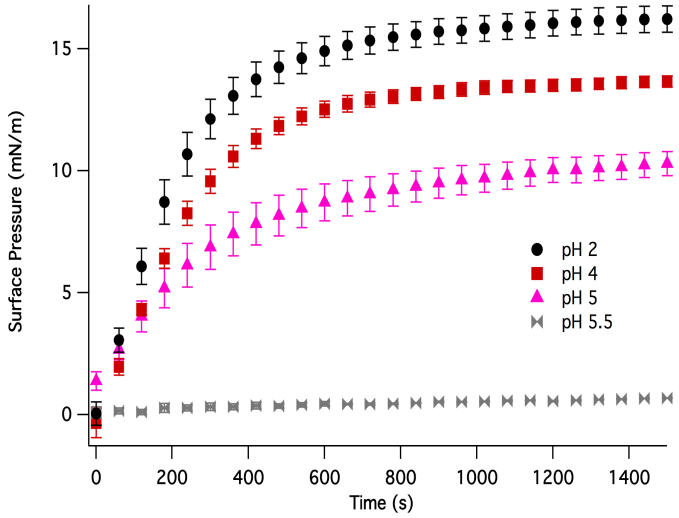

Figure 4.3. Surface pressure data for 3 kD sPMA (5 ppm) at different pHs as a function of time. The error bars represent the standard error.

The surface pressure value of the 3 kD sPMA at pH 5.5 is ~0 mN/m. This confirms that at pH 5.5 the 3 kD sPMA does not adsorb to the interface and that the absence of VSF signal is not indicative of disordered sPMA at the interface. This lack of polymer adsorption at higher pHs is attributed to the charge on the polymer making water solvation more favorable than adsorption. The equilibrium surface pressure values increase slightly as the pH is decreased from 5 to 2. The equilibrium surface pressure value is ~10 mN/m at pH 5, ~12 mN/m at pH 4, and ~16 mN/m at pH 2. This indicates that the relative amount of 3 kD sPMA adsorbed to the CCl_4-H_2O interface increases from pH 5 to 2.

Interestingly, the surface pressure measurements take ~10 minutes to reach

equilibrium for all pHs. In contrast, the VSF signal intensity does not show a similar slow rise but instead reaches the constant value within one minute of interface preparation that is seen in Figures 4.1 and 4.2. This behavior has been observed in previous studies of PAA, [24-26] and as was also observed in Chapter III. This indicates that the VSF experiment detects only the oriented polymer layer that immediately adsorbs to the interface. What adsorbs over time is disordered material that cannot be detected with VSF spectroscopy, but can be detected with the surface pressure measurements. As discussed in Chapter III, this behavior is attributed to the inherent electric field present at the CCl_4-H_2O interface that is known to assist in the adsorption of ions.[36] This field assists in the quick adsorption of highly oriented material to the oil-water interface, yet does not penetrate deep enough into the bulk water to orient the slower adsorbing material, which then adsorbs in a disordered fashion. These disordered polymers, however, continue to adsorb to the interface due to favorable hydrophobic interactions between the top-most ordered layer and disordered material that subsequently adsorbs.

What is apparent is that a decrease in pH leads to both an increase in the total amount of polymer adsorbed to the interface, as seen in the surface pressure data, as well as an increase in the number of ordered carboxylic acid groups that comprise the initially adsorbed polymer layer, as seen in the VSF data. In the first case, the increase in the total amount of polymer adsorbed at the interface is attributed to more favorable hydrophobic interactions between the initially adsorbed polymer layer and the slower adsorbing disordered polymer layer. This is due to fewer charges on the polymer chains as the carboxylate groups become protonated, leading to fewer charge-charge repulsion interactions between the initially adsorbed layer and the slower adsorbing layer. Likewise,

the decrease in pH and subsequent protonation of carboxylate groups leads to an increase in the number of carboxylic acid groups on the polymer chains. Along with the greater ability of the initially adsorbed polymer to tightly pack at the interface due to minimized charge-charge repulsions, the greater number of carboxylic acid groups is most likely what contributes to the increase in VSF signal as the pH of the solution is decreased.

Overall, the VSF spectroscopic and interfacial tension data lead to picture in which a pH change from 5 to 2 leads to an increase in the total amount of adsorbed 3 kD sPMA at the interface, specifically the amount of disordered polymer that adsorbs to the interface after the initial adsorption of an ordered polymer layer. This pH decrease additionally leads to a decrease in the amount of charge at the interface and subsequently an increase in the degree of oriented carboxylic acid groups on the polymer chains that initially adsorb to the interface. The water solvated carboxylate groups are unable to line up at the interface, since they adopt opposite orientations on the polymer chains to minimize charge-charge repulsions. Once these groups are protonated and their charges are neutralized, the resulting carboxylic acid groups are able to orient themselves normal to the interface, with the carbonyl groups pointing both into the oil phase and the water phase, and with the carboxylic acid OH groups pointing into the water phase.

Interfacial Assembly of High Molecular Weight sPMA

VSF spectra and surface pressure data were also taken for 28 kD sPMA at varying pHs to elucidate the effect of charge distribution among polymer chains on interfacial adsorption and assembly. Described below and shown in Figure 4.4 are the VSF spectra for

the samples at pH 2 and 4 (A, B) as well as pD 2 (C). Data were also obtained at pH 3 and the results fall within the trend of the other solutions studied. These data is not included in the figure for the sake of clarity.

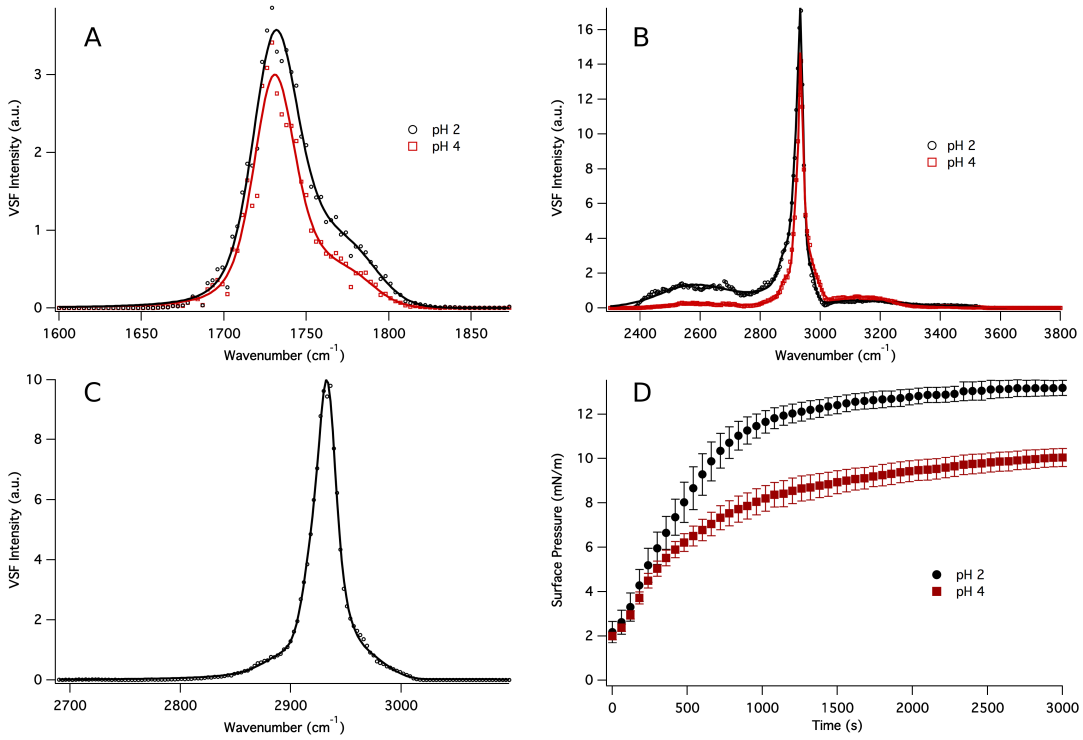

Figure 4.4. VSF spectra (*ssp* polarization) and surface pressure data for 28 kD sPMA (5 ppm) at pH 4, 2, and pD 2. (A) VSF spectra in the carbonyl stretching region. (B) VSF spectra in the CH/OH stretching region. (C) VSF spectrum of 28 kD sPMA in D_2O in the CH stretching region. (D) Surface pressure data as a function of time. The error bars represent the standard error. Solid lines are fits to the data.

Figure 4.4A shows the VSF spectra in the carbonyl stretching region. At pH 4 and 2, the spectra appear similar to the 3 kD sPMA data. Again, two peaks are present and are attributed to carbonyl groups in a more water rich environment (1730 cm^{-1}) and carbonyl groups in a more oil-rich environment (1790 cm^{-1}). As the pH decreases from 4 to 2, the amplitudes of both peaks increase, consistent with an increase in the number of oriented carbonyl groups at the interface that was also seen in the 3 kD sPMA VSF spectroscopic data of the carbonyl stretching region.

Small differences can be seen, however, in the CH stretching region of the 28 kD sample compared to the 3 kD sample. A spectrum of the 28 kD sample was taken in D_2O at pD 2 (Fig. 4.4C) and the fitting parameters were compared to the corresponding spectrum for the 3 kD sample (Fig. 4.2B) in order to elucidate the cause of the differences between the two spectra. The spectra were fit using a global routine in which all parameters were held constant except for peak amplitudes and Gaussian widths. Peak frequencies were constrained to be within the error from fits of each individual spectrum. Results from the fits indicate that the only significant difference between the two spectra is a decrease in the peak amplitude near 2888 cm^{-1} for the 28 kD sample. We attribute this to the smaller number of polymer end groups at the interface for the 28 kD sample compared to the 3 kD sPMA sample rather than a change in the overall orientation of the backbone or methyl groups. As both the 28 kD and 3 kD sPMA samples were prepared with the same monomer concentration, the 28 kD sPMA samples contain about ten times fewer chains in solution than the 3 kD sPMA samples. The data is therefore consistent with the fact that the 28 kD sPMA sample has ten times fewer polymer end groups than the 3 kD sPMA sample.

The corresponding spectra for both polymer sizes in H_2O show very similar behavior from pH 4 to 2. For the 28 kD sPMA sample, the water spectra in Figure 4.4B were fit using the same method as described for the 3 kD sPMA H_2O spectra shown in Figure 4.2A. Results from the fits show an increase in the number of oriented carboxylic acid groups from pH 4 to 2, as seen from the amplitude increase of the peak assigned to the carboxylic acid OH stretching mode (2534 cm^{-1}). Additionally, there is a slight decrease in the amplitude of the peak assigned to the water OH stretching mode near 3200 cm^{-1}, again indicating a decrease in interfacial water structure due to charge neutralization of the

interfacial polymer as the pH decreases from 4 to 2. There is, however, an insignificant change in amplitude of the peak near 3400 cm^{-1} as the pH decreases from 4 to 2. This is not surprising, as the change in amplitude of this peak in the water spectra of the 3 kD sPMA sample was not very large. Finally, small amplitude changes of the CH stretching mode peaks as the pH decreases indicate a change in backbone packing and/or orientation as the carboxylic acid groups become more ordered at the interface.

Surface pressure data were also collected for the 28 kD sPMA sample and are shown in Figure 4.4D. Again, the equilibrium surface pressure of the pH 2 sample (~12 mN/m) is slightly higher than the pH 4 sample (~9 mN/m), suggesting that there is an increase in the amount of disordered polymer adsorbed to the interface as the pH is decreased. While it is obvious that the surface pressure of the 28 kD sPMA sample takes nearly 1 h longer to reach equilibrium than the 3 kD sPMA, this is not surprising. It has been observed in studies of different molecular weight polymers that polymer accumulation at fluid interfaces is limited by diffusion, with the time for interfacial tension values to reach equilibrium longer for larger polymers compared to smaller polymers.[25, 151]

Overall, at pH ≤ 4 the 28 kD and 3 kD sPMA polymers behave very similarly at the CCl_4-H_2O interface, with strong VSF signal due to the high degree of order of the polymer methylene backbone, carboxylic acid, and methyl groups at the interface. For both sPMA sizes, a decrease in pH results in an increased degree of order of the carboxylic acid groups, with the carbonyl groups able to reside in both oil rich and water rich environments. Although the dynamics of the interfacial tension are different between the two sizes, both polymers show a time dependence that is not seen in the VSF spectroscopic data that indicates the fast adsorption of highly oriented polymer chains to the interface followed by

the accumulation of disordered material to the interface over time.

The interfacial behavior for the two different sized polymers was observed to be different in the pH region from 4-5. The adsorption of the 28 kD sPMA to the CCl_4-H_2O interface only occurs at pH<5, as indicated by both the similarity of the OH stretching region spectrum to that of the neat CCl_4-H_2O interface (Fig. 2.4), and a surface pressure value close to 0 mN/m. However, the 3 kD sPMA does adsorb to the interface at pH 5, showing strong VSF signal and a significant increase in the surface pressure compared to the neat CCl_4-H_2O interface (10 mN/m).

Between pH 4 and 5, the 28 kD sPMA does adsorb to the interface, yet the polymer interfacial behavior in this pH region is very different than it is for pH≤4. This is apparent from the time dependence of the VSF signal seen for samples studied in the pH 4-5 region. A plot of VSF signal at 2940 cm^{-1} and 1730 cm^{-1} as a function of time is shown in Figure 4.5 for a 28 kD sPMA sample at pH 4.4.

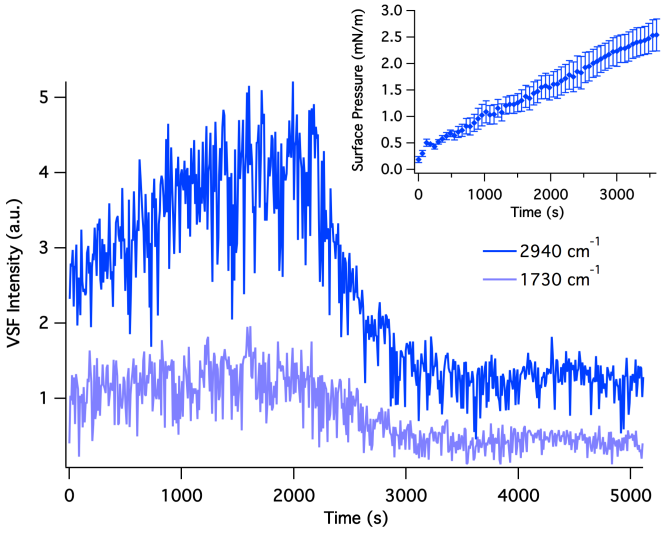

Figure 4.5. VSF signal intensity (*ssp* polarization) at 1730 cm^{-1} corresponding to the carbonyl stretching mode region and 2940 cm^{-1} corresponding to the CH stretching mode region as a function of time for 28 kD sPMA (5 ppm) at pH 4.4. The inset is the surface pressure data plotted as a function of time for the corresponding solution.

As can be seen, the intensity of the signal at both 1730 cm^{-1} (carbonyl stretching mode region) and 2940 cm^{-1} (CH stretching mode region) initially increases with time. Once maximum intensity is reached, the signal intensity suddenly decreases until a constant value is reached. This behavior is similar for samples studied between pH 4.2-4.9. In contrast, at pH 2-4, signal is observed within ~1 minute of interfacial preparation once data collection begins and remains at the same value for ~3 hours when data collection is complete. Since a change in VSF signal intensity can be due to either a change in the numbers of molecules at the interface, a change in the orientation of interfacial molecules, or both of the factors, interfacial tension data is essential for elucidating the cause of the signal intensity changes. The surface pressure data for the 28 kD sPMA at pH 4.4 is shown in the inset of Figure 4.5. As can be seen, the surface pressure value continues to increase with time even after the VSF signal intensity reaches its constant value at a much earlier time. This indicates that adsorption of polymer to the interface continues over the time period in which changes are seen in the VSF signal intensity. While this suggests that the initial increase in VSF signal intensity is due to an increase in the number of oriented polymer segments through adsorption to the interface, the decrease in signal is due to polymer reorientation rather than desorption. The increase in surface pressure after the VSF signal intensity reaches equilibrium is attributed to the accumulation of disordered polymer to the interface, albeit less than what was observed for the lower pH samples, as the surface pressure value for the pH 4.4 sample is ~2.5 mN/m at 3000 s while the value for the pH 2 sample is ~12 mN/m at 3000 s.

The VSF spectra of the carbonyl stretching region and the CH/OH stretching region, shown in Figure 4.6, indicate that the top-most layer of 28 kD sPMA absorbed to

the interface between pH 4-5 is quite different than at pH≤4.

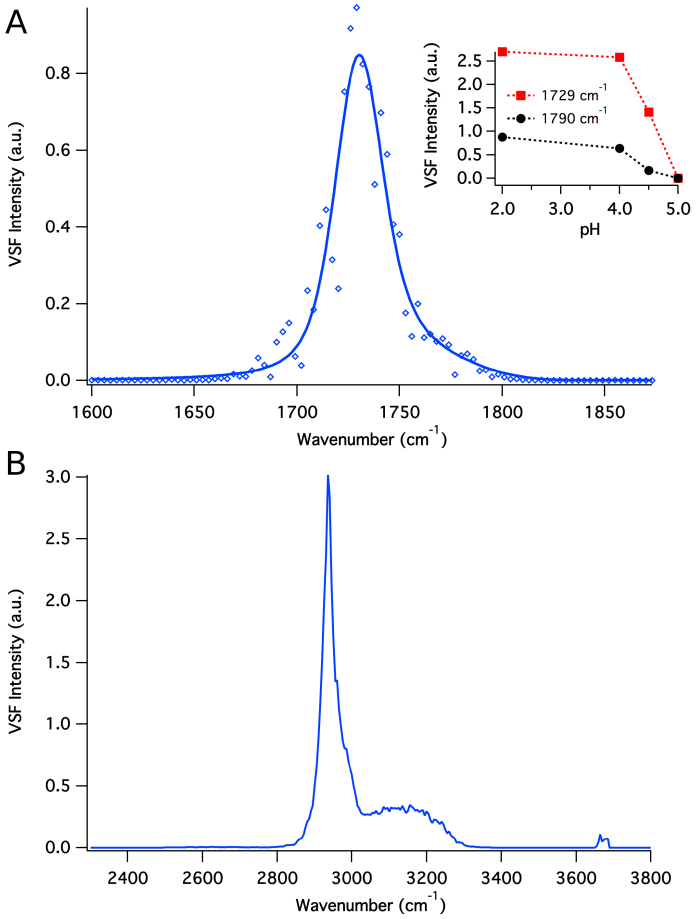

Figure 4.6. Equilibrium VSF spectra (*ssp* polarization) of 28 kD sPMA (5 ppm) at pH 4.4 in the carbonyl stretching region (top) and CH/OH stretching region (bottom). The inset shows the fit amplitudes for the peaks at 1730 cm^{-1} and 1790 cm^{-1} as a function of pH.

As with the VSF spectroscopic data taken in the carbonyl stretching region at pH≤4, the spectrum in Figure 4.6A was fit to a peak near 1730 cm^{-1} (carbonyl groups in a water rich environment) and near 1790 cm^{-1} (carbonyl groups in an oil-rich environment). The result of the fit shows that the intensities of the 1730 cm^{-1} and 1790 cm^{-1} peaks for the sample at pH 4.4 are much less than what was seen for the lower pH samples. This is represented in the inset of Figure 4.6A and indicates that overall there are fewer oriented

carbonyl groups at the interface for the pH 4.4 sample compared to the lower pH samples. The spectrum in the CH/OH stretching region shown in Figure 4.6B confirms this picture. It is quite obvious that the peak near 2534 cm^{-1} attributed to the carboxylic acid OH stretching mode is absent in this spectrum, while strong signal due to the coordinated water OH stretching mode is present. Additionally, the peak near 3670 cm^{-1} is assigned to the free-OH stretching mode (Fig. 2.4) and indicates that there is not complete coverage of the interface by the polymer,[42, 90] consistent with the relatively low surface pressure values. This mode was not present for samples of 28 kD sPMA at pH≤4, indicative of full coverage of the interface by sPMA at these lower pH values. Finally, the intensities of the CH stretching mode peaks are much weaker for the pH 4.4 sample compared to the lower pH samples, consistent with the carbonyl stretching mode data.

A picture consistent with the data discussed above for the 28 kD sPMA samples between pH 4-5 is one in which ordered polymer chains initially adsorb to the interface, with continued adsorption of oriented material until a critical point. At this point, chain segments rearrange at the interface, until an equilibrium polymer surface structure is attained that is more disordered than the initially adsorbed polymer. After this point, disordered polymer continues to adsorb to the interface, yet this accumulation does not lead to complete coverage of the interface. For 3 kD sPMA between pH 4-5, full coverage of the interface occurs within minutes of interface preparation, as observed by both the strong VSF signal attributed to the polymer along with the lack of a peak at ~3670 cm^{-1} attributed to the free-OH stretching mode. A constant VSF signal at both ~1730 cm^{-1} and ~2940 cm^{-1} indicates no rearrangement of the initially adsorbed polymer layer with time. Again, the decrease in the interfacial tension value with time indicates the accumulation of disordered

polymer to the interface with time.

It is obvious that between pH 4-5, polymer chain length plays a role in sPMA interfacial adsorption behavior. As stated in the introduction of this chapter, the charge distribution among polymer chains for the 28 kD sPMA samples, with ~326 monomers per chain, will be different than the charging of the 3 kD sPMA samples, with ~34 monomers per chain. The solutions were made with the same number of monomers such that at 5 ppm, solutions of both 28 kD sPMA and 3 kD sPMA have a monomer concentration of ~0.06 mM. This results in the 3 kD solutions containing overall ~10x the number of polymer chains in solution as the 28 kD solutions. Because of this, the 3 kD samples contain a relatively large number of chains in solution in which a small number of charges can accumulate on each chain, whereas the 28 kD samples contain a relatively small number of chains in solution in which a large number of charges accumulate on each chain.

In order to give an idea of the approximate number of charges per chain as the solution pH decreases from 5 to 2, titration data for sPMA from previous work by Kawaguchi et al will be discussed.[152] At pH ~5, approximately 20% of monomers in solution will be charged, corresponding to ~7 charges/chain for the 3 kD sPMA (34 monomers/chain) and ~65 charges/chain for the 28 kD sPMA (325 monomers/chain). At pH ~4, approximately 5% of monomers in solution will be charged, corresponding to ~1 charge/chain for the 3 kD sPMA and ~16 charges/chain for the 28 kD sPMA. By pH 3, only approximately 1% of monomers in solution will be charged, corresponding to less than 1 charge/chain for the 3 kD sPMA and ~3 charges/chain for the 28 kD sample. That the larger sPMA can accumulate so many more charges per chain than the smaller sPMA between pH 4-5 appears to play a key role in the greater surface activity of the 3 kD sPMA

compared to the 28 kD sPMA in this pH range.

Previous work on polyelectrolytes in bulk aqueous solution has suggested that cooperative effects allow charges on polymer chains to accumulate near each other.[153] In previous studies, this effect was used to explain why PAA desorbs so readily from the CCl_4-H_2O interface in a very narrow pH region, and specifically that deprotonation occurs on carboxylic acid functional groups near each other such that sections of the chain become so hydrophilic that solvation is more favorable than adsorption.[24-26] It is concluded here that the same effect is at play with the two different sized sPMA polymers. As discussed above, the 28 kD sPMA is able to accumulate more charges per chain than the 3 kD sPMA polymer. These charges have the ability to accumulate near each other on the chain, creating sections of the polymer that are very hydrophilic. The result is that when both polymer solutions are at the same pH, the larger polymer will be more hydrophilic than the smaller polymer. This explains why the smaller polymer is able to adsorb to the CCl_4-H_2O interface at higher pHs than the larger polymer.

Additionally, this polyelectrolyte charging behavior explains the time dependence of the VSF signal observed for the 28 kD sPMA between pH 4-5. For the sPMA samples where there is no observed time dependence of the VSF signal, the polymer chains are able to adsorb to and spread out at the interface so quickly that these steps are not observed in the spectroscopy. The disordered polymer that continues to adsorb to the interface is only observed in the interfacial tension data. For the 28 kD sPMA between pH 4-5, however, the hydrophilic nature of the polymer causes the adsorption of oriented material to be quite slow. Despite the hydrophilic nature of 28 kD sPMA at this pH, the initial adsorption of oriented polymer segments is assisted by the inherent electric field present at the CCl_4-H_2O

interface.[36] Once a critical amount of polymer adsorbs to the interface, such that when the VSF signal is at a maximum, reorientation of polymer occurs until an equilibrium surface structure is reached. Due to the accumulation of charges near each other on the polymer chain, it is likely that the critical amount of polymer adsorption correlates to a critical amount of highly charged chain sections at the interface. The reorientation of these sections would thus be due to the solvation of these highly charged chain sections to minimize the charge-charge repulsions that would be present if these chains were spread out in an extended configuration at the oil-water interface.

Since the surface pressure does not change much for these systems compared to the lower pH samples, it shows that the degree of polymer accumulation after the top-most equilibrium surface layer is attained is much less than for the lower pH 28 kD sPMA samples. This is consistent with the fact that the multilayer adsorption is ascribed to favorable hydrophobic interactions between the top-most adsorbed layer and the disordered material that subsequently adsorbs to the interface.[24-26] This has also been noted in adsorption studies of biological polyelectrolytes.[21, 127] For the 28 kD sPMA in the pH region from 4-5, these favorable hydrophobic interactions are minimal due to the highly hydrophilic nature of the polymer.

A cartoon depicting the surface structure of the 3 kD and 28 kD sPMA polymers between pH 4-5 is shown in Figure 4.7. Overall, the smaller 3 kD sPMA polymer adsorbs to the interface at lower pH values than the 28 kD sPMA polymer. Specifically, for the 3 kD sPMA polymer, a change in pH from 5 to 2 results in only a gradual increase in the number of ordered of carboxylic acid groups as the carboxylate groups become protonated, as well as an increase in the amount of disordered polymer adsorbed to the interface.

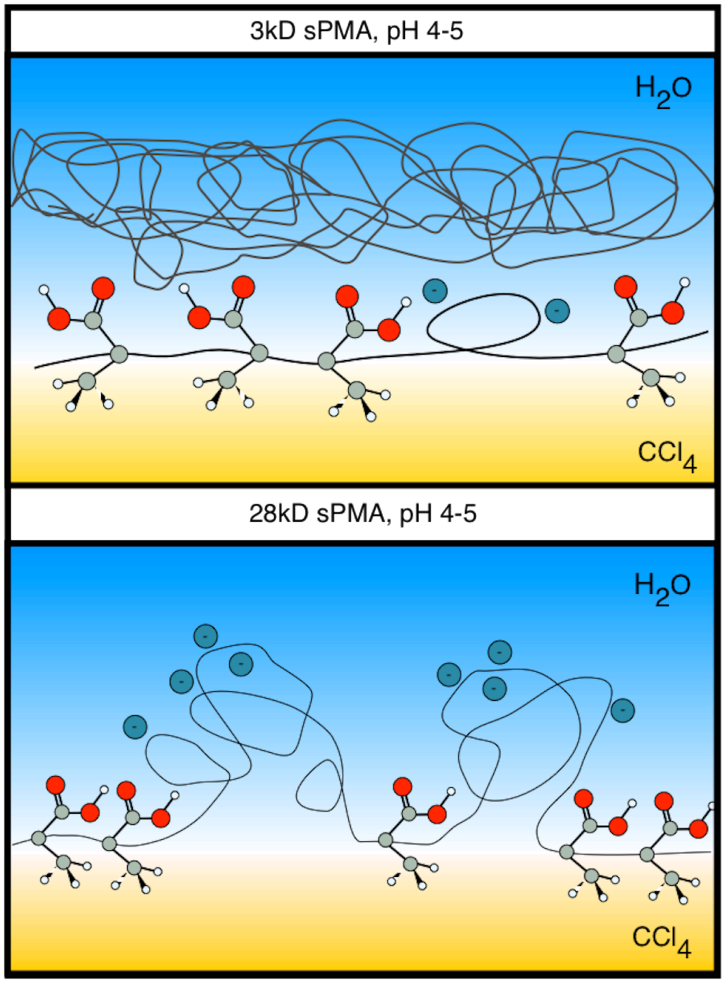

Figure 4.7. Cartoon depicting the interfacial behavior of sPMA at 5>pH>4 for the 3 kD polymer (top) and the 28 kD polymer (bottom).

The 28 kD sample, however, experiences different pH-dependent adsorption behavior. In the region from pH 4-5, adsorption is followed by polymer chain reorientation to minimize charge-charge interactions and is due to the ability of the 28 kD sPMA polymer to accumulate more charges on the chains compared to the 3 kD sPMA polymer. In the region of pH ≤ 4, the 28 kD sPMA adsorption behavior is very similar to the 3 kD sPMA polymer. By this point, charge accumulation on the chain must be minimal so that polymer adsorption and accumulation at the interface is more favorable than both complete solvation and polymer chain reorientation to solvate highly charged chain sections.

Summary and Conclusions

Through VSF spectroscopic and surface pressure measurements, it is demonstrated how the distribution of charges among different sized polymer chains in solution influences polyelectrolyte behavior at an oil-water interface. The differences between the interfacial behavior of the large and small sPMA polymers occurs only between a narrow pH range, from pH 4 to pH 5. For the larger sPMA polymer in this pH range, the ability to accumulate a greater number of charges per chain compared to the smaller sPMA polymer makes the larger polymer overall more hydrophilic; the highly charged chain segments of the larger adsorbed polymer protrude into the aqueous phase and do not allow full coverage of the interface. In contrast, the smaller polymer, with only a few charges per chain, is better able to pack at the interface. Overall, the smaller polymer appears to behave more like an alkyl surfactant than the larger polymer.

The sensitivity of these polyelectrolyte systems on specific solution conditions has implications for oil recovery and environmental remediation processes that utilize the adsorption of natural polyelectrolytes to an oil-water interface. By fine-tuning factors such as macromolecular size and placement of ionizable groups, it seems possible to engineer natural polyelectrolyte mimetics and analogs that will accumulate at the oil-water interface under any set of environmental conditions. As natural polyelectrolyte substances are known to be polydisperse and structurally very complex, it may also be possible to select specific sizes and structures of humic or fulvic acids that will behave ideally at environmental oil-water interfaces, either for the purpose of recovering a natural fuel source or for remediating waters contaminated by toxic materials. The following chapter, which explores

the difference in the interfacial assembly between different PMA isomers with metal ions, further demonstrates the sensitivity of interfacial adsorption and assembly on the specific arrangement of the ionizable groups along the polymer backbone as well as on the degree of polymer charging.

CHAPTER V

METAL ION INDUCED ADSORPTION AND ORDERING OF CHARGED MACROMOLECULES AT THE OIL-WATER INTERFACE

Whether or not a charged macromolecule remains solvated or adsorbs to the interface between two immiscible fluids depends on a variety of complex factors. Ions, in particular, have the capacity to affect the degree of polyelectrolyte hydrophobicity and conformation through electrostatic screening and site-specific interactions. In this chapter, the adsorption dynamics, conformation, and extent of carboxylate-cation interactions of poly(methacrylic acid) at the carbon tetrachloride-water interface is deduced as a function of $CaCl_2$ and KCl ionic strength. Additionally, the role of polymer backbone configuration in the degree of polyelectrolyte-ion interactions and subsequent interfacial behavior is explored through isomer specific studies. Results show that ion binding and charge screening induce the adsorption of the isotactic isomer of poly(methacrylic acid) to the oil-water interface under solution conditions unfavorable to surface adsorptivity, and that the degree of cation-carboxylate interactions strongly affects the adsorption dynamics and interfacial structure of the adsorbed polymer. The backbone structure of syndiotactic PMA does not allow for strong interactions with cations, and so remains water solvated in the presence of salt. This work was submitted to the *Journal of Physical Chemistry C,* with Andrew P. Carpenter, Courtney M. Olson, and Geraldine L. Richmond as coauthors. I wrote the paper and performed the spectroscopic measurements, Andrew P. Carpenter and Courtney M. Olson performed the interfacial tension measurements, and Geraldine L. Richmond provided editorial assistance.

Introduction

Metal ion binding to charged macromolecules is a ubiquitous process in several systems ranging from biological,[1, 154], to environmental,[155, 156] to industrial.[157-162] In biology, several classes of proteins and enzymes require a bound metal ion, such as copper, zinc, or calcium, in order for them to function properly.[154] In the environment, humic acids can strongly bind to both toxic metal ions, such as lead and mercury, as well as biologically important ions like calcium and copper, and can therefore play an important role in the fate and transport of toxins as well as the bio-availability of nutrients.[155, 156, 160, 163] Industrial polyelectrolytes are often designed to selectively bind certain ions as a means of remediating contaminated water.[157-159] Additionally, certain pharmaceutical polymers are used to bind metal ion-containing drugs for enhance drug delivery.[162, 164]

As has been shown thus far, polyelectrolyte assembly at the liquid-liquid interface is an essential process for the types of charged macromolecules discussed above, and this is especially true in the case of polymer interactions with metal ions. For instance, humic substances are surface-active macromolecules that bind toxic metals,[4, 5, 155, 156, 165-170] which can result in the accumulation of such toxins at environmental interfaces. In biology, the misfolding of amyloid proteins on the surface of cells is known to result in neurodegenerative diseases such as Alzheimer's, and has been linked to interactions of the protein with metal ions.[117-122] The binding of metal ions is also known to assist in the transport of charged polymers across fluid interfaces, which can be important in the use of polyelectrolytes as drug delivery vehicles for metal-containing pharmaceuticals.[162, 164] Ions, in general, are prevalent aqueous species that can encounter and interact with

polyelectrolytes in bulk solution, which has the potential to affect polyelectrolyte interfacial behavior. The studies in this chapter elucidate the factors that dictate the behavior of carboxylic acid-containing polymers at the oil-water interface by specifically probing the manner in which different cations alter polyelectrolyte hydrophobicity and conformation and thus interfacial activity and structure.

For highly charged polyelectrolytes in the absence of salt, the bulk conformation is that of a rigid, extended coil due to charge-charge repulsions between neighboring monomers.[89] Different counterions can interact with polyelectrolytes in various ways that can change this bulk conformation, and these interactions have been studied extensively both theoretically[89, 171-181] and experimentally[164, 182, 183] for polyelectrolytes in bulk solution. For poly(carboxylic acids) in particular, monovalent and divalent cations play distinctly different roles in terms of electrostatic charge screening and binding, which in turn affect macromolecular bulk conformation and hydrophobicity.[184-191] Monovalent cations are known to interact with anionic carboxylate groups through non-specific electrostatic interactions. These cations only disrupt the second solvation shell of the polyelectrolyte and can move freely over the polyelectrolyte surface.[89] The addition of monovalent cations acts to screen the polymer charges, and thus shrinks the dimension of the polymer conformation to that of the undissociated state.[89]

In contrast, in bulk aqueous solution divalent cations interact specifically with the carboxylate groups on the polymer.[89] The extent of these interactions depends on several factors, such as polymer backbone configuration, distance between charged groups, molecular weight, and polymer charge density.[164] Site-bound cations disrupt both the first and second solvation shell of the polymer, and, depending on the nature of the divalent ion-

carboxylate complex, can cause dehydration of the polyelectrolyte. Such an increase in polyelectrolyte hydrophobicity can result in the collapse and extensive coiling of the bulk conformations of the chains. Consequently, interactions of poly(carboxylic acids) with both mono and divalent cations in bulk solution that lead to changes in charging, hydrophobicity, and structural characteristics have the potential to greatly affect polyelectrolyte behavior at the oil-water interface where metal ion binding is quite relevant.

In this chapter, vibrational sum frequency (VSF) spectroscopy is used to probe the molecular-level effects of ions on the oil-water interfacial behavior of poly(methacrylic acid) (PMA), a model poly(carboxylic acid). Previous studies have detailed the binding of metal ions to carboxylic acid containing surfactants using both VSF[39, 192-194] and surface infrared[195-198] spectroscopic techniques at the oil-water interface, but results from Chapter IV have clearly shown that polyelectrolyte interfacial behavior is quite different from that of a simple alkyl surfactant. A few studies have probed metal ion binding to carboxylic acid containing polymers at the air-water interface using VSF spectroscopy,[72, 74] but these studies focused only on the CH/OH stretching spectral region and did not explore adsorption dynamics.

In this chapter, studies specifically show how the biologically and environmentally relevant divalent and monovalent cations, Ca^{2+} and K^{+}, affect the carbon tetrachloride-water (CCl_4-H_2O) interfacial behavior of PMA under solution conditions for which it is not normally surface active. Here, the polymer CH, carbonyl, and carboxylate stretching modes, as well as the water OH stretching modes are probed in order to gain a complete understanding of the interactions of the metal ions with the carboxylate groups and how these interactions affect polymer adsorption dynamics and resulting interfacial

conformation. In order to further understand how polymer backbone structure affects metal ion interactions and thus interfacial behavior, both the syndiotactic (sPMA) and isotactic (iPMA) isomers of PMA were studied. The chemical structure of iPMA and sPMA were shown in Figure 3.1. As discussed previously, it is well known that the tacticity of PMA plays a strong role in the charging behavior and hydrophobicity of the polymer.[83-86] For iPMA, all the carboxyl groups are on the same side of the polymer when in the *all anti*-conformation, while for sPMA, the carboxyl groups are located on each side of the polymer and alternate every monomer when in the *all anti*-conformation. The closeness of the carboxylic acid groups to each other in iPMA gives it a local charge density higher than that of sPMA. Studies have shown that the greater charge density of iPMA allows it to interact more strongly with oppositely charged species compared to sPMA.[83, 85, 86] By studying both isomers of PMA with K^+ and Ca^{2+}, the ability of ions to alter polyelectrolyte hydrophobicity and conformation is demonstrated, and how these characteristics affect polyelectrolyte interfacial activity, adsorption dynamics, and resulting structure at the oil-water interface is shown.

Calcium-Induced Adsorption of iPMA

The CH/OH stretching region spectrum of surface adsorbed iPMA at pH 6 in the absence of $CaCl_2$ is shown in Figure 5.1A (gray trace). This spectrum shows the characteristic OH stretching signal from interfacial water molecules of the neat CCl_4-H_2O interface. There is relatively strong and broad signal in the region between 2800-3400 cm^{-1} corresponding to various degrees of hydrogen bonding of interfacial water molecules, and

the sharp peak near 3670 cm^{-1} due to the free-OH oscillators of the top-most water molecules. As the intensity of this peak in the gray trace of Figure 5.1A is very close to that of the neat CCl_4-H_2O interface (Fig. 2.4), it is very likely that only a trace amount of iPMA has adsorbed to the interface at pH 6.

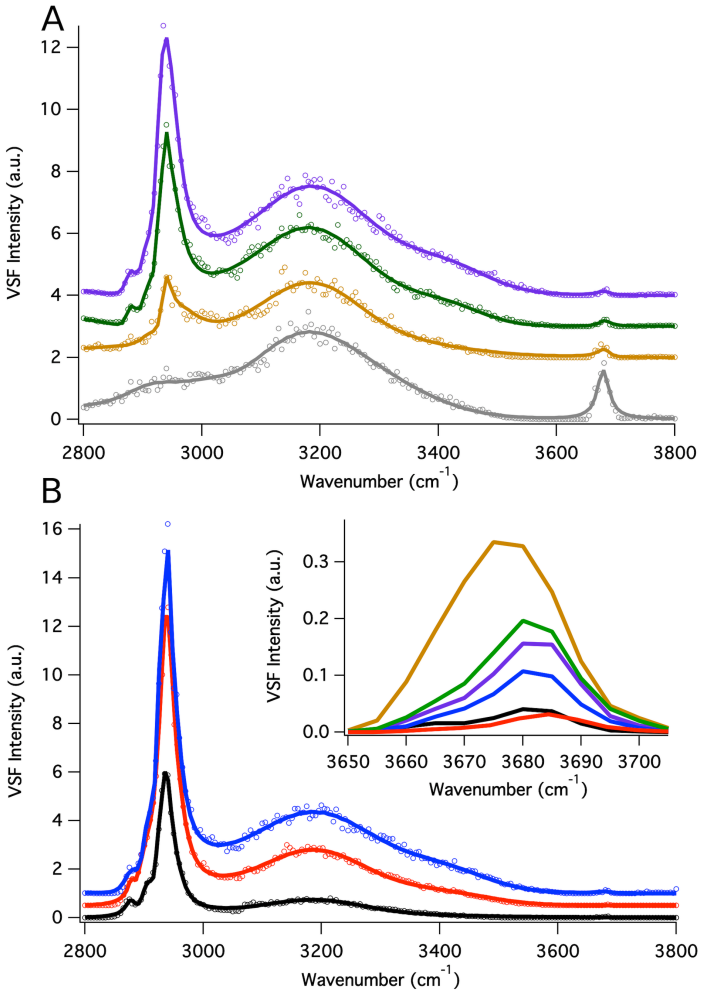

Figure 5.1. VSF spectra (*ssp* polarization) of 3 kD iPMA (5 ppm, pH 6) in the CH/OH stretching region as a function of $CaCl_2$ ionic strength. (A) 0 mM (gray), 0.1 mM (yellow), 0.175 mM (green), and 0.25 mM (purple) $CaCl_2$. (B) 0.5 mM (blue), 1 mM (red), and 10 mM (black) $CaCl_2$. Solid lines are fits to the data. The spectra are offset for clarity. The inset of B displays the free-OH peak near 3670 cm^{-1} as a function of $CaCl_2$ ionic strength, and the solid lines are guides for the eye.

The pK_a of PMA in bulk water was measured to be 7.3,[199] so at pH 6 it is estimated that a little less than half of the carboxyl groups are charged. That only a trace amount of polymer adsorbs to the interface is consistent with the degree of charging of iPMA. This was shown in the pH-dependent adsorption behavior of sPMA in Chapter III, in which strong adsorption to the interface occurred only at pH≤5. It is clear that under these pH conditions when iPMA is significantly charged, the adsorption of polymer to the oil-water interface is not favorable. However, the addition of $CaCl_2$ can reduce the degree of polymer charging, leading to conditions that favor iPMA adsorption over solvation.

This can be seen in the spectra in the CH/OH stretching region of iPMA with added $CaCl_2$ (Fig. 5.1). The interface clearly changes upon the addition of 0.1 mM $CaCl_2$ as shown in the yellow trace of Figure 5.1A. The most distinct changes are the stronger and more defined peaks near 2800-3000 cm^{-1} corresponding to the CH stretching modes of the polymer, and a decrease in intensity of the water free-OH peak near 3670 cm^{-1}. Both of these features indicate that the calcium ions drive iPMA to the CCl_4-H_2O interface and that the adsorbed polymer has an average net orientation of the methyl and methylene groups normal to the plane of the interface. An increase in $CaCl_2$ ionic strength acts to further increase the ordered adsorption of iPMA to the oil-water interface, as shown in the green (0.175 mM $CaCl_2$) and purple (0.25 mM $CaCl_2$) traces in Figure 5.1A, and the blue trace (0.5 mM $CaCl_2$) in Figure 5.1B. These spectra show further increases in the intensities of the peaks between 2800-3000 cm^{-1} concomitant with a decrease in the intensity of the water free-OH peak near 3670 cm^{-1}. Fits to the data specifically shows peaks near 2881 cm^{-1}, 2918 cm^{-1}, 2927 cm^{-1}, and 2936 cm^{-1}. The high density of modes in this region makes specific assignment difficult. The increased addition of Ca^{2+} clearly acts to further increase

the adsorption of iPMA to the interface, with the adsorbed polymer backbone and methyl groups displaying a strong net orientation normal to the plane of the interface. By an ionic strength of 1 mM (Fig. 5.1B, red trace) and 10 mM (Fig. 5.1B, black trace) $CaCl_2$, the free-OH peak intensities are close to zero, indicating nearly full coverage of the interface with the polymer.

Despite this high degree of interfacial coverage at higher $CaCl_2$ ionic strength, fits to the data for these higher ionic strengths show an overall decrease in amplitude for the peaks attributed to CH stretching modes. A decrease in VSF peak amplitude is due to either a decrease in the number of molecules at the interface or a reorientation of functional groups, or a combination of both effects. As discussed previously, interfacial tension measurements are implemented to decouple these different factors, as they give information about the interfacial concentration of molecules and is not as sensitive to orientational changes. However, Chapter II showed that even though VSF signal is observed from iPMA adsorbed at the interface at low pH, the interfacial tension measurement is insensitive to this adsorption due to the formation of a single polymer layer. Consistent with this, interfacial tension measurements of iPMA as a function of $CaCl_2$ ionic strength also did not reveal large surface pressure increases, as shown in Figure 5.2.

As can be seen, there is no trend in the surface pressure data for iPMA with $CaCl_2$ ionic strengths between 0.1 mM and 10 mM. The 10 mM $CaCl_2$ surface pressure value is likely close to 0 mN/m due to the relatively high salt concentration. The corresponding spectroscopic measurement shows that the free-OH intensity is smaller in both the 1 mM and 10 mM spectra compared to that in the 0.5 mM spectrum (Fig. 5.1B inset), indicative

of sustained surface adsorption with ion concentration. The decreases in CH peak amplitudes at higher $CaCl_2$ ionic strength are therefore attributed to a change in the orientation of the adsorbed polymer rather than a decreased number density. The most likely explanation for this increased coverage and decreased VSF amplitude of iPMA at the higher ion concentration is Ca^{2+} binding to the negatively charged carboxylate groups that induce adsorption and reordering of iPMA at the interface.

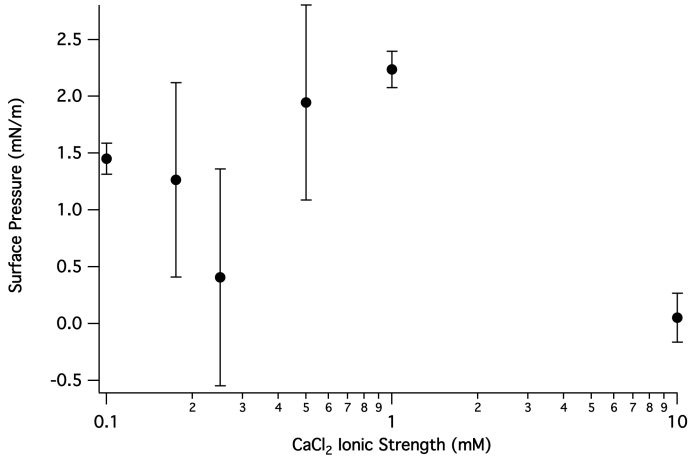

Figure 5.2. Surface pressure data for iPMA at pH 6 as a function of $CaCl_2$ ionic strength.

In order to elucidate how interactions between the Ca^{2+} ions and carboxylate groups affect iPMA adsorption and interfacial assembly, spectra were obtained in the carboxylate stretching region, shown in Figure 5.3, and carbonyl stretching region, shown in Figure 5.4 as a function of $CaCl_2$ ionic strength. At an ionic strength of 0.1 mM $CaCl_2$ (Fig. 5.3, yellow trace), a very weak signal is seen in the carboxylate stretching region. This suggests that even though this small amount of Ca^{2+} has induced the adsorption of iPMA to the interface (as demonstrated by the CH region data in Fig. 5.1A), there are insufficient interactions with the carboxylate groups to cause them to have a strong net orientation

normal to the plane of the interface. However, by an ionic strength of 0.175 mM $CaCl_2$, (Fig. 5.3, green trace) a peak is clearly seen near 1400 cm^{-1}, which increases in intensity as the ionic strength increases. A second smaller peak is observed on the low energy side of the spectra near 1360 cm^{-1}. Both of these peaks are attributed to the carboxylate stretching mode of dissociated carboxylic acid moieties, with the low energy peak due to carboxylate groups in a more strongly water hydrogen-bonded environment.[29]

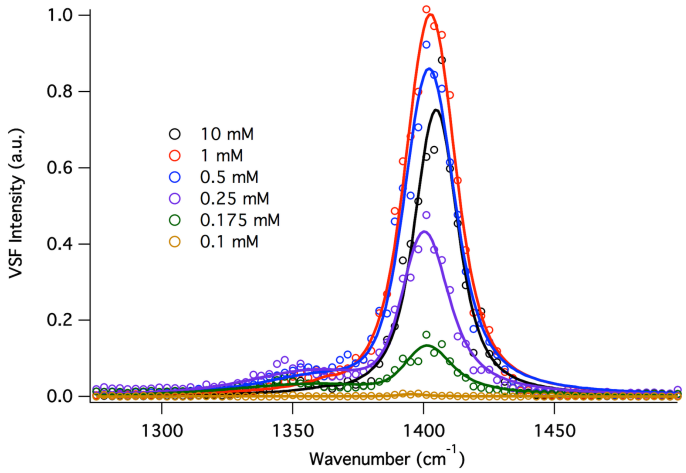

Figure 5.3. VSF spectra (*ssp* polarization) of 3 kD iPMA (5 ppm, pH 6) in the carboxylate stretching regions as a function of $CaCl_2$ ionic strength: 0.1 mM (yellow), 0.175 mM (green), 0.25 mM (purple), 0.5 mM (blue), 1 mM (red), and 10 mM (black). The solid lines are fits to the data.

Fits to the COO^- data in Figure 5.3 indicate that as the ionic strength of $CaCl_2$ increases from 0.175 mM to 10 mM, the carboxylate peak gradually shifts from 1400 cm^{-1} to 1405 cm^{-1}. Additionally, the width of the carboxylate peak in the 10 mM $CaCl_2$ spectra is significantly narrower than the peaks in the lower ionic strength spectra. These changes in the carboxylate peak frequency and width are indicative of an increase in the degree of specific binding between the negatively charged carboxylate groups and the positively charged Ca^{2+} ions. Specifically, the shifting to higher wavenumbers and peak narrowing

indicate a lesser degree of hydrogen bonding to the carboxylate groups due to the displacement of solvating water molecules by the calcium cations.[39]

In the carbonyl stretching region (Fig. 5.4), a single peak is observed near 1711 cm^{-1} and is assigned to the carbonyl functional groups of the protonated carboxylic acids. This peak initially increases with increasing the $CaCl_2$ ionic strength up to 0.25 mM (Fig. 5.4A, purple trace). By an ionic strength of 0.5 mM (Fig. 4B, blue trace), the intensity of this peak begins to decrease and is close to zero by an ionic strength of 10 mM (Fig. 5.4B, black trace).

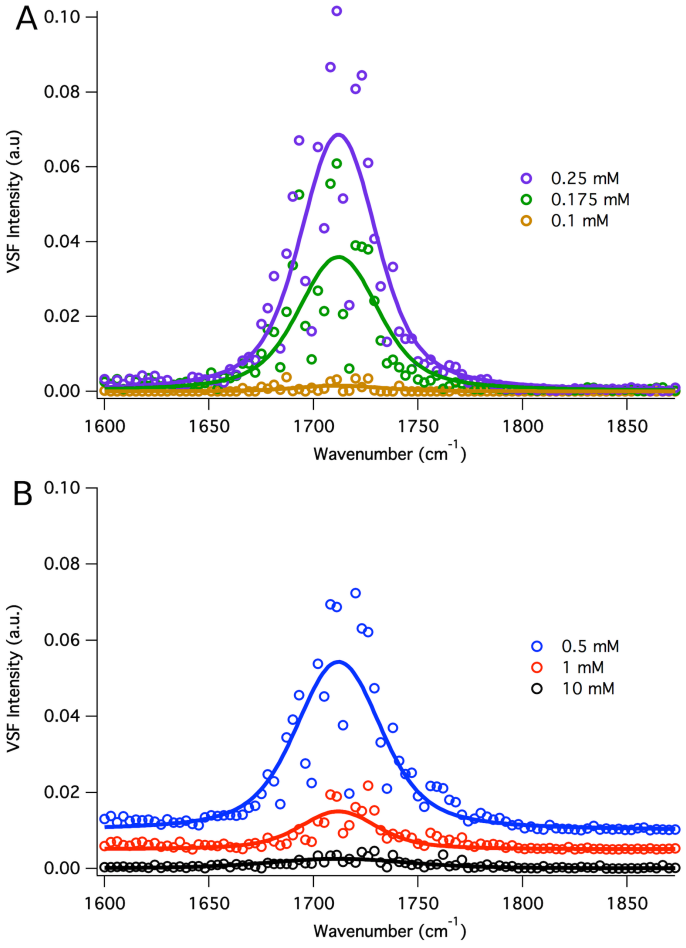

Figure 5.4. VSF spectra (*ssp* polarization) of 3 kD iPMA (5 ppm, pH 6) in the carbonyl stretching regions as a function of $CaCl_2$ ionic strength. (A) 0.1 mM (yellow), 0.175 mM (green), and 0.25 mM (purple). (B) 0.5 mM (blue), 1 mM (red), and 10 mM (black). The data are offset for clarity. The solid lines are fits to the data.

To understand the factors contributing to these observations, the square roots of the intensities for the peaks near 1400 cm^{-1} (carboxylate peak, squares), 1711 cm^{-1} (carbonyl peak, triangles), and 2927 cm^{-1} (CH peak, circles) are plotted as a function of $CaCl_2$ ionic strength in Figure 5.5. The peak amplitudes were obtained from global fitting routines of each spectral region. As discussed above, the square root of the intensity of the CH peak increases with increasing ionic strength up to 0.5 mM, and then decreases at higher ionic strengths. The square root of the carboxylate peak intensity does not follow this trend. Instead, it increases with increasing ionic strength up to 1 mM and then does not change significantly at 10 mM. The square root of the carbonyl peak intensity follows neither the trend seen in for the CH peak nor the carboxylate peak. Instead, as stated above, the intensity increases until an ionic strength of 0.25 mM and then decreases with further increases in ionic strength.

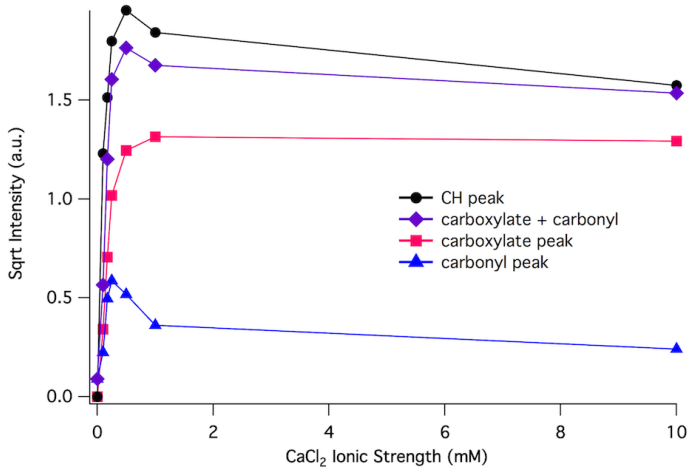

Figure 5.5. Square roots of the fitted intensities (3 kD iPMA, 5 ppm, pH 6) for the peaks near 1711 cm^{-1} (carbonyl peak, triangles), 1400 cm^{-1} (carboxylate peak, squares), 2927 cm^{-1} (CH peak, circles), and the sum of the square root intensities for the peaks near 1400 cm^{-1} and 1711 cm^{-1} (carboxylate + carbonyl, diamonds) as a function of $CaCl_2$ ionic strength. The lines are guides for the eye. All intensities are within ±0.1 a.u.

Because neither the carboxylate nor the carbonyl peak intensities track the changes seen with the CH peak, it is likely that both the total number and orientation of these functional groups are changing with increasing $CaCl_2$ ionic strength. This is not surprising, as Ca^{2+} ions are known to deprotonate poly(carboxylic acids), which would cause an increase in the number of carboxylate groups and a decrease in the number of carbonyl groups.[200] In general, the presence of ions in solution induces the deprotonation of polyacids due to their ability to screen the charges of the carboxylate groups.[89] Deprotonation of the carboxylic acid groups would thus lead to an increase in the number of Ca^{2+}-carboxylate interactions.

The initial increase in the carboxylate peak intensity with increasing $CaCl_2$ ionic strength is therefore attributed to an increase in the number of ordered surface carboxylate groups as more polymer molecules adsorb to the interface. This is consistent with bulk studies, which show that calcium cations are known to bind specifically to carboxylate groups and that these dehydrated Ca^{2+}-COO^- complexes cause an increase in overall polymer hydrophobicity.[184-186, 188-190] This increasing degree of hydrophobicity with increasing $CaCl_2$ ionic strength acts to drive oriented polymer to the interface. The leveling off of the intensity is attributed to an increase in number of carboxylate groups at the interface as the carboxylic acid groups become deprotonated, and an increase in polymer disorder as more carboxylate groups bind Ca^{2+} ions. Previous bulk studies of poly(carboxylic acids) have shown that at high enough Ca^{2+} concentrations, one Ca^{2+} cation is able to interact with two carboxylate groups to form divalent complexes.[164, 184, 185, 188, 201, 202] These studies showed that the complexes mostly form between two neighboring carboxylate groups, but there is the potential for a small number of inter- and intra-

molecular bridging complexes to form.[186, 203] It is therefore likely that the interfacial carboxylate groups become disordered at these higher ionic strengths due to such an increase in the number of neighboring $Ca^{2+}(COO^{-})_2$ complexes.

The trend seen in the carboxylate intensity is consistent with the behavior of the carbonyl peak intensity, which initially increases with increasing $CaCl_2$ ionic strength due to adsorption of iPMA to the interface. The observed decreases in intensity with the further increases in $CaCl_2$ ionic strength is due to both the deprotonation of the carboxylic acid groups by the calcium ions and an overall decrease in polymer ordering at the interface. When both the carboxylate and carbonyl peak intensities are considered together in Figure 5.5 (carboxylate + carbonyl, diamonds), it is clear that the trend seen in the intensity with increasing $CaCl_2$ ionic strength follows that of the CH peak intensity. This indicates an initial increase in ordered iPMA adsorption up to an ionic strength of 0.5 mM due to an increase in polymer hydrophobicity. By 1 mM, the adsorbed polymer structure becomes disordered, due to the increase in the number of neighboring $Ca^{2+}(COO^{-})_2$ complexes, with an increasing degree of disorder seen at 10 mM.

A developing picture of the induced iPMA adsorption through Ca^{2+} binding that is consistent with the data presented thus far is depicted in Figure 5.6. The top panel shows that with small amounts of added $CaCl_2$, iPMA is driven to the interface due to a decrease in the degree of polymer charging. At such low ionic strengths, very little ordering of the polymer is observed, and there is incomplete coverage of the interface. This is attributed to a significant amount of charge remaining on the polymer resulting in unfavorable charge-charge repulsions that cause large segments of the polymer to prefer bulk water solvation rather than surface adsorption, as was seen in Chapter IV.

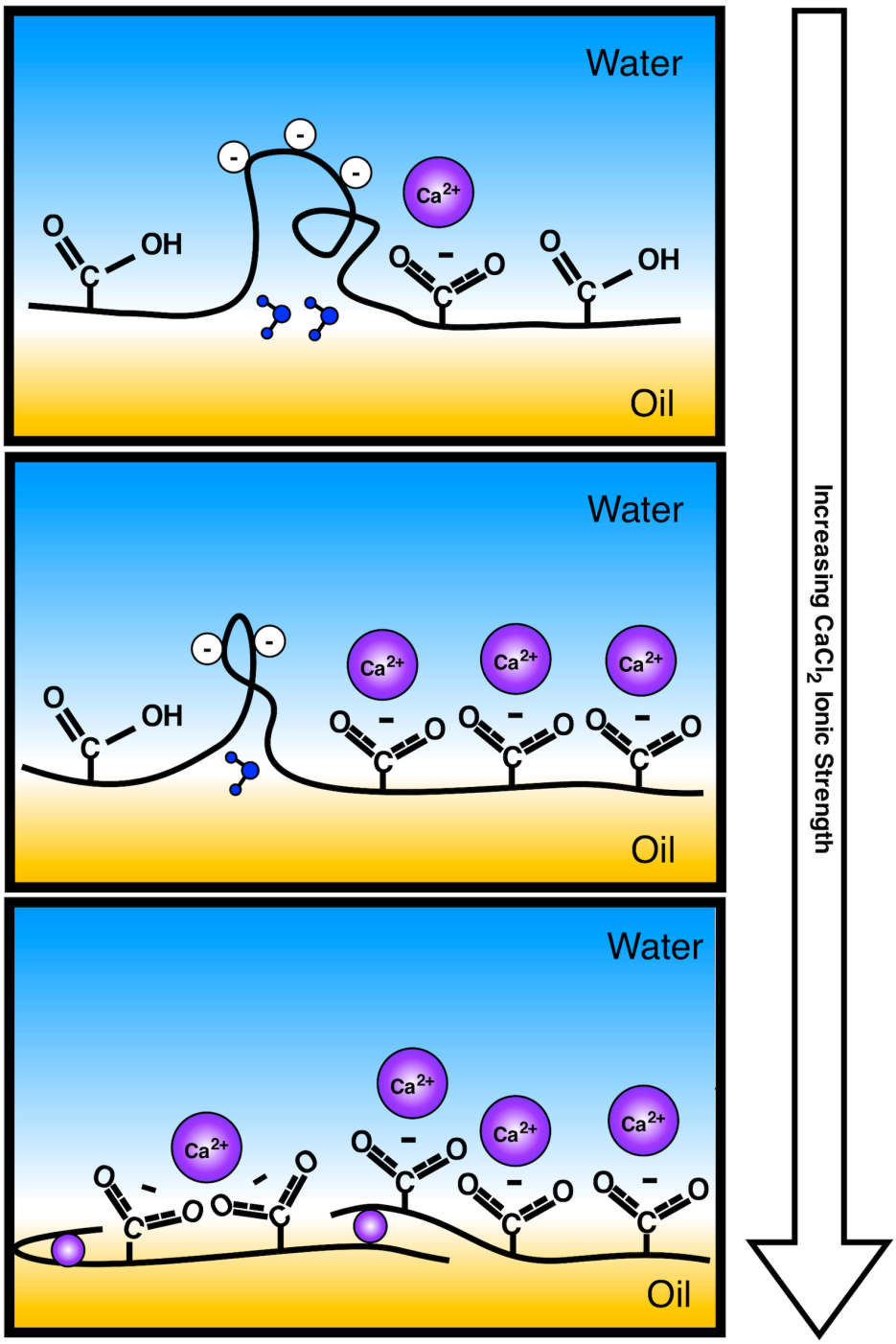

Figure 5.6. Cartoon representing the adsorption and assembly behavior of 3 kD iPMA at the oil-water interface as a function of $CaCl_2$ ionic strength.

The middle panel of Figure 5.6 shows that as more $CaCl_2$ is added to solution, the number of the Ca^{2+}-COO^- complexes increases. This increasing degree of polymer

hydrophobicity increases the degree of iPMA adsorption to the interface. The adsorbed species are highly ordered normal to the plane of the interface due to favorable interactions between the hydrophobic moieties and the oil phase, and those between the carboxylate groups and the calcium ions. At these higher $CaCl_2$ ionic strengths, Ca^{2+} is able to induce the deprotonation of iPMA. As the ionic strength of $CaCl_2$ is further increased, full coverage of the interface is attained, but the structure of the adsorbed polymer becomes disordered due to an increase in the number neighboring $Ca^{2+}(COO^-)_2$ complexes as the polymer becomes completely deprotonated. This is depicted in the bottom panel of Figure 5.6.

Interfacial Dynamics of Adsorbed iPMA-Ca^{2+} Complexes

A more complete picture of Ca^{2+}-induced iPMA adsorption can be attained by considering adsorption dynamics. For the spectra shown in the previous section, the intense peaks were not observed initially after interface preparation. For most of the solutions studied, there was a strong time dependence seen in the data, with the time for the peak intensities to stop changing taking up to several hours. Because of this, all spectra shown were obtained several hours after the interface was initially prepared. The interface was specifically prepared by depositing the aqueous solution of interest on top of the CCl_4 layer in the sample cell. Within a minute, data collection began by plotting the sum frequency intensity of the signal at 2940 cm^{-1} with time. Spectra were only obtained after the variation in the sum frequency signal was less than 1% over an hour. This is referred to as the point when the signal stabilizes, although slow dynamic processes may be occurring on a longer

time scale.

Representative time-dependent VSF signal intensities at 2940 cm^{-1} are plotted in Figure 5.7 as a function of $CaCl_2$ ionic strength. As shown, the magnitude of the intensity at 2940 cm^{-1} increases with ionic strength as does the time to achieve equilibrium adsorption. At 0.1 mM $CaCl_2$ (Fig. 5.7, yellow markers), signal does not appear to significantly change with time due to the low degree of surface adsorption (consistent with Fig. 5.1A, yellow trace). For $CaCl_2$ ionic strengths of 0.175 mM (Fig. 5.7, green markers), 0.25 mM (Fig. 5.7, purple markers), and 0.5 mM (Fig. 5.7, blue markers), the time for the VSF signal to stabilize is on the order of a couple of hours. For both 1 mM (Fig. 5.7 inset, red markers) and 10 mM (Fig. 5.7 inset, black markers) $CaCl_2$, the time for the signal to stabilize is on the order of 12 hours. The spectra obtained for these higher ionic strengths were obtained after leaving the samples in the cell for ~24 hours.

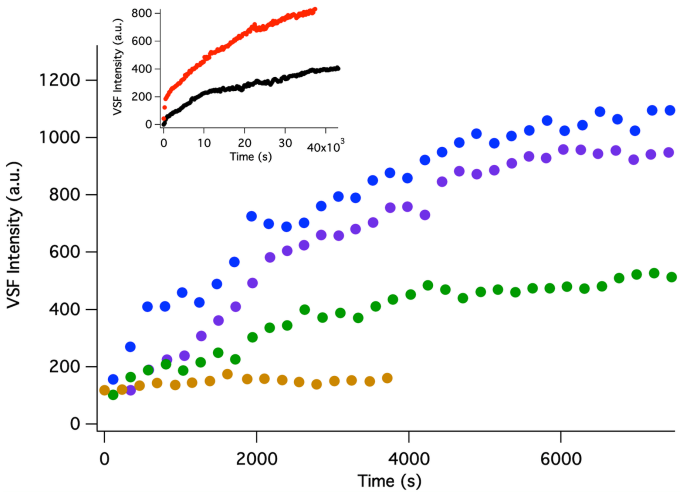

Figure 5.7. Time-dependent VSF (*ssp* polarization) of the signal at 2940 cm^{-1} (corresponding to the most intense peak in the CH/OH spectra) as a function of $CaCl_2$ ionic strength: 0.1 mM (yellow), 0.175 mM (green), 0.25 mM (purple), 0.5 mM (blue), 1 mM (red, inset), and 10 mM (black, inset).

Ions can impact the adsorption dynamics via at least two mechanisms. The first is purely electrostatic in nature whereas the second is through interactions with the adsorbate. The inherent electric field at the oil-water interface[90] is known to assist in the rapid adsorption of charged macromolecules.[25] For the first mechanism, ions cause electrostatic screening of the interfacial field,[36] thereby affecting the dynamics of macromolecular adsorption. This is thought to be the case for the adsorption of iPMA to the oil-water interface at pH 2 in the presence of 10 mM $CaCl_2$. At pH 2, not only is iPMA strongly surface active as shown in Chapter III, but the low polymer charge density should preclude a strong interaction of Ca^{2+} with charged carboxylate groups. In the previous section, it was shown that Ca^{2+} can induce the deprotonation of iPMA at pH~6. However, at pH 2, where there are excess hydronium ions in solution, the equilibrium should favor the protonated carboxylic acid rather than the Ca^{2+} bound carboxylate.[188, 189]

As shown in Figure 5.8, the addition of excess $CaCl_2$ does alter the adsorption of iPMA to the interface when the polymer is largely uncharged. In the absence of $CaCl_2$ (Fig. 5.8A), the water free-OH signal is initially zero, while the polymer CH signal is very intense and changes little with time. This indicates that soon after the interface is prepared, full coverage of the interface is attained, with insignificant change in intensity with time. The time-dependent data of iPMA with 1 mM $CaCl_2$ (Fig. 5.8B) looks very similar to the salt-free data. This is not the case for the time-dependent data of iPMA with 10 mM $CaCl_2$ (Fig. 5.8C). Here, after the aqueous layer is deposited on top of the oil layer, the CH signal is zero, while the intensity of the water free-OH signal is close to that for the neat CCl_4-H_2O interface. This indicates that shortly after the interface is initially prepared, no oriented iPMA has adsorbed to the interface. However, the water free-OH signal decreases to zero

while the polymer CH signal increases over 20 mins, indicating that oriented polymer adsorbs to the interface over time and eventually completely covers the interface.

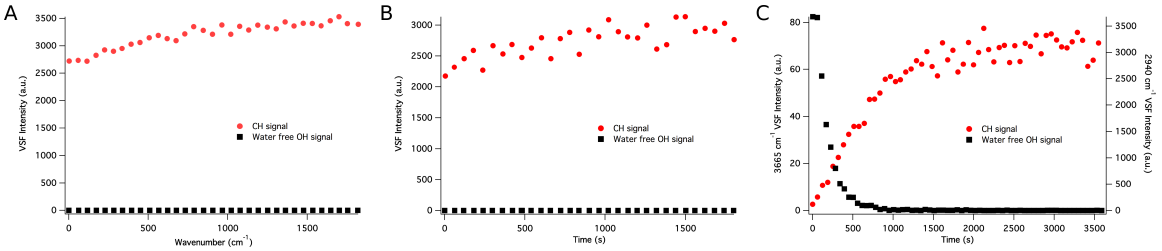

Figure 5.8. Time-dependent VSF signal (*ssp* polarization) for iPMA (5 ppm, pH 2) at 2940 cm^{-1} (CH signal, circles) and 3665 cm^{-1} (water free-OH signal, squares) in the presence of 0 mM $CaCl_2$ (A), 1 mM $CaCl_2$ (B), and 10 mM $CaCl_2$ (C).

The spectra of iPMA at pH 2 in Figure 5.9 demonstrate only very small changes with increasing $CaCl_2$ ionic strength. Fits to the data in the CH/OH spectral region (Fig. 5.9A) show peaks for the CH modes between 2800-3000 cm^{-1} as well as an additional broad peak near 2534 cm^{-1} assigned to the carboxylic acid OH stretching mode. According to the fits and also inspection, very small but measureable amplitude decreases for the iPMA peaks are observed with increasing Ca^{2+} concentration. In the carbonyl stretching region (Fig 5.9B), the spectra again look very similar. Here, two peaks are observed near 1730 cm^{-1} and 1790 cm^{-1}, and are both assigned to carbonyl stretching modes. The lower frequency peak corresponds to carbonyl groups in a more water solvated environment, while the higher frequency peak corresponds to carbonyl groups in a less water solvated environment. Again, the amplitudes of these peaks slightly decrease as Ca^{2+} concentration increases. Even though no signal was seen near 1400 cm^{-1}, indicating the absence of ordered carboxylate groups at the interface, it is possible that the small changes in peak amplitudes discussed above are due to a small number of Ca^{2+}-COO^- interactions.

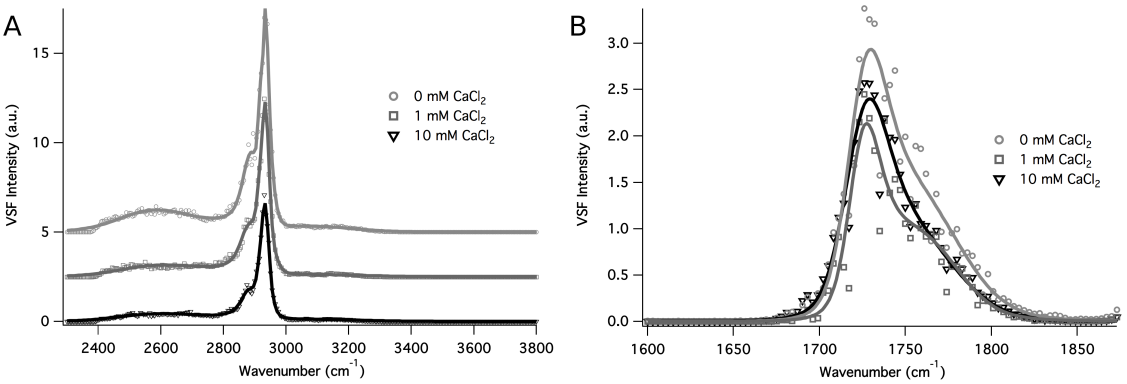

Figure 5.9. VSF spectra (*ssp* polarization) of iPMA (5 ppm, pH 2) as a function of $CaCl_2$ ionic strength in the CH/OH (A) and carbonyl (B) stretching regions. The spectra in (A) are offset for clarity. The solid lines are fits to the data.

Both the time-dependent data and the spectra taken for iPMA at pH 2 as a function of $CaCl_2$ ionic strength indicate that excess calcium acts to slow the adsorption of iPMA by means other than Ca^{2+}-COO^- interactions. For both the salt-free sample and the sample with 1 mM $CaCl_2$, the interface is quickly covered by a layer of ordered iPMA. With 10 mM $CaCl_2$, however, it takes several minutes for full coverage of the interface by oriented iPMA to occur. As discussed in Chapter III, rapid PMA adsorption at low pH has been attributed in part to the inherent interfacial field present at the interface. In order to determine if significant screening of the interfacial field occurs with excess $CaCl_2$ such that it no longer plays a significant role in polymer interfacial adsorption, a spectrum was obtained of a CCl_4-10 mM $CaCl_2$ aqueous interface and is shown in Figure 5.10.

If such an interfacial field screening effect is operative it should be observable by a significant decrease in the OH stretch mode intensities in the 3200-3600 cm^{-1} region of the VSF spectrum. As can be seen here, decreases in OH mode intensities are indeed observed for the CCl_4-aqueous salt interface compared to that of the neat CCl_4-H_2O interface, suggesting that the time dependence seen in the adsorption of iPMA to the oil-water

interface with 10 mM $CaCl_2$, both at pH 2 and 6, is in part due to electrostatic screening of the interfacial field by the added ions. It is therefore concluded that the decrease in the interfacial field due to the presence of ions contributes to the time dependence of iPMA adsorption at pH 6, although only at the higher ionic strengths.

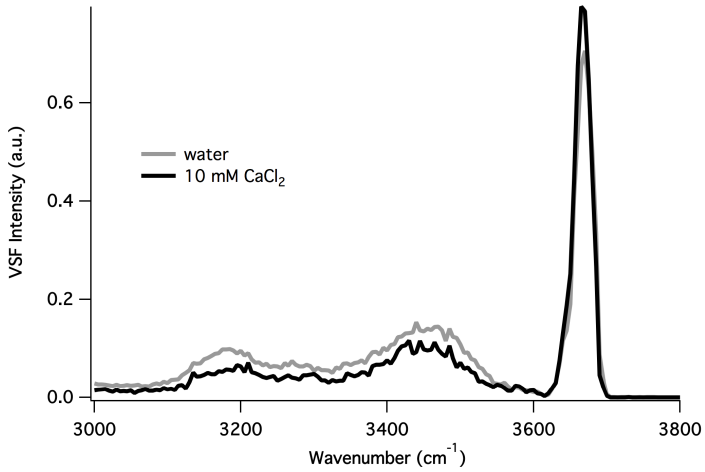

Figure 5.10. VSF spectra (*ssp* polarization) in the water OH stretching region of the neat CCl_4-H_2O interface (gray trace), and the CCl_4-10 mM $CaCl_2$ aqueous interface (black trace).

For the second mechanism, interactions between ions can influence adsorption dynamics by changing the conformation of polymer chains in bulk solution. For poly(carboxylic acids), it is well established that calcium binding to the carboxylate groups causes a change in the bulk conformation of the polymer chains.[184-191] In particular, light scattering techniques have shown that there is a gradual increase in the degree of coiling of poly(carboxylic acids) with increasing the number of bound cations.[202] The polymer chains completely collapse at high enough Ca^{2+} concentrations when most of the cations are interacting with two neighboring carboxylate groups and the polymer chains become completely dehydrated.[184, 185] Because such strong VSF signal is seen from the adsorbed

polymer at significantly high $CaCl_2$ ionic strengths after enough time, it is unlikely that the equilibrium polymer conformation at the interface is that of a coil or collapsed structure. Such structures would produce little or no VSF signal due to their overall disordered nature. A more consistent interpretation of the data is that the initially coiled or collapsed structures adsorb to the interface quite quickly and then reconfigure over a long time into a more extended structure that can maximize the interactions of the polar carboxyl groups with the aqueous phase and the hydrophobic interactions with the organic phase. Such a mechanism for adsorption is depicted in Figure 5.11.

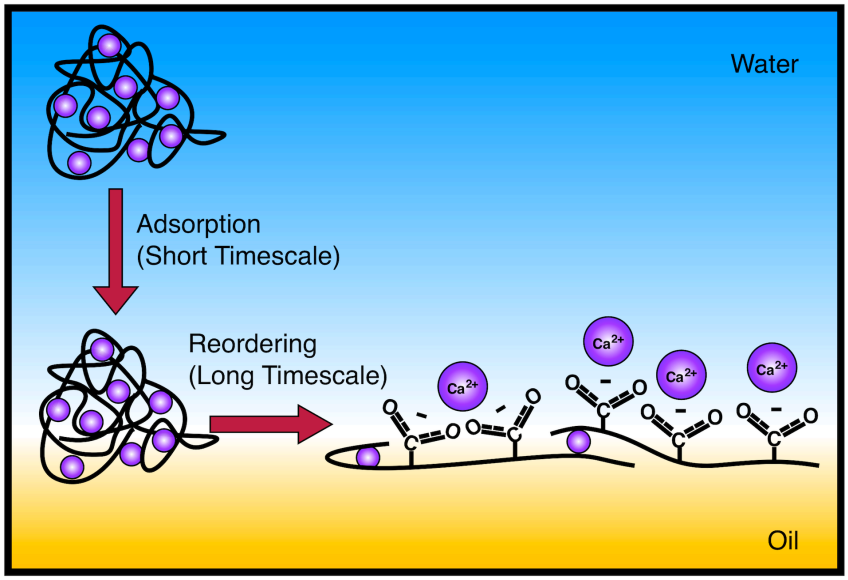

Figure 5.11. Cartoon depicting the mechanism for the adsorption and reordering of initially coiled 3 kD iPMA-Ca^{2+} complexes into more extended structures at the oil-water interface.

The time for spreading of the iPMA chains at the interface increases with the degree of binding between the calcium ions and the carboxylate groups. As the polymer becomes deprotonated, the increased degree of metal ion binding induces more stability of the adsorbed coiled polymer structures. At $CaCl_2$ ionic strengths of 1 mM and 10 mM, the

extremely long time dependence is attributed to the adsorption of collapsed chain structures at the interface in which several $Ca^{2+}(COO^-)_2$ complexes exist. The liberation of water from the solvation shells of the polymer chains due to ion binding in the bulk is driven by an increase in entropy of the system.[202] This, along with the favorable binding interactions between the carboxylate groups and calcium ions, cause the collapsed structures to be extremely stable. The spreading of such structures at the interface would decrease the entropy of the system through restricting the conformation of the adsorbed polymer[126] and potentially changing the water structure around the adsorbed polymer. These factors likely contribute to the long time dependences seen in the spreading of iPMA at the interface with high $CaCl_2$ ionic strengths. That the adsorbed structures reconfigure at the interface at all is attributed to an increase in the degree of favorable hydrophobic interactions of the methyl/methylene groups with the oil phase and the hydrophilic groups with the aqueous phase, thus decreasing the total free energy of the system. The resulting interfacial structures retain some degree of disorder due to the significant numbers of $Ca^{2+}(COO^-)_2$ complexes. This is consistent with both polymer and protein systems that show long surface rearrangement dynamics when the bulk macromolecular conformation is stabilized, such as through disulfide bonds[127] or the crosslinking of functional groups.[151]

This picture is further supported by data taken of 28 kD iPMA with 10 mM $CaCl_2$ (not shown). Compared to 3 kD iPMA, which has ~34 monomers per chain, 28 kD iPMA has ~326 monomers per chain, and so several more $Ca^{2+}(COO^-)_2$ complexes will form for the longer chains compared to the shorter chains. This should act to stabilize the collapsed coil structures of the longer chains to a greater extent than the shorter chains. It was observed that the time-dependent CH VSF signal intensity for the 28 kD polymer with

$CaCl_2$ increases very little over several hours. The equilibrium spectrum in the CH/OH stretching region displays the characteristic decrease in free-OH intensity that is associated with adsorbates at the interface. The intensity of this peak is similar to that seen with 3 kD iPMA + 10 mM $CaCl_2$, suggesting a similar degree of adsorption for both polymer sizes. Additionally, the 28 kD spectrum shows an absence of the water stretching peaks from 3000 cm^{-1} - 3600 cm^{-1}. The intensity of the CH signal near 2927 cm^{-1} for the 28 kD iPMA, however, is ~1/4 of that seen in the 3 kD iPMA spectrum (Fig. 5.1B, black trace), which is consistent with less oriented polymer at the interface due to the polymer existing as a disordered coil structure.

These results are very similar to those obtained by Hu et al, who studied the behavior of partially hydrolyzed polyacrylamide at the air-water interface using heterodyne-detected VSF spectroscopy.[72] They attributed the results to the amorphous nature of the polymer surface structure due to several $Ca^{2+}(COO^-)_2$ interactions. Such an interfacial structure did not allow for the ordering of either the polymer functional groups or the water molecules near the surface of adsorbed polymer. The same conclusion can be applied to the 28 kD iPMA chains with 10 mM $CaCl_2$. The high degree of $Ca^{2+}(COO^-)_2$ complexation for the longer iPMA chains cause extensive stabilization of the collapsed coil conformation such that favorable interactions between the hydrophobic moieties of the polymer and the oil phase are not enough of a driving force to cause the adsorbed polymer structure to spread at the interface. For the smaller iPMA chains, with fewer $Ca^{2+}(COO^-)_2$ complexes and thus a lesser degree of collapsed coil stabilization, these hydrophobic interactions are a major driving force in the uncoiling of the polymer chains at the interface.

Potassium-Induced Adsorption of iPMA

To explore further the differing roles of ions in inducing poly(carboxylic acid) adsorption through charge screening, rather than specific binding to carboxylate groups, spectra were taken of iPMA at pH 6 with the addition of KCl and are shown in Figure 5.12. As stated previously, monovalent cations are known to interact less strongly with polycarboxylate charges than divalent cations: monovalent cations only bind territorially, while divalent cations bind specifically to the polymer carboxylate groups. These studies with K^+ will therefore demonstrate if purely electrostatic screening interactions are sufficient to induce the ordered adsorption of iPMA to the oil-water interface.

As shown in Figure 5.1A (gray trace), iPMA is not strongly surface active at pH 6 due to a high charge density that renders the polymer chains water-soluble. For iPMA with KCl, it is clear from the CH/OH stretching region (Fig. 5.12A, triangles) that 1 mM KCl does induce the adsorption of iPMA to the interface, but not to the same extent as 1 mM $CaCl_2$ (Fig. 5.1B, red trace). With 1 mM KCl, while small peaks due to the polymer appear from 2800-3000 cm^{-1}, the peak attributed to the water free-OH stretching mode near 3670 cm^{-1} is still present and indicates incomplete surface coverage by the polymer. More significant, however, is the absence of a VSF signal in either the carbonyl (Fig. 5.12B, triangles) or carboxylate (Fig. 5.12C, triangles) regions with 1 mM KCl. This is quite different than what is seen with 1 mM $CaCl_2$, which results in strong adsorption and ordering of the polymer alkyl (Fig. 2B, red trace), and carboxylate (Fig. 3, red trace) groups.

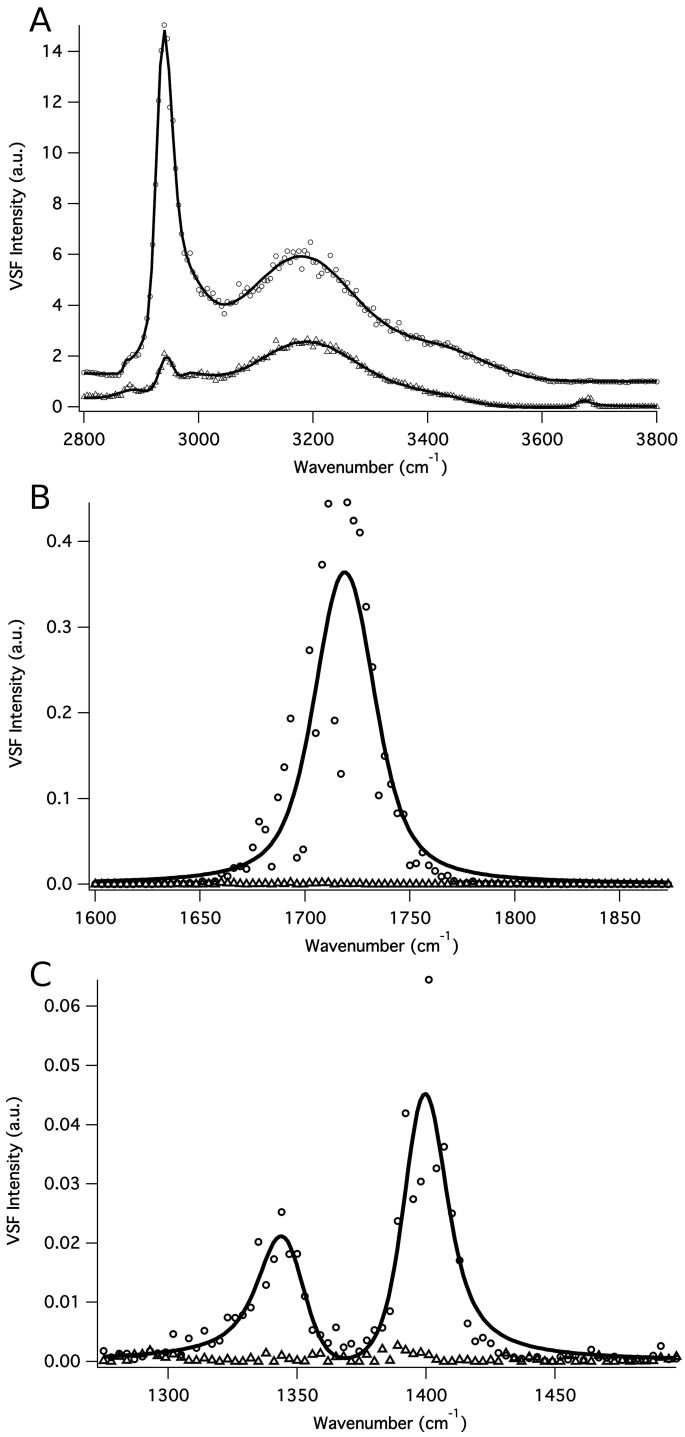

Figure 5.12. VSF spectra (*ssp* polarization) of 3 kD iPMA (5 ppm, pH 6) with 1 mM KCl (triangles) and 10 mM KCl (circles) in the CH/OH (A), carbonyl (B), and carboxylate (C) stretching regions. The spectra in (A) are offset for clarity. The solid lines are fits to the data.

At 10 mM KCl, however, complete coverage of the interface by ordered iPMA is achieved. In the CH/OH stretching region (Fig. 5.12A, circles), the signal due to the water free-OH stretch is almost zero, while intense CH peaks due to the polymer methyl and methylene groups appear from 2800-3000 cm^{-1}. Additionally, the peaks attributed to the coordinated water OH stretching modes near 3200 cm^{-1} and 3450 cm^{-1} are relatively strong compared to the iPMA spectra with Ca^{2+} (Fig. 5.1), indicating that the water molecules are more aligned at the interface for the case of iPMA with K^+. This suggests that the charges of the interfacial polymer are less effectively neutralized by K^+ compared to Ca^{2+}. The greater degree of charging of the adsorbed iPMA+K^+ acts to align the dipoles of the interfacial water to a greater extent than is seen with the adsorbed iPMA+Ca^{2+}.

The weaker interactions of the carboxylate groups of iPMA with K^+ compared to those with Ca^{2+} can also be observed in the spectra of the carbonyl (Fig. 5.12B, circles) and carboxylate (Fig. 5.12C, circles) stretching regions. At 10 mM KCl, peaks appear near 1719 cm^{-1} and 1400 cm^{-1}. Compared to the corresponding spectra of iPMA with 10 mM $CaCl_2$ (Figs. 5.3 and 5.4B, black traces), the amplitude of the carbonyl peak is larger, while the amplitude of the carboxylate peak is smaller. Thus, for 10 mM KCl with iPMA compared to 10 mM $CaCl_2$ with iPMA, there are more oriented carbonyl groups and fewer oriented carboxylate groups at the interface. This suggests that Ca^{2+} is able to deprotonate the carboxylic acid groups of iPMA to a greater extent than K^+ is able to do, as expected. Additionally, it is likely that K^+ is unable to cause a strong net orientation of carboxylate groups normal to the plane of the interface, consistent with bulk studies the suggest monovalent cations are not well able to penetrate the second solvation shell of poly(carboxylic acids).[89]

As with all other interfacial tension measurements of iPMA, K^+ does not appear to increase the surface pressure of iPMA by very much. The surface pressure values for iPMA with 1 and 10 mM KCl were both ~1 mN/m. It is therefore difficult to say whether or not Ca^{2+} drives more polymer to the interface than K^+ or vice versa. This lack of change of iPMA interfacial tension with either Ca^{2+} or K^+, however, indicates that neither ion acts to increase favorable hydrophobic interactions between the initially adsorbed oriented polymer layer and polymer in bulk solution.

The time for the ordered adsorption of iPMA with KCl to occur at the oil-water interface is relatively short. Similar to 0.5 mM $CaCl_2$ with iPMA (Fig. 5.7, blue markers), the time for the CH signal to stabilize is observed to be ~2 hours for 10 mM KCl with iPMA (not shown). Some of the initial time dependence may be due to a screening of the interfacial field by KCl, as shown by the depression of the coordinated water signal in the VSF spectrum of the CCl_4-10 mM KCl aqueous interface in Figure 5.13.

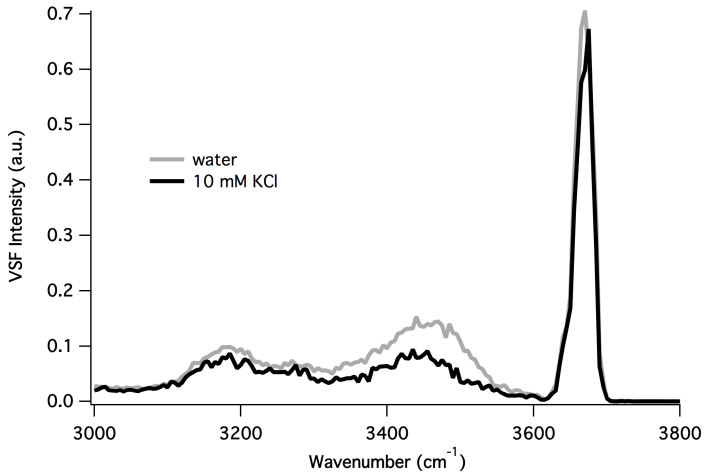

Figure 5.13. VSF spectra (*ssp* polarization) in the water OH stretching region of the neat CCl_4-H_2O interface (gray trace), and the CCl_4-10 mM KCl aqueous interface (black trace).

That the signal does not take several hours to stabilize confirms that K^+ does not interact strongly enough with the carboxylate groups to result in the long time scale process

associated with the collapse of the polymer chains in solution and subsequent spreading and reordering at the interface. The mechanism for K^+ induced iPMA adsorption consistent with the spectroscopic results is one in which electrostatic screening, rather than direct binding, of the charged carboxylate groups increases the hydrophobicity of the polymer, driving it to the oil-water interface.

Effect of Ions on sPMA Interfacial Behavior

In order to determine the role of polymer backbone configuration in the ion induced adsorption of PMA, Ca^{2+} and K^+ were also studied with sPMA. As seen in Chapter III, the specific stereochemistry of the monomers along the polymer backbone play a large role in the difference in the adsorption behavior of sPMA compared iPMA. That sPMA adsorbs as multiple layers while iPMA adsorbs as a single layer is ascribed to the different configurations of the two isomers, such that favorable hydrophobic interactions between the initially adsorbed layer and polymer in the bulk exists for sPMA but not for iPMA. It is therefore apparent that the backbone configuration of the different polymer isomers plays a major role in the adsorption of iPMA and sPMA to the oil-water interface.

The important role of backbone configuration can also be seen on examination of the VSF spectra in the CH/OH stretching region both with and without added salt, as shown in Figure 5.14. In the absence of salt (Fig. 5.14, black trace), the spectrum of sPMA at pH 6 looks very similar to that of the neat CCl_4-H_2O interface (Fig. 2.4), suggesting that polymer has not adsorbed to the interface. This is different than what is seen with iPMA at pH 6 (Fig. 5.1A, gray trace), in which stronger coordinated water signal seen from 2800-

3600 cm^{-1} suggests a trace amount of polymer at the interface. Quite significantly, unlike with iPMA, the addition of either 10 mM $CaCl_2$ (Fig. 5.14, purple trace) or 10 mM KCl (Fig. 5.14, red trace) does not significantly change the appearance of the VSF spectra, showing that these ions do not induce the adsorption of sPMA to the interface.

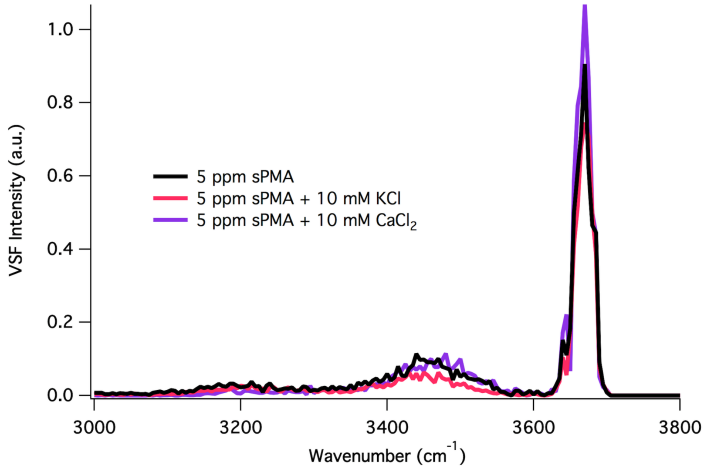

Figure 5.14. VSF spectra (*ssp* polarization) of sPMA (5 ppm, pH 6) in the presence of no added salt (black), KCl (red), and $CaCl_2$ (purple).

Different factors could be at play in determining why Ca^{2+} and K^+ are able to induce the adsorption of iPMA to the interface at this pH, but not sPMA. These factors, however, all relate to the differences in the backbone configuration of the different PMA isomers. First, even in the absence of salt, it is apparent that a trace amount of iPMA adsorbs to the CCl_4-H_2O interface at pH 6, yet there is no evidence of sPMA at the interface at this pH. This is attributed to the placement of the methyl groups along the backbone of iPMA compared to sPMA. As stated previously, the carboxyl groups of the iPMA isomer are on the same side of the polymer chain, while those of sPMA are on both sides of the chain and alternate every monomer. Both experimental and computation studies have shown that iPMA is overall more hydrophobic than sPMA.[83-88] Additionally, while the pK_a of both sPMA and iPMA is known to be ~7.3, iPMA is slightly less acidic than sPMA due to the

fact that the ionizable groups of iPMA are close to each other on the same side of the polymer chain, and hence more difficult to deprotonate compared to sPMA.[87] Thus, at pH 6, iPMA is slightly more protonated than sPMA and as a result slightly surface active. Both of these factors likely contribute to the trace amount of iPMA, yet complete lack of sPMA adsorption, observed at the CCl_4-H_2O interface at pH 6. Since iPMA is more hydrophobic than sPMA at pH 6, this may contribute to its increased adsorption with ions.

The greater localized charge density of iPMA compared to sPMA most likely also explains the large effects of ions on the surface behavior of iPMA.[83, 85, 86] It is known that iPMA interacts quite strongly with cations and surfactants due to the nearness of the charged groups to each other. Cations and surfactants interact much less strongly with sPMA because the charged groups are on opposite sides of the chain and the methyl groups hinder the electrostatic interactions between the charged groups and the ions. It is therefore likely that the Ca^{2+} and K^+ are able to more effectively bind to and screen the charges of iPMA compared to sPMA, thereby driving iPMA to the interface but not sPMA.

Summary and Conclusions

An illustration that summarizes the behavior of PMA in the presence of ions at the oil-water interface is shown in Figure 5.15. The above results show that cations are able to induce the adsorption of iPMA to this interface when it is not otherwise surface active through different mechanisms, but that the mechanisms all involve increasing polymer hydrophobicity through cation-carboxylate interactions. For Ca^{2+}-induced adsorption (Fig. 15, top panel), the divalent cations are able to bind specifically to the carboxylate groups of

iPMA. This results in dehydration of the polymer, which increases its hydrophobicity and drives it to the interface. The strength of the binding interactions between Ca^{2+} and the polymer carboxylate groups is demonstrated by the fact that the divalent cations are able to induce the deprotonation of the carboxylate groups at high enough ionic strengths. Additionally, the results indicate that at these higher $CaCl_2$ ionic strengths there are a significant number of $Ca^{2+}(COO^-)_2$ complexes. These complexes lead to disordered structures in the bulk that initially adsorb to the oil-water interface. Favorable hydrophobic interactions between the nonpolar groups of the polymer and the oil phase result in the uncoiling of the polymer chains at the interface over several hours. The resulting adsorbed polymer configuration is extended, yet retains some disorder at high enough ionic strengths when several $Ca^{2+}(COO^-)_2$ complexes are likely.

For K^+ (Fig. 5.15, middle panel), the induced adsorption occurs through non-specific electrostatic screening of the charged carboxylate groups of iPMA. These weaker cation-polymer interactions require much more KCl than $CaCl_2$ to cause complete interfacial coverage by the polymer. Additionally, the weaker interactions of K^+ with iPMA result in neither the significant deprotonation of the carboxylic acid groups nor ordering of the charged carboxylate groups. With sPMA (Fig. 5.15, bottom panel), neither Ca^{2+} nor K^+ is able to induce the adsorption of sPMA to the CCl_4-H_2O interface at pH 6 due to the alternating positions of the charged carboxylate groups and bulky methyl groups on the chains such that direct binding and electrostatic interactions of the ions with the polymer are hindered.

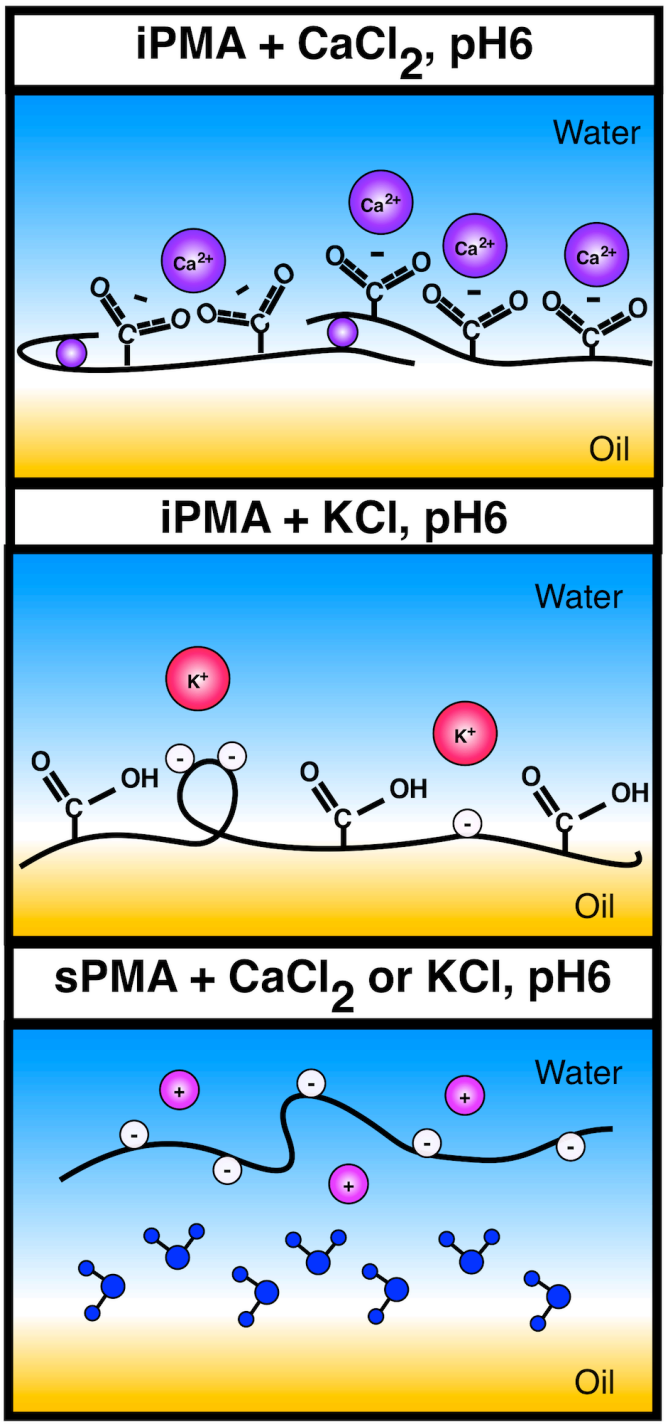

Figure 5.15. Cartoon depicting the effects of Ca^{2+} and K^{+} on the interfacial behavior of 3 kD iPMA and sPMA at pH 6.

This study clearly shows that both aqueous solution conditions and polymer structure greatly affect the oil-water interfacial behavior of a carboxylic acid-containing

macromolecule. The degree of polymer charging obviously dictates water solvation vs. adsorption. The way in which the charges are arranged on the polymer backbone additionally affects the extent to which counter ions bind to and screen these charges, with strong cation-carboxylate interactions increasing polymer hydrophobicity and driving it to the interface. It has been demonstrated that direct ion binding has an effect on polymer adsorption behavior and resulting surface structure that is different from induced adsorption due to purely electrostatic interactions between the carboxylate groups and cations.

The results have implications for understanding a multitude of important macromolecular interfacial processes. For one, humic substances are a class of complex macromolecules with a variety of structures. These findings imply that certain humic structures that are prone to counter ion binding and charge screening may be more likely to accumulate toxins at environmental interfaces. These results are also relevant to biological processes. Specifically, metal ion binding is linked to the misfolding of amyloid proteins at cell interfaces, which can result in neurodegenerative diseases like Alzheimer's. That the conformation of polyelectrolyte chains in bulk solution may not be the most favorable interfacial conformation, and that the resulting adsorbed polymer structure depends on the degree of metal ion binding, has implications for understanding the misfolding of proteins involved in neurodegenerative diseases. While this chapter showed the effects of polyelectrolyte interfacial behavior on the interactions between positively charged inorganic ions and the negatively charged groups of the polymer, the next chapter shows the effects that originate when these electrostatic interactions occur between oppositely charged groups that comprise the same polymer.

CHAPTER VI

ORDERED MACROMOLECULAR ASSEMBLY: UNDERSTANDING PEPTOID BEHAVIOR AT THE OIL-WATER INTERFACE

The vibrational sum frequency spectroscopic and interfacial tension measurements presented in this chapter were obtained as part of a collaborative project with Ronald Zuckermann's group from the Molecular Foundry at Lawrence Berkeley National Laboratory (LBNL). The Zuckermann group synthesizes peptoid polymers that assemble into two-dimensional nanomaterials via a key interfacial monolayer intermediate. Not only have our studies of different peptoid polymer monolayers at the oil-water interface assisted the LBNL group in characterizing the molecular-level details of the key monolayer intermediate, but have also allowed for the opportunity to probe more complex aspects of polyelectrolyte adsorption and assembly behavior at the hydrophobic liquid-water interface. Specifically, these studies show the influential role of intermolecular electrostatic interactions between adsorbed polyelectrolyte chains, which was not possible to determine from studies of the simpler poly(methacrylic acid) polymers as discussed in Chapters III-V. This work has been submitted to *PNAS,* with Gloria K. Oliver, Menglu Quan, Caroline Proulx, Ronald N. Zuckermann, and Geraldine L. Richmond. I wrote the section of the paper and performed all of the experimental measurements that appear in this chapter, Gloria K. Oliver, Caroline Proulx, and Menglu Quan from LBNL graciously provided the peptoid samples for these studies, and all coauthors provided editorial assistance.

Introduction

The self-assembly of ordered monolayers to the interface between two immiscible fluids is important to the fabrication of novel materials. For instance, it has been well established that the oil-water interface serves as a platform for the synthesis of nanoparticles.[132, 204-206] More recently, both the air-water and oil-water interfaces have been shown to catalyze the assembly of two-dimensional organic nanomaterials known as peptoid nanosheets.[207, 208] These biomimetic materials are only two molecules thick yet span microns in the lateral direction, and have potential applications in catalysts, molecular sensors, and artificial enzymes.[208-210] The mechanism for nanosheet synthesis first involves the assembly of a peptoid polymer monolayer at the interface, with a subsequent compression leading to monolayer collapse and formation of stable bilayer structures. The oil-water interface is a particularly interesting avenue for nanosheet formation, as it has the potential to offer synthetic advantages and increase nanosheet stability and functionality.[207] The amphiphilic peptoid polymers that are used to make nanosheets have a nonpolar side composed of ethyl phenyl groups, and a hydrophilic side composed of carboxylic acid and amine groups. In the resulting bilayer structures, the nonpolar moieties are on the interior of the sheets, and the polar moieties are on the exterior of the sheets. A representation of a cross section of a nanosheet is depicted in Figure 6.1.

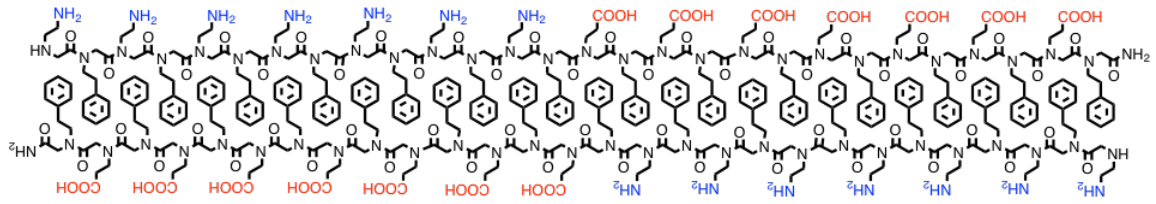

Figure 6.1. Depiction of a peptoid bilayer nanosheet cross section.

In order to increase the complexity and functionality of these novel nanomaterials, it is essential to understand the molecular-level details of the key monolayer intermediate. In particular, it is important to understand how different characteristics of the peptoid monolayer (such as degree of backbone and side chain ordering, intermolecular interactions, and packing density) either hinder or enhance the ability of these polymers to form nanosheets. For instance, it has been shown by the Zuckermann group that certain peptoids form nanosheets, while others do not.[207] Chemical structures of such peptoids are shown in Figure 6.2, in which peptoid **1** has both amine and carboxylic acid groups and forms nanosheets when both groups are fully charged, while peptoid **2** has only carboxylic acid groups and does not form nanosheets when fully charged. Understanding the behavior of the adsorbed peptoids on the molecular-level is essential in determining how monolayer characteristics relate to the ability of peptoids to form nanosheets.

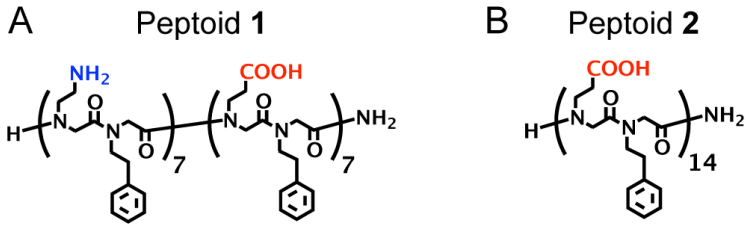

Figure 6.2. Chemical structures of (A) peptoid **1** containing both amine and carboxylic acid groups; and (B) peptoid **2** having only carboxylic acid groups. Peptoid **1** formed nanosheets whereas **2** did not.

This chapter explores the molecular-level behavior of the two different peptoids at the carbon tetrachloride-water (CCl_4-H_2O) interface using vibrational sum frequency (VSF) spectroscopy and interfacial tension measurements. In addition, examination of these different peptoids at pH 8, in which peptoid **1** has both positive and negative charges and peptoid **2** has only negative charges, allows for further determination of the role of

electrostatic interactions in poly(carboxylic acid) behavior at the oil-water interface. While the previous chapter explored such roles through studies of PMA with inorganic counter ions, the studies in this chapter probe assembly behavior of polyelectrolytes with the potential for electrostatic interactions between co-adsorbed organic species. Results show the importance of such electrostatic interactions, both in the ordered assembly of polyelectrolyte monolayers as well as the ability for peptoid polymers to form nanosheets. Additionally, concentration studies of peptoid **1** show that the degree of these interactions are enhanced with increasing monolayer packing density.

Ordering of Peptoid Monolayers at the Oil-Water Interface

In order to determine when a full peptoid monolayer is achieved at the CCl_4-H_2O interface, surface pressure data were obtained for **1** as a function of bulk aqueous peptoid concentration, as shown in Figure 6.3.

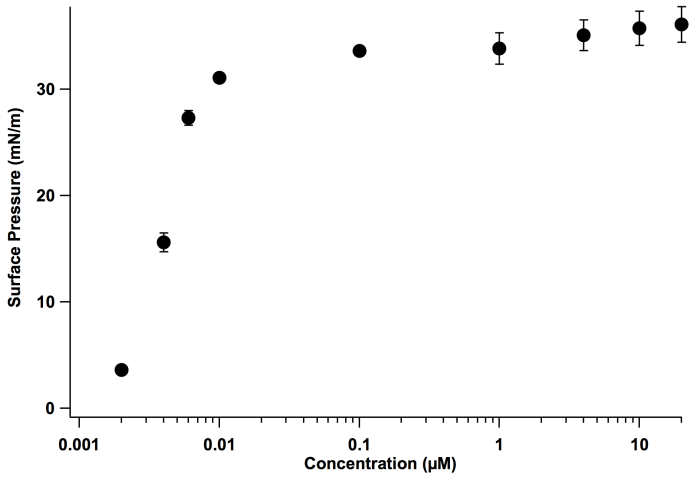

Figure 6.3. Interfacial pressure of peptoid **1** at the CCl_4-H_2O interface as a function of peptoid concentration (in 10 mM Tris buffer, pH 8.0).

Clearly, adsorption to the CCl_4-H_2O interface begins at an extremely low bulk peptoid concentration of 0.02 μM (~4 mN/m). The amount of adsorbed peptoid continues to increase with concentration until ~1 μM (36 mN/m), at which point an increase in concentration does not result in a significant change in surface pressure. VSF spectra of **1** at 20 μM were obtained at the CCl_4-H_2O interface after allowing the peptoid monolayer to equilibrate for at least 1 h and are shown in Figure 6.4. At this concentration, a full peptoid monolayer of **1** is achieved according to the interfacial tension measurements.

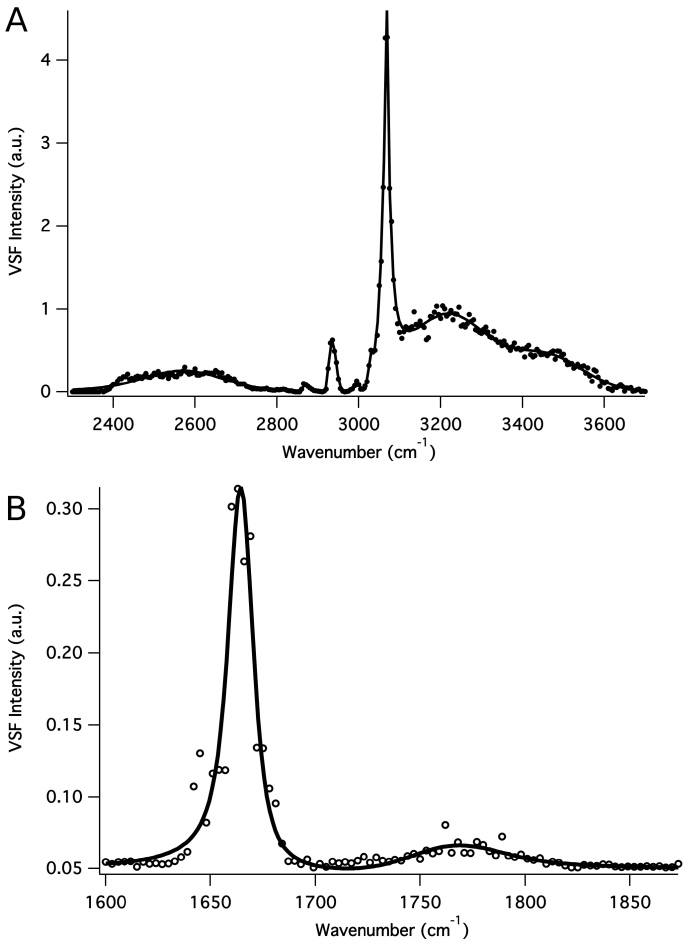

Figure 6.4. VSF spectra (*ssp* polarization) of peptoid **1** in the CH/OH stretching region (A) and the amide/carbonyl stretching region (B). All spectra were collected using a 20 μM peptoid concentration in pH 8.0, 10 mM Tris buffer. The solid lines are representative fits to the data.

In the CH/OH stretching region for **1** (Fig. 6.4A), the peak near 2590 cm^{-1} is assigned to the carboxylic acid OH stretching mode.[125] Although most of the polar residues of **1** are expected to be charged at pH 8.0, some of the carboxyl groups are still protonated, as seen by the small intensity carbonyl stretching mode peak near 1760 cm^{-1} (Fig. 6.4B). The peaks that appear from 2800-3000 cm^{-1} are assigned to alkyl CH_2 stretching modes that originate from the methylene groups in the peptoid backbone and side-chains,[123] whereas the peaks at 3000-3100 cm^{-1} are assigned to the aromatic CH stretching modes of the phenyl functional groups.[123] The broad peaks that appear from 3100-3600 cm^{-1} are assigned to the coordinated water OH stretching modes.[34, 90, 150] The NH_3^+ stretching mode is also known to appear in the 3100-3600 cm^{-1} region,[123] but is difficult to distinguish from the relatively strong water signal.

The VSF spectrum of the 20 μM peptoid **1** monolayer reveals that **1** adsorbs at the CCl_4-H_2O interface into an equilibrated film that completely covers the water surface. This is demonstrated by the lack of a free-OH oscillator peak near 3670 cm^{-1}, indicating that water molecules in the top-most interfacial layer are not present.[90] There is also strong evidence from the VSF spectrum that the interfacial peptoid layer is highly ordered. This can be observed from the strong intensity of the aromatic CH stretching mode peak that appears near 3066 cm^{-1}, indicating that the phenyl groups have a strong net orientation normal to the plane of the interface. The methylene groups also show a degree of ordering, but not due to a fully extended backbone conformation as depicted in Figure. 6.2. Since a net orientation of functional groups is required for generating VSF signal, the orientation depicted in Fig. 6.2, in which all of the methylene groups pointing

into the oil phase have the exact opposite orientation as those pointing into the water phase, would cause cancelation of any signal in the region from 2800-3000 cm^{-1}.

The lack of a fully extended peptoid backbone conformation is confirmed by the spectrum taken in the amide I/carbonyl region of **1** (Fig. 6.4B). Here, the sharp peak that appears near 1665 cm^{-1} is assigned to the amide I stretching mode[123] and indicates that the amide groups along the peptoid backbone have a net orientation normal to the plane of the interface. The peptoid backbone therefore must not be in a fully extended conformation at the interface, but contain some intra-chain disorder such that peaks due to the methylene and amide groups appear in the spectra. This conformational freedom of the interfacial peptoids is not surprising, since peptoid backbones are known to be quite flexible.[211] Additionally, the CCl_4-H_2O interface provides a fluid environment in which side-chains can interact with both the oil and the water phases.[29]

Interfacial peptoid ordering can also be observed in the carboxylate stretching region of **1**, shown in Figure 6.5. The strong intensity of the peak near 1405 cm^{-1} indicates that the carboxylate groups are also highly oriented normal to the plane of the interface. An additional peak appears in the spectrum near 1360 cm^{-1}, which is assigned to carboxylate groups in a stronger water hydrogen bonding environment than those that correspond to the 1405 cm^{-1} peak.[29] Lastly, a third peak appears in the spectrum of **1** near 1440 cm^{-1}. Similar carboxylate peak frequencies have been observed in VSF spectroscopic studies of carboxylate-metal ion complexes, which were attributed to the disruption of carboxylate solvation shells due to the closeness of the cations.[39, 192, 194] FTIR studies of simple carboxylic acids have additionally shown that the frequency of the peak attributed to the COO^- antisymmetric stretch of a carboxylate-amine complex is blue

shifted by ~40 cm^{-1} relative to that of a fully water solvated carboxylate group.[212] The peak that appears near 1440 cm^{-1} is therefore assigned to a direct ionic interaction between the negatively charged carboxylate groups and the positively charged amine groups. This direct interaction acts to disrupt the water solvation shell of the carboxylate groups, causing the peak frequency to shift to higher wavenumbers due to a lack of hydrogen bonding from water molecules.

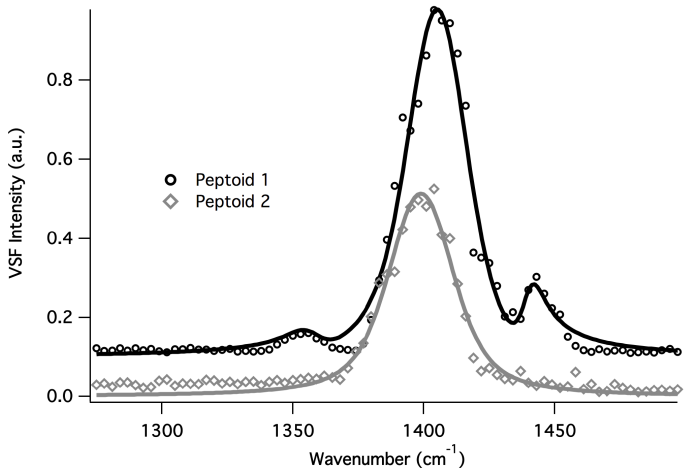

Figure 6.5. VSF spectra (*ssp* polarization) of the carboxylate stretching region of peptoid **1** (black circles) and peptoid **2** (gray diamonds). All spectra were collected using a 20 μM peptoid concentration in pH 8.0, 10 mM Tris buffer. The solid lines are representative fits to the data. The data are offset for clarity.

In order to confirm the assignment of the peak near 1440 cm^{-1}, the VSF spectrum of **1** (Fig. 6.5, black trace) was compared with that of **2** (Fig. 6.5, gray trace) which lacks the ability to form attractive electrostatic interactions. It is clear from the spectrum of **2** that only a single peak appears near 1400 cm^{-1}. This peak is slightly red-shifted relative to the peak of **1** at 1405 cm^{-1}, indicating a greater degree of water hydrogen bonding of the carboxylate groups of **2** compared to **1**. Additionally, the presence of the peak near 1440

cm^{-1} for **1** and the lack of this peak for **2** confirms that a direct ionic interaction exists between some of the negatively charged carboxylate groups and some of the positively charged amine groups in the **1** monolayer.

The lack of cationic groups in peptoid **2** strongly affects the spectrum in the CH/OH and amine/carbonyl stretching regions, as shown in Figure 6.6. Compared to the spectrum for **1** (Fig. 6.4A), the amplitudes of the peaks assigned to the coordinated water OH stretching modes from 3100-3600 cm^{-1} are much larger for **2** (Fig. 6.6A) than for **1**. This is attributed to a difference in the charge of the peptoid monolayers at the oil-water interface. As with **1**, there is minimal protonation of the carboxylic acid groups of **2** at pH 8.0, as evidenced by the small carbonyl peak near 1730 cm^{-1} (Fig. 6.6B). Since **2** contains mostly negatively charged carboxylate groups, the lack of positively charged amines to counterbalance the net charge of the carboxylates creates an electric field at the interface of **2** that acts to orient the dipoles of water molecules near the interface. The electrostatic interactions between the carboxylate and amine groups of **1** reduce the interfacial field, resulting in fewer oriented water molecules near the interface of **1** compared to **2**. The alkyl CH_2 stretches are also quite different between the two peptoids. The widths of the peaks due to the CH_2 stretching modes for **2** (Fig. 6.6A) are overall broader compared to those for **1 (**Fig. 6.4A). This indicates that the backbone and/or side-chain conformations are different between the two different peptoid monolayers, with **2** exhibiting a wider range of methylene groups in different chemical environments than **1**.

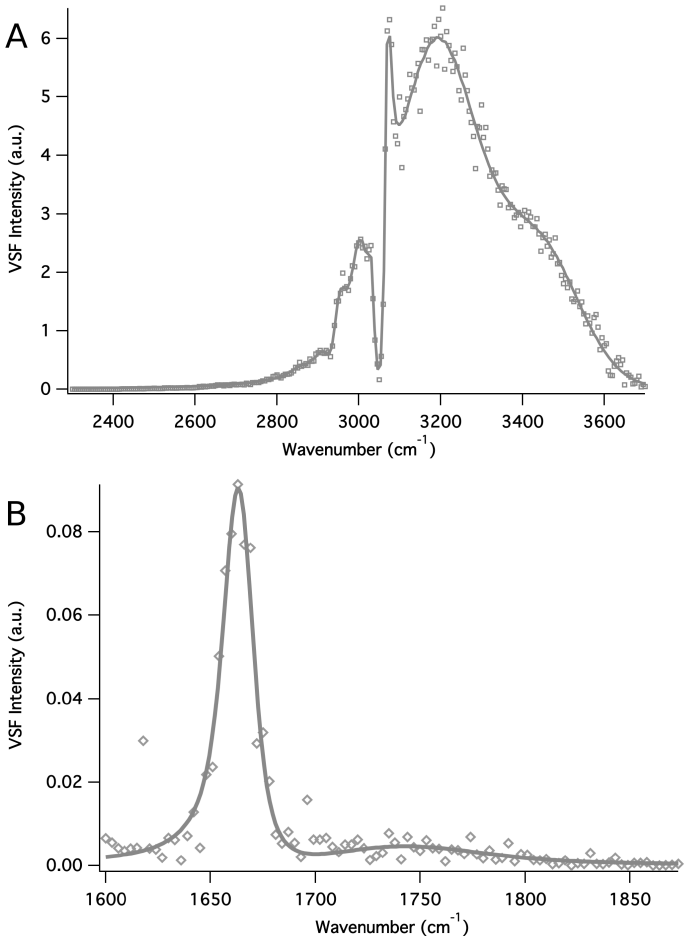

Figure 6.6. VSF spectra (*ssp* polarization) of peptoid **2** in the CH/OH stretching region (A) and the amide/carbonyl stretching region (B). All spectra were collected using a 20 μM peptoid concentration in pH 8.0, 10 mM Tris buffer. The solid lines are representative fits to the data.

These differences in the surface structure of **1** and **2** are also supported by surface pressure measurements collected with 20 μM peptoid at the CCl_4-H_2O interface. The **1** monolayer exhibited a higher surface pressure (36 mN/m) than that of **2** (24 mN/m), indicating a greater degree of adsorption and packing at the interface is achieved by **1** compared to **2**. The lower packing density of **2** is attributed to charge-charge repulsions that exists between neighboring charged carboxylate groups at the interface. These repulsive interactions may also increase the heterogeneity around the methylene groups

of **2** such that broader peaks attributed to the CH_2 stretching modes are seen in the spectrum of **2** compared to those seen in the spectrum of **1**.

As the degree of peptoid packing appears to play a large role in the conformation of the peptoid within the interfacial monolayer, spectra of **1** were obtained in the CH/OH stretching region as a function of bulk peptoid concentration and are shown in Figure 6.7.

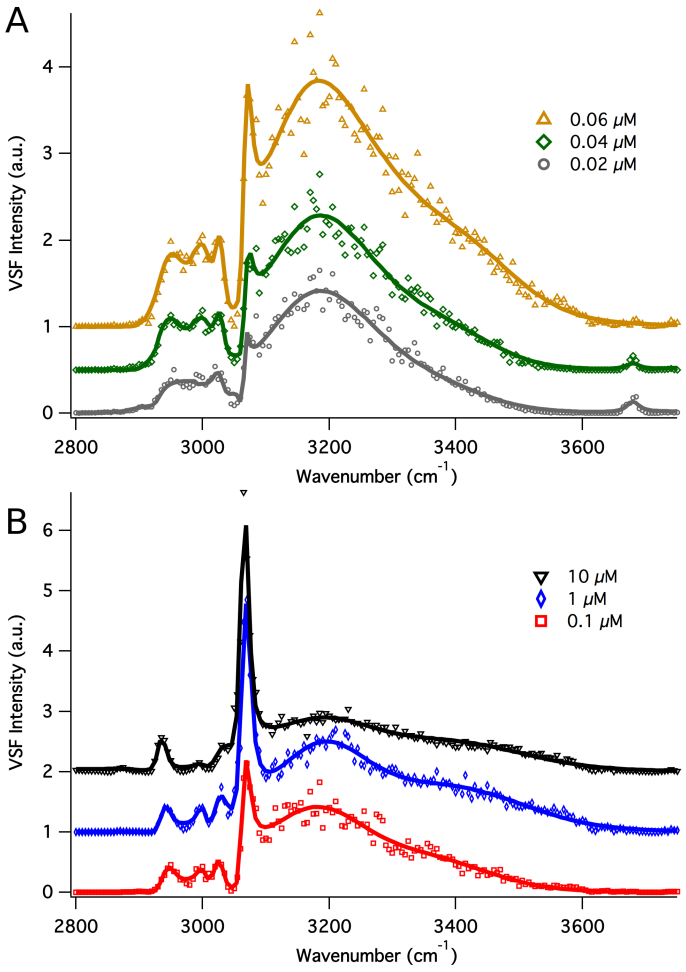

Figure 6.7. VSF spectra (*ssp* polarization) of peptoid **1** as a function of peptoid concentration in the CH/OH stretching region (in 10 mM Tris buffer, pH 8.0). (A) 0.02 μM (gray), 0.04 μM (green), and 0.06 μM (yellow). (B) 0.1 μM (red), 1 μM (blue), and 10 μM (black). The solid lines are representative fits to the data. The data are offset for clarity.

From a bulk peptoid concentration of 0.02-0.06 μM, increases in amplitude from the peptoid alkyl and aromatic CH peaks are seen (Fig. 6.7A). The increase in surface pressure over this concentration range from ~4 mN/m to ~27 mN/m indicates an increase in the number of interfacial peptoid molecules. By a concentration of 0.06 μM, the free-OH peak near 3670 cm^{-1} has disappeared, indicating full coverage of the oil-water interface by the peptoid.

As the concentration increases from 0.02-0.06 μM, there is also a drastic increase in amplitude of the peak near 1400 cm^{-1} due to a large increase in the number of oriented carboxylate groups at the interface, as shown in Figure 6.8. The carboxylate-amine charge complex peak near 1440 cm^{-1} does not appear until a peptoid concentration of 0.1 μM, with a corresponding surface pressure of ~31 mN/m.

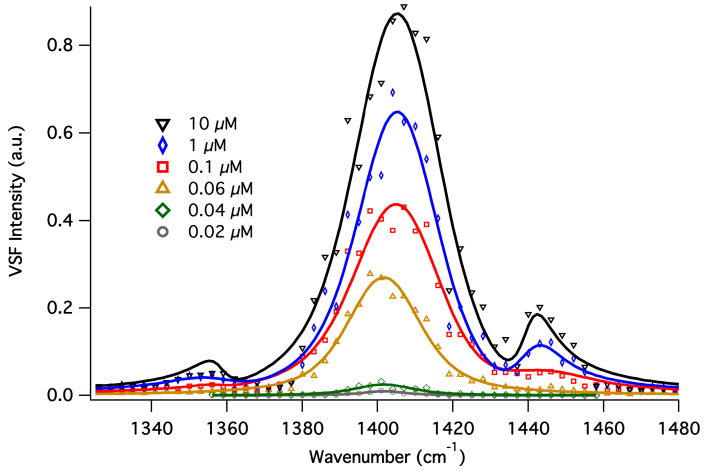

Figure 6.8. VSF spectra (*ssp* polarization) of peptoid **1** as a function of peptoid concentration in the carboxylate stretching region (in 10 mM Tris buffer, pH 8.0). The solid lines are representative fits to the data.

The amplitude of this peak and the water solvated carboxylate peak near 1405 cm^{-1} continue to grow with increasing concentration through 10 μM, with a

corresponding surface pressure of ~36 mN/m. These data overlay almost perfectly with those at 20 μM. The shift in frequency of the solvated carboxylate peak from ~1400 cm^{-1} to ~1405 cm^{-1} suggests a decrease in the degree of hydrogen bonding from water as the monolayer packing density increases. Over this concentration range in the CH/OH stretching region (Fig. 6.7B), there is also a continual increase in amplitude of the aromatic CH stretch peak near 3066 cm^{-1}. Additionally, there is a narrowing of the alkyl CH_2 stretch peak near 2940 cm^{-1}, indicating a decrease in the number of methylene chemical environments as more peptoids pack at the interface. These combined spectral changes are consistent with an increase in monolayer packing and subsequent ordering of the peptoid backbone, side-chains, and functional groups.

It is interesting to note that the data at 0.06 μM for **1** is similar to the data for **2** at 20 μM. For both peptoid monolayers, the spectra show strong signal from the water, broad methylene peaks, and only one peak in the carboxylate stretching region. The lack of a charge complex in the spectra of **2** is attributed to its lack of amine groups. No complex is observed with **1** at 0.06 μM because a full monolayer has not been attained at the oil-water interface. The peptoid chains within this partially filled monolayer presumably lack the alignment and close-packing required for the amine groups to interact with the carboxylate groups.

Summary and Conclusions

Figure 6.9 summarizes the key results obtained from these studies. First, panel A shows that electrostatic interactions between the positively charged amine and negatively

charge carboxylate groups assists in the ordered assembly of a highly packed monolayer of peptoid **1** that is capable of collapsing into nanosheets upon compression. These favorable interactions are seen through the peak near 1440 cm^{-1} that is attributed to direct electrostatic interactions between the carboxylate and amine groups, which cause a high degree of ordering of the ethyl phenyl and carboxylate groups.

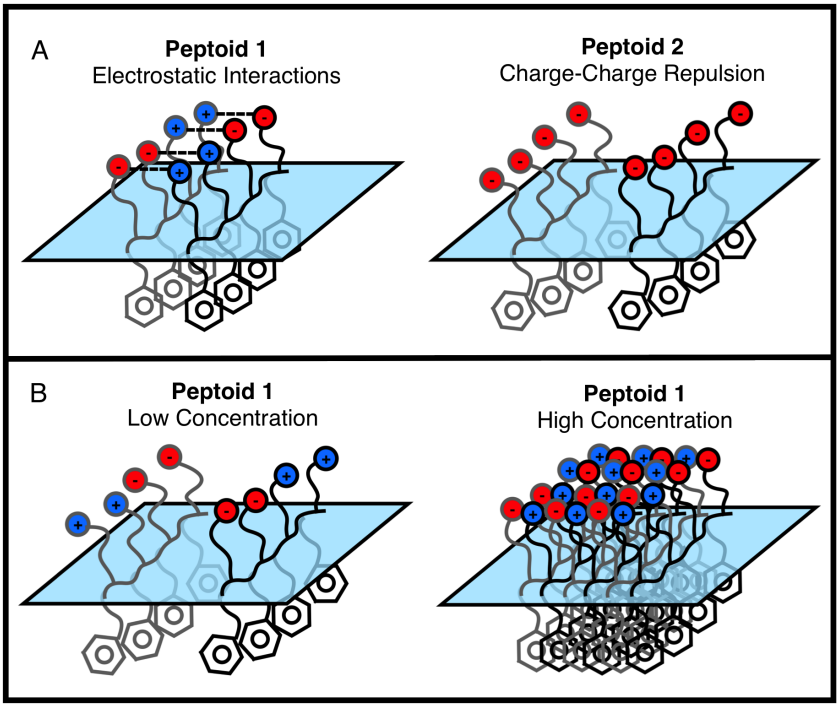

Figure 6.9. Cartoon summarizing findings from the peptoid studies. (A) Depiction of electrostatic interactions seen in monolayers of peptoid **1**, and electrostatic repulsions seen in monolayers of peptoid **2**. (B) Depiction of increasing packing density of peptoid **1** with increasing concentration.

For peptoid **2**, although the ethyl phenyl and carboxylate groups are somewhat ordered, packing at the interface is hindered due to charge-charge repulsions between the negatively charged carboxylate groups. The intense peaks near 3200 cm^{-1} and 3400 cm^{-1} that are due to the coordinated surface water OH modes demonstrates the high degree of

charging of the interfacial layer. This results in an interfacial monolayer that is overall less ordered than that of peptoid **1**. These factors likely contribute to the inability of peptoid **2** to form nanosheets.

Panel B of Figure 6.9 depicts the increase in favorable electrostatic interactions and subsequent ordering observed in the monolayer of peptoid **1** as the surface concentration increases. Overall, the structures of both pepoid **1** and **2** are not as rigid as depicted in Figure 6.2. A degree of flexibility exists for the interfacial peptoids such that the VSF signal from the amide modes does not cancel.

The results presented in this chapter have implications both for understanding nanosheet formation via the assembly of a peptoid monolayer at the interface, and also for understanding general polyelectrolyte oil-water interfacial behavior. Understanding the role that each molecular moiety plays in peptoid assembly into the key monolayer intermediate is essential to effectively designing peptoids that will increase the complexity and functionality of these novel nanomaterials. In general, polyelectrolytes are often used with oppositely charged organic species, such as surfactants or other polyelectrolytes, to invoke synergistic adsorption effects. Often, these adsorption processes are complicated and not well understood.[213] Understanding the molecular-level details of co-adsorbed species has the potential to elucidate the nature of synergistic adsorption effects. The results given here have demonstrated that studying oppositely-charged polyelectrolyte systems with VSF spectroscopy and interfacial tension have the capability to de-convolute complicated factors often involved in the oil-water interfacial behavior of such binary systems.

CHAPTER VII

CONCLUSIONS

The assembly of polyelectrolytes to the interface between nonpolar and aqueous liquids is an important process to several applications ranging from biological, to environmental, to industrial. It is therefore important to identify and understand which polyelectrolyte characteristics as well as aqueous solution conditions enable charged macromolecules to adsorb to liquid-liquid interfaces. Additionally, it is critical to acquire specific details of the adsorption process itself, as well as the resulting interfacial structure. Specific questions can be asked in terms of polyelectrolyte behavior at the oil-water interface: What characteristics of the polyelectrolyte and aqueous solution promote the ordered assembly of polyelectrolytes at the interface? What factors determine the degree to which polyelectrolytes accumulate at the interface? How can the interactions of polyelectrolytes with counterions induce adsorption and affect polyelectrolyte adsorption dynamics and resulting interfacial structure? What is the effect of electrostatic interactions between adsorbed polyelectrolyte chains?

The studies presented in this dissertation have provided insight into these questions by probing the molecular-level details associated with the behavior of simple carboxylic acid-containing polyelectrolytes at a model oil-water interface with vibrational sum frequency (VSF) spectroscopic and interfacial tension measurements. Studies presented in Chapter III indicated that polyelectrolyte backbone structure is an essential parameter for determining the degree to which poly(methacrylic acid) (PMA) accumulates at the oil-water interface. The backbone structure of isotactic PMA

(iPMA) and syndiotactic PMA (sPMA) are very different from each other, which in turn affects the bulk and interfacial behavior of each isomer. For sPMA, the results indicated that the structure of polymer that initially adsorbs to the interface is such that hydrophobic moieties of the adsorbed polymer chain are exposed to the aqueous phase. The coiled sPMA that remains in bulk solution is therefore able to accumulate at the interface to due to favorable hydrophobic interactions between the initially adsorbed polymer layer and what adsorbs over time. For iPMA, on the other hand, the structure of the polymer that initially adsorbs to the interface is one in which the hydrophobic moieties are not exposed to the aqueous phase. Specifically, such orientation prevents further accumulation of iPMA to the interface over time.

The results presented in Chapter IV indicated that charging behavior plays a key role in the oil-water interfacial activity of polyelectrolytes. Specifically, sPMA only adsorbs to the interface when it is not highly charged. Collective interactions cause charges to accumulate near each other, which induces the solvation of polymer chains at relatively low charge densities. It was found that these collective interactions are quite evident for long sPMA chains, which can accumulate several charges per chain. Here, the charged segments remain water soluble, while the un-charged segments assemble at the interface.

In Chapter V, the role of metal ions in the induced adsorption of PMA was explored. Here, it was shown that both monovalent and divalent cations are able to induce the adsorption of iPMA to the interface under solution conditions when it is not normally surface active. For Ca^{2+}, results are consistent in surface adsorption driven by site-specific interactions of the cations with the polymer carboxylate groups.

Importantly, these interactions also greatly affect adsorption dynamics and the resulting polymer interfacial structure. K^+, on the other hand, appears to induce the adsorption of iPMA through electrostatic screening of the charged polymer chain. Neither cation, however, is able to induce the adsorption of sPMA to the oil-water interface due to the backbone structure of this isomer of PMA sterically hindering the interaction of the cations with the carboxylate groups.

Lastly, Chapter VI showed the influence of electrostatic interactions between adsorbed polymer chains on the assembly of peptoids at the oil-water interface and on their ability to form nanosheets. Here, peptoids with both positively charged amine groups and negatively charged carboxylate groups were found to be able to adsorb to the oil-water interface in a highly ordered manner due to direct interactions between the oppositely charged groups. These favorable intermolecular interactions result in the formation of nanosheets via the oil-water interface. For peptoids that had only negatively charged carboxylate groups, results indicate that charge-charge repulsions between adsorbed chains hinder the highly ordered assembly at the oil-water interface, which in turn prevents these peptoids from forming nanosheets.

The results presented in this dissertation have thus provided an in depth molecular-level picture for describing polyelectrolyte behavior at the oil-water interface. In particular, these results have implications for a variety of fields in which polyelectrolyte assembly between two immiscible liquids is important, such as for describing the behavior of proteins at the surface of a cell, understanding the fate and transport of toxins and nutrients in the environment via humic acids, or determining the ability of polyelectrolytes to stabilize emulsions for enhanced oil-recovery. These

studies have paved the way for future studies aimed at exploring more complex polyelectrolytes systems, such as polyelectrolytes with co-adsorbates, at the oil-water interface with VSF spectroscopy that have prevalence in more realistic systems.

APPENDIX A

FITTING PARAMETERS FOR PMA IN THE ABSENCE OF METAL IONS

Table A.1. Parameters used to fit the iPMA and sPMA (pH ≤4) spectra in Chapters III and IV.

Peak Position (cm^{-1})	Phase (Rad.)	$\Gamma_L^{100\text{-}103}$ (cm^{-1})	Assignment
1729 ± 2	3.14	5	Carbonyl stretch (water rich)
1788 ± 3	0	5	Carbonyl stretch (oil rich)
2534 ± 7	3.14	5	Carboxylic acid OH stretch
2888 ± 2	0	2	End cap methyl/methylene stretches
2928 ± 2	0	2	Methyl stretch
2934 ± 2	0	2	Methyl stretch
2980 ± 4	3.14	2	Methylene stretch
3111 ± 37	0	5	Coordinated surface water OH stretches
3496 ± 18	3.14	5	

APPENDIX B

FITTING PARAMETERS FOR iPMA IN THE PRESENCE OF METAL IONS

Table B.1. Parameters used to fit the iPMA+$CaCl_2$ spectra in Chapter V.

Peak Position (cm^{-1})	Phase (Rad.)	$\Gamma_L^{100\text{-}103}$ (cm^{-1})	Assignment
1365 ± 3	3.14	5	Carboxylate stretch (high water solvation)
1400 ± 4	3.14	5	Carboxylate stretch (low water solvation)
1712 ± 2	3.14	5	Carbonyl stretch
2732 ± 4	3.14	5	Carboxylic acid OH stretch
2881 ± 2	3.14	2	Methyl/methylene stretches
2917 ± 2	0	2	
2927 ± 2	3.14	2	
2937 ± 2	3.14	2	
3196 ± 2	0	5	Surface coordinated water OH stretches
3463 ± 3	3.14	5	
3681 ± 3	0	12	Free-OH stretch

Table B.2. Parameters used to fit the iPMA+KCl spectra in Chapter V.

Peak Position (cm^{-1})	Phase (Rad.)	$\Gamma_L^{100\text{-}103}$ (cm^{-1})	Assignment
1346 ± 2	3.14	5	Carboxylate stretch (high water solvation)
1398 ± 2	3.14	5	Carboxylate stretch (low water solvation)
1719 ± 2	3.14	5	Carbonyl stretch
2700 ± 11	3.14	5	Carboxylic acid OH stretch
2868 ± 2	3.14	2	Methyl/methylene stretches
2923 ± 3	3.14	2	
2936 ± 9	0	2	
2956 ± 7	0	2	
3178 ± 2	0	5	Surface coordinated water OH stretches
3484 ± 6	3.14	5	

APPENDIX C

FITTING PARAMETERS FOR PEPTOID STUDIES

Table C.1. Parameters used to fit the peptoid spectra in Chapter VI.

Peak Position (cm^{-1})	Phase (Rad.)	$\Gamma_L^{100\text{-}103}$ (cm^{-1})	Assignment
1357 ± 2	3.14	5	Carboxylate stretch (high water solvation)
1404 ± 2	3.14	5	Carboxylate stretch (low water solvation)
1440 ± 2	3.14	5	Carboxylate stretch (NH^{3+}:COO^- ion pair)
1665 ± 2	3.14	5	Amide I stretch
1761 ± 8	3.14	5	Carbonyl stretch
2592 ± 16	3.14	5	Carboxylic acid OH stretch
2898 ± 12	0	2	Alkyl methylene stretches
2925 ± 6	0	2	
2937 ± 2	3.14	2	
2990 ± 72	0	2	
3007 ± 2	0	2	Aromatic CH stretches
3029 ± 2	0	2	
3065 ± 2	3.14	2	
3141 ± 4	0	5	Surface coordinated water OH stretches
3301 ± 4	3.14	5	
3413 ± 3	3.14	5	Amine stretch?
3680 ± 7	0	12	Free-OH stretch

REFERENCES CITED

1. Voet, D.; Voet, J. G.; Pratt, C. W., *Fundamentals of Biochemistry: Life at the Molecular Level*. Wiley: 2006.

2. Molson, J. W.; Frind, E. O.; Van Stempvoort, D. R.; Lesage, S. Humic Acid Enhanced Remediation of an Emplaced Diesel Source in Groundwater. 2. Numerical Model Development and Application. *J. Contam. Hydrol.* **2002,** *54*, 277-305.

3. Rebhun, M.; Meir, S.; Laor, Y. Using Dissolved Humic Acid to Remove Hydrophobic Contaminants from Water by Complexation-Flocculation Process. *Environ. Sci. Technol.* **1998,** *32*, 981-986.

4. Zhang, J.; Li, G.; Yang, F.; Xu, N.; Fan, H.; Yuan, T.; Chen, L. Hydrophobically Modified Sodium Humate Surfactant: Ultra-Low Interfacial Tension at the Oil/Water Interface. *Appl. Surf. Sci.* **2012,** *259*, 774-779.

5. Quadri, G.; Chen, X.; Jawitz, J. W.; Tambone, F.; Genevini, P.; Faoro, F.; Adani, F. Biobased Surfactant-Like Molecules from Organic Wastes: The Effect of Waste Composition and Composting Process on Surfactant Properties and on the Ability to Solubilize Tetrachloroethene (PCE). *Environ. Sci. Technol.* **2008,** *42*, 2618-2623.

6. Abdul, A. S.; Gibson, T. L.; Rai, D. N. Use of Humic-Acid Solution to Remove Organic Contaminants from Hydrogeologic Systems. *Environ. Sci. Technol.* **1990,** *24*, 328-333.

7. van Stempvoort, D. R.; Lesage, S. Binding of Methylated Naphthalenes to Concentrated Aqueous Humic Acid. *Adv. Environ. Res.* **2002,** *6*, 495-504.

8. van Stempvoort, D. R.; Lesage, S.; Novakowski, K. S.; Millar, K.; Brown, S.; Lawrence, J. R. Humic Acid Enhanced Remediation of an Emplaced Diesel Source in Groundwater. 1. Laboratory-Based Pilot Scale Test. *J. Contam. Hydrol.* **2002,** *54*, 249-276.

9. Kan, A. T.; Tomson, M. B. Ground Water Transport of Hydrophobic Organic Compounds in the Presence of Dissolved Organic Matter. *Environ. Toxicol. Chem.* **1990,** *9*, 253-264.

10. Chiou, C. T.; Malcolm, R. L.; Brinton, T. I.; Kile, D. E. Water Solubility Enhancement of Some Organic Pollutants and Pesticides by Dissolved Humic and Fulvic Acids. *Environ. Sci. Technol.* **1986,** *20*, 502-508.

11. Magee, B. R.; Lion, L. W.; Lemley, A. T. Transport of Dissolved Organic Macromolecules and Their Effect on the Transport of Phenanthrene in Porous Media. *Environ. Sci. Technol.* **1991,** *25*, 323-331.

12. Schlautman, M. A.; Morgan, J. J. Binding of a Fluorescent Hydrophobic Organic Probe by Dissolved Humic Substances and Organically-Coated Aluminum Oxide Surfaces. *Environ. Sci. Technol.* **1993,** *27*, 2523-2532.

13. Becher, P., *Encyclopedia of Emulsion Technology: Applications*. Marcel Dekker Incorporated: 1985.

14. Galindo-Alvarez, J.; Kim-Anh, L.; Sadtler, V.; Marchal, P.; Perrin, P.; Tribet, C.; Marie, E.; Durand, A. Enhanced Stability of Nanoemulsions Using Mixtures of Non-Ionic Surfactant and Amphiphilic Polyelectrolyte. *Colloids Surf., A* **2011,** *389*, 237-245.

15. Michaut, F.; Hebraud, P.; Perrin, P. Amphiphilic Polyelectrolyte for Stabilization of Multiple Emulsions. *Polym. Int.* **2003,** *52*, 594-601.

16. Perrin, P.; Millet, F.; Charleux, B. Emulsions Stabilized by Polyelectrolytes. *Surfactant Science Series* **2001**, 363-446.

17. Perrin, P.; Lafuma, F.; Audebert, R., Emulsions Stabilized with Hydrophobically Modified Poly(Acrylic Acid). In *Trends in Colloid and Interface Science xi*, Rosenholm, J. B.; Lindman, B.; Stenius, P., Eds. Steinkopff: 1997; Vol. 105, pp 228-238.

18. Urzua, M. D.; Mendizabal, F. J.; Cabrera, W. J.; Rios, H. E. Interfacial Properties of Poly(Maleic Acid-Alt-1-Alkene) Disodium Salts at Water/Hydrocarbon Interfaces. *J. Colloid Interface Sci.* **2005,** *281*, 93-100.

19. Yuan, W.; Mok, M. M.; Kim, J.; Wong, C. L. H.; Dettmer, C. M.; Nguyen, S. T.; Torkelson, J. M.; Shull, K. R. Behavior of Gradient Copolymers at Liquid/Liquid Interfaces. *Langmuir* **2010,** *26*, 3261-3267.

20. Amjad, Z., *Water Soluble Polymers - Solution Properties and Applications*. Springer - Verlag: pp 1-22.

21. Beverung, C. J.; Radke, C. J.; Blanch, H. W. Adsorption Dynamics of l-Glutamic Acid Copolymers at a Heptane/Water Interface. *Biophys. Chem.* **1998,** *70*, 121-132.

22. Rotureau, E.; Leonard, M.; Dellacherie, E.; Durand, A. Amphiphilic Derivatives of Dextran: Adsorption at Air/Water and Oil/Water Interfaces. *J. Colloid Interface Sci.* **2004,** *279*, 68-77.

23. Tsetska Radeva, Ed., *Physical Chemistry of Polyelectrolytes*. Marcel Dekker, Inc. : New York, 2001; p 882.

24. Beaman, D. K.; Robertson, E. J.; Richmond, G. L. Unique Assembly of Charged Polymers at the Oil-Water Interface. *Langmuir* **2011,** *27*, 2104-2106.

25. Beaman, D. K.; Robertson, E. J.; Richmond, G. L. Ordered Polyelectrolyte Assembly at the Oil-Water Interface. *Proc. Natl. Acad. Sci. U. S. A.* **2012,** *109*, 3226-3231.

26. Beaman, D. K.; Robertson, E. J.; Richmond, G. L. Metal Ions: Driving the Orderly Assembly of Polyelectrolytes at a Hydrophobic Surface. *Langmuir* **2012,** *28*, 14245-14253.

27. Walker, D. S.; Moore, F. G.; Richmond, G. L. Vibrational Sum-Frequency Spectroscopiy and Molecular Dynamics Simulations of the Carbon Tetrachloride-Water and 1,2-Dichloroethane-Water Interfaces. *J. Phys. Chem. C,* **2007**, *111*, 6103-6112.

28. Richmond, G. L. Vibrational Spectroscopy of Molecules at Liquid/Liquid Interfaces. *Anal. Chem.* **1997,** *69*, A536-A543.

29. Beaman, D. K.; Robertson, E. J.; Richmond, G. L. From Head to Tail: Structure, Solvation, and Hydrogen Bonding of Carboxylate Surfactants at the Organic-Water Interface. *J. Phys. Chem. C* **2011,** *115*, 12508-12516.

30. Conboy, J. C.; Messmer, M. C.; Richmond, G. L. Investigation of Surfactant Conformation and Order at the Liquid-Liquid Interface by Total Internal Reflection Sum-Frequency Vibrational Spectroscopy. *J. Phys. Chem.* **1996,** *100*, 7617-7622.

31. Gragson, D. E.; Richmond, G. L. Probing the Intermolecular Hydrogen Bonding of Water Molecules at the CCl_4/Water Interface in the Presence of Charged Soluble Surfactant. *J. Chem. Phys.* **1997,** *107*, 9687-9690.

32. Gragson, D. E.; Richmond, G. L. Probing the Structure of Water Molecules at an Oil/Water Interface in the Presence of a Charged Soluble Surfactant through Isotopic Dilution Studies. *J. Phys. Chem. B* **1998,** *102*, 569-576.

33. Watry, M. R.; Richmond, G. L. Vibrational Sum Frequency Spectroscopic Investigations of Molecular Interactions at Liquid/Liquid Interfaces. In *Interfacial Nanochemistry,* Watarai, H., Ed. Kluwer Academic/Plenum Publishers: 2005, pp 25-56.

34. McFearin, C. L.; Beaman, D. K.; Moore, F. G.; Richmond, G. L. From Franklin to Today: Toward a Molecular Level Understanding of Bonding and Adsorption at the Oil-Water Interface. *J. Phys. Chem. C* **2009,** *113*, 1171-1188.

35. McFearin, C. L.; Richmond, G. L. Understanding How Organic, Solvent Polarity Affects Water Structure and Bonding at Halocarbon-Water Interfaces. *J. Mol. Liq.* **2007,** *136*, 221-226.

36. McFearin, C. L.; Richmond, G. L. The Role of Interfacial Molecular Structure in the Adsorption of Ions at the Liquid-Liquid Interface. *J. Phys. Chem. C* **2009,** *113*, 21162-21168.

37. McFearin, C. L.; Richmond, G. L. The Unique Molecular Behavior of Water at the Chloroform-Water Interface. *Appl. Spectrosc.* **2010,** *64*, 986-994.

38. Moore, F. G.; Richmond, G. L. Integration or Segregation: How Do Molecules Behave at Oil/Water Interfaces? *Acc. Chem. Res.* **2008,** *41*, 739-748.

39. Robertson, E. J.; Beaman, D. K.; Richmond, G. L. Designated Drivers: The Differing Roles of Divalent Metal Ions in Surfactant Adsorption at the Oil-Water Interface. *Langmuir* **2013,** *29*, 15511-15520.

40. Robertson, E. J.; Richmond, G. L. Chunks of Charge: Effects at Play in the Assembly of Macromolecules at Fluid Surfaces. *Langmuir* **2013,** *29*, 10980-10989.

41. Scatena, L. F.; Richmond, G. L. Orientation, Hydrogen Bonding, and Penetration of Water at the Organic/Water Interface. *J. Phys. Chem. B* **2001,** *105*, 11240-11250.

42. Scatena, L. F.; Richmond, G. L. Isolated Molecular Ion Solvation at an Oil/Water Interface Investigated by Vibrational Sum-Frequency Spectroscopy. *J. Phys. Chem. B* **2004,** *108*, 12518-12528.

43. Scatena, L. F.; Richmond, G. L. Aqueous Solvation of Charge at Hydrophobic Liquid Surfaces. *Chem. Phys. Lett.* **2004,** *383*, 491-495.

44. Smiley, B. L.; Richmond, G. L. Assembly of Long Chain Phosphatidylcholines at a Liquid-Liquid Interface. *Biopolymers* **2000,** *57*, 117-125.

45. Walker, R. A.; Conboy, J. C.; Richmond, G. L. Molecular Structure and Ordering of Phospholipids at a Liquid-Liquid Interface. *Langmuir* **1997,** *13*, 3070-3073.

46. Walker, R. A.; Gruetzmacher, J. A.; Richmond, G. L. Phosphatidylcholine Monolayer Structure at a Liquid-Liquid Interface. *J. Am. Chem. Soc.* **1998,** *120*, 6991-7003.

47. Watry, M. R.; Richmond, G. L. Comparison of the Adsorption of Linear Alkanesulfonate and Linear Alkylbenzenesulfonate Surfactants at Liquid Interfaces. *J. Am. Chem. Soc.* **2000,** *122*, 875-883.

48. Watry, M. R.; Richmond, G. L. Orientation and Conformation of Amino Acids in Monolayers Adsorbed at an Oil/Water Interface as Determined by Vibrational Sum-Frequency Spectroscopy. *J. Phys. Chem. B* **2002,** *106*, 12517-12523.

49. Kim, G.; Gurau, M.; Kim, J.; Cremer, P. S. Investigations of Lysozyme Adsorption at the Air/Water and Quartz/Water Interfaces by Vibrational Sum Frequency Spectroscopy. *Langmuir* **2002,** *18*, 2807-2811.

50. Wang, J.; Buck, S. M.; Chen, Z. Sum Frequency Generation Vibrational Spectroscopy Studies on Protein Adsorption. *J. Phys. Chem. B* **2002,** *106*, 11666-11672.

51. Wang, J.; Buck, S. M.; Chen, Z. The Effect of Surface Coverage on Conformation Changes of Bovine Serum Albumin Molecules at the Air-Solution Interface Detected by Sum Frequency Generation Vibrational Spectroscopy. *Analyst* **2003,** *128*, 773-778.

52. Fu, L.; Ma, G.; Yan, E. C. Y. In Situ Misfolding of Human Islet Amyloid Polypeptide at Interfaces Probed by Vibrational Sum Frequency Generation. *J. Am. Chem. Soc.* **2010,** *132*, 5405-5412.

53. Wang, Z.; Fu, L.; Yan, E. C. Y. C–H Stretch for Probing Kinetics of Self-Assembly into Macromolecular Chiral Structures at Interfaces by Chiral Sum Frequency Generation Spectroscopy. *Langmuir* **2013,** *29*, 4077-4083.

54. Kim, G.; Gurau, M. C.; Lim, S. M.; Cremer, P. S. Investigations of the Orientation of a Membrane Peptide by Sum Frequency Spectroscopy. *J. Phys. Chem. B* **2003,** *107*, 1403-1409.

55. Chen, X. Y.; Clarke, M. L.; Wang, J.; Chen, Z. Sum Frequency Generation Vibrational Spectroscopy Studies on Molecular Conformation and Orientation of Biological Molecules at Interfaces. *Int. J. Mod. Phys. B* **2005,** *19*, 691-713.

56. Ye, S.; Nguyen, K. T.; Le Clair, S. V.; Chen, Z. In Situ Molecular Level Studies on Membrane Related Peptides and Proteins in Real Time Using Sum Frequency Generation Vibrational Spectroscopy. *J. Struct. Biol.* **2009,** *168*, 61-77.

57. Wang, J.; Clarke, M. L.; Zhang, Y. B.; Chen, X. Y.; Chen, Z. Using Isotope-Labeled Proteins and Sum Frequency Generation Vibrational Spectroscopy to Study Protein Adsorption. *Langmuir* **2003,** *19*, 7862-7866.

58. Even, M. A.; Wang, J.; Chen, Z. Structural Information of Mussel Adhesive Protein Mefp-3 Acquired at Various Polymer/Mefp-3 Solution Interfaces. *Langmuir* **2008,** *24*, 5795-5801.

59. Wang, J.; Even, M. A.; Chen, X. Y.; Schmaier, A. H.; Waite, J. H.; Chen, Z. Detection of Amide I Signals of Interfacial Proteins in Situ Using SFG. *J. Am. Chem. Soc.* **2003,** *125*, 9914-9915.

60. Wang, J.; Buck, S. M.; Even, M. A.; Chen, Z. Molecular Responses of Proteins at Different Interfacial Environments Detected by Sum Frequency Generation Vibrational Spectroscopy. *J. Am. Chem. Soc.* **2002,** *124*, 13302-13305.

61. Wang, J.; Chen, X. Y.; Clarke, M. L.; Chen, Z. Detection of Chiral Sum Frequency Generation Vibrational Spectra of Proteins and Peptides at Interfaces in Situ. *Proc. Natl. Acad. Sci. U. S. A.* **2005,** *102*, 4978-4983.

62. Paszti, Z.; Wang, J.; Clarke, M. L.; Chen, Z. Sum Frequency Generation Vibrational Spectroscopy Studies of Protein Adsorption on Oxide-Covered Ti Surfaces. *J. Phys. Chem. B* **2004,** *108*, 7779-7787.

63. Wang, J.; Chen, X. Y.; Clarke, M. L.; Chen, Z. Vibrational Spectroscopic Studies on Fibrinogen Adsorption at Polystyrene/Protein Solution Interfaces: Hydrophobic Side Chain and Secondary Structure Changes. *J. Phys. Chem. B* **2006,** *110*, 5017-5024.

64. Han, X.; Soblosky, L.; Slutsky, M.; Mello, C. M.; Chen, Z. Solvent Effect and Time-Dependent Behavior of C-Terminus-Cysteine-Modified Cecropin P1 Chemically Immobilized on a Polymer Surface. *Langmuir* **2011,** *27*, 7042-7051.

65. Yang, P.; Ramamoorthy, A.; Chen, Z. Membrane Orientation of MSI-78 Measured by Sum Frequency Generation Vibrational Spectroscopy. *Langmuir* **2011,** *27*, 7760-7767.

66. Chen, X.; Wang, J.; Boughton, A. P.; Kristalyn, C. B.; Chen, Z. Multiple Orientation of Melittin inside a Single Lipid Bilayer Determined by Combined Vibrational Spectroscopic Studies. *J. Am. Chem. Soc.* **2007,** *129*, 1420-1427.

67. Nguyen, K. T.; Soong, R.; Im, S.-C.; Waskell, L.; Ramamoorthy, A.; Chen, Z. Probing the Spontaneous Membrane Insertion of a Tail-Anchored Membrane Protein by Sum Frequency Generation Spectroscopy. *J. Am. Chem. Soc.* **2010,** *132*, 15112-15115.

68. Chen, X.; Boughton, A. P.; Tesmer, J. J. G.; Chen, Z. In Situ Investigation of Heterotrimeric G Protein Beta Gamma Subunit Binding and Orientation on Membrane Bilayers. *J. Am. Chem. Soc.* **2007,** *129*, 12658.

69. Yang, P.; Wu, F.-G.; Chen, Z. Lipid Fluid-Gel Phase Transition Induced Alamethicin Orientational Change Probed by Sum Frequency Generation Vibrational Spectroscopy. *J. Phys. Chem. C* **2013,** *117*, 17039-17049.

70. Fu, L.; Liu, J. Yan,; E. C. Y. Chiral Sum Frequency Generation Spectroscopy for Characterizing Protein Secondary Structures at Interfaces. *J. Am. Chem. Soc.* **2011,** *133*, 8094-8097.

71. Doyle, A. W.; Fick, J.; Himmelhaus, M.; Eck, W.; Graziani, I.; Prudovsky, I.; Grunze, M.; Maciag, T.; Neivandt, D. J. Protein Deformation of Lipid Hybrid Bilayer Membranes Studied by Sum Frequency Generation Vibrational Spectroscopy. *Langmuir* **2004,** *20*, 8961-8965.

72. Hu, D.; Yang, Z.; Chou, K. C. Interactions of Polyelectrolytes with Water and Ions at Air/Water Interfaces Studied by Phase-Sensitive Sum Frequency Generation Vibrational Spectroscopy. *J. Phys. Chem. C* **2013,** *117*, 15698-15703.

73. Liu, G.; Wu, D.; Ma, C.; Zhang, G.; Wang, H.; Yang, S. Insight into the Origin of the Thermosensitivity of Poly 2-(Dimethylamino)Ethyl Methacrylate. *ChemPhysChem* **2007,** *8*, 2254-2259.

74. Kherb, J.; Flores, S. C.; Cremer, P. S. Role of Carboxylate Side Chains in the Cation Hofmeister Series. *J. Phys. Chem. B* **2012,** *116*, 7389-7397.

75. Kim, J.; Cremer, P. S. IR−Visible Sfg Investigations of Interfacial Water Structure Upon Polyelectrolyte Adsorption at the Solid/Liquid Interface. *J. Am. Chem. Soc.* **2000,** *122*, 12371-12372.

76. Kim, J.; Kim, G.; Cremer, P. S. Investigations of Polyelectrolyte Adsorption at the Solid/Liquid Interface by Sum Frequency Spectroscopy: Evidence for Long-Range Macromolecular Alignment at Highly Charged Quartz/Water Interfaces. *J. Am. Chem. Soc.* **2002,** *124*, 8751-8756.

77. Kett, P. J. N.; Casford, M. T. L.; Yang, A. Y.; Lane, T. J.; Johal, M. S.; Davies, P. B. Structural Changes in a Polyelectrolyte Multilayer Assembly Investigated by Reflection Absorption Infrared Spectroscopy and Sum Frequency Generation Spectroscopy. *J. Phys. Chem. B* **2009,** *113*, 1559-1568.

78. Windsor, R.; Neivandt, D. J.; Davies, P. B. Adsorption of Sodium Dodecyl Sulfate in the Presence of Poly(Ethylenimine) and Sodium Chloride Studied Using Sum Frequency Vibrational Spectroscopy. *Langmuir* **2001,** *17*, 7306-7312.

79. Windsor, R.; Neivandt, D. J.; Davies, P. B. Temperature and pH Effects on the Coadsorption of Sodium Dodecyl Sulfate and Poly(Ethylenimine). *Langmuir* **2002,** *18*, 2199-2204.

80. Shi, Q.; Ye, S.; Spanninga, S. A.; Su, Y.; Jiang, Z.; Chen, Z. The Molecular Surface Conformation of Surface-Tethered Polyelectrolytes on PDMS Surfaces. *Soft Matter* **2009,** *5*, 3487-3494.

81. Roger, G. M.; Durand-Vidal, S.; Bernard, O.; Meriguet, G.; Altmann, S.; Turq, P. Characterization of Humic Substances and Polyacrylic Acid: A High Precision Conductimetry Study. *Colloids Surf. A* **2010,** *356*, 51-57.

82. Eisenberg, H. Thermodynamics and the Structure of Biological Macromolecules - Rozhinkes-Mit-Mandeln. *Eur. J. Biochem.* **1990,** *187*, 7-22.

83. Jerman, B.; Breznik, M.; Kogej, K.; Paoletti, S. Osmotic and Volume Properties of Stereoregular Poly(Methacrylic Acids) in Aqueous Solution: Role of Intermolecular Association. *J. Phys. Chem. B* **2007,** *111*, 8435-8443.

84. Jerman, B.; Kogej, K. Fluorimetric and Potentiometric Study of the Conformational Transition of Isotactic and Atactic Poly(Methacrylic Acid) in Mixed Solvents. *Acta Chim. Slov.* **2006,** *53*, 264-273.

85. Jerman, B.; Podlipnik, C.; Kogej, K. Molecular Dynamics Simulation of Poly(Methacrylic Acid) Chains in Water. *Acta Chim. Slov.* **2007,** *54*, 509-516.

86. Vlachy, N.; Dolenc, J.; Jerman, B.; Kogej, K. Influence of Stereoregularity of the Polymer Chain on Interactions with Surfactants: Binding of Cetylpyridinium Chloride by Isotactic and Atactic Poly(Methacrylic Acid). *J. Phys. Chem. B* **2006,** *110*, 9061-9071.

87. Nagasawa, M.; Murase, T.; Kondo, K. Potentiometric Titration of Stereoregular Polyelectrolytes. *J. Phys. Chem.* **1965,** *69*, 4005-&.

88. van den Bosch, E.; Keil, Q.; Filipesei, G.; Berghmans, H.; Reynaers, H. Structure Formation in Isotactic Poly (Methacrylic Acid). *Macromolecules* **2004,** *37*, 9673-9675.

89. Oosawa, F., *Polyelectrolytes*. Marcel Dekker, Inc. : New York, 1971.

90. Richmond, G. L. Molecular Bonding and Interactions at Aqueous Surfaces as Probed by Vibrational Sum Frequency Spectroscopy. *Chem. Rev. (Washington, DC, U. S.)* **2002,** *102*, 2693-2724.

91. Lambert, A. G.; Davies, P. B.; Neivandt, D. J. Implementing the Theory of Sum Frequency Generation Vibrational Spectroscopy: A Tutorial Review. *Appl. Spectrosc. Rev.* **2005,** *40*, 103-145.

92. Miranda, P. B.; Shen, Y. R. Liquid Interfaces: A Study by Sum-Frequency Vibrational Spectroscopy. *J. Phys. Chem. B* **1999,** *103*, 3292-3307.

93. Shen, Y. R. Surface-Properties Probed by 2nd-Harmonic and Sum-Frequency Generation. *Nature* **1989,** *337*, 519-525.

94. Shen, Y. R., *The Principles of Nonlinear Optics*. Wiley-Interscience: 2003.

95. Boyd, R. W., *Nonlinear Optics*. Elsevier Science: 2008.

96. McGilp, J. F. A Review of Optical Second-Harmonic and Sum-Frequency Generation at Surfaces and Interfaces. *J. Phys. D: Appl. Phys.* **1996,** *29*, 1812.

97. Zhu, X. D.; Suhr, H.; Shen, Y. R. Surface Vibrational Spectroscopy by Infrared-Visible Sum Frequency Generation. *Phys. Rev. B* **1987,** *35*, 3047-3050.

98. Moore, F. G.; Becraft, K. A.; Richmond, G. L. Challenges in Interpreting Vibrational Sum Frequency Spectra: Deconvoluting Spectral Features as Demonstrated in the Calcium Fluoride-Water-Sodium Dodecylsulfate System. *Appl. Spectrosc.* **2002,** *56*, 1575-1578.

99. Bain, C. D.; Davies, P. B.; Ong, T. H.; Ward, R. N.; Brown, M. A. Quantitative-Analysis of Monolayer Composition by Sum-Frequency Vibrational Spectroscopy. *Langmuir* **1991,** *7*, 1563-1566.

100. Lim, M.; Hochstrasser, R. M. Unusual Vibrational Dynamics of the Acetic Acid Dimer. *J. Chem. Phys.* **2001,** *115*, 7629-7643.

101. Goates, S. R.; Schofield, D. A.; Bain, C. D. A Study of Nonionic Surfactants at the Air–Water Interface by Sum-Frequency Spectroscopy and Ellipsometry. *Langmuir* **1999,** *15*, 1400-1409.

102. Brown, M. G.; Raymond, E. A.; Allen, H. C.; Scatena, L. F.; Richmond, G. L. The Analysis of Interference Effects in the Sum Frequency Spectra of Water Interfaces. *J. Phys. Chem. A* **2000,** *104*, 10220-10226.

103. Ota, S. T.; Richmond, G. L. Uptake of SO_2 to Aqueous Formaldehyde Surfaces. *J. Am. Chem. Soc.* **2012,** *134*, 9967-9977.

104. Richmond, G. L. Structure and Bonding of Molecules at Aqueous Surfaces. *Annu. Rev. Phys. Chem.* **2001,** *52*, 357-389.

105. Hore, D. K.; Walker, D. S.; Richmond, G. L. Water at Hydrophobic Surfaces: When Weaker Is Better. *J. Am. Chem. Soc.* **2008,** *130*, 1800.

106. Walker, D. S.; Richmond, G. L. Depth Profiling of Water Molecules at the Liquid-Liquid Interface Using a Combined Surface Vibrational Spectroscopy and Molecular Dynamics Approach. *J. Am. Chem. Soc.* **2007,** *129*, 9446-9451.

107. Chang, T. M.; Dang, L. X. Molecular Dynamics Simulations of CCl_4-H_2O Liquid-Liquid Interface with Polarizable Potential Models. *J. Chem. Phys.* **1996,** *104*, 6772-6783.

108. Hore, D. K.; Walker, D. S.; Richmond, G. L. Layered Organic Structure at the Carbon Tetrachloride-Water Interface. *J. Am. Chem. Soc.* **2007,** *129*, 752-753.

109. Ezell, R. G.; McCormick, C. L. Electrolyte- and pH-Responsive Polyampholytes with Potential as Viscosity-Control Agents in Enhanced Petroleum Recovery. *J. Appl. Polym. Sci.* **2007,** *104*, 2812-2821.

110. Huang, J. S.; Varadaraj, R. Colloid and Interface Science in the Oil Industry. *Curr. Opin. Colloid Interface Sci.* **1996,** *1*, 535-539.

111. Kristen, N.; Vuellings, A.; Laschewsky, A.; Miller, R.; von Klitzing, R. Foam Films from Oppositely Charged Polyelectolyte/Surfactant Mixtures: Effect of Polyelectrolyte and Surfactant Hydrophobicity on Film Stability. *Langmuir* **2010,** *26*, 9321-9327.

112. Sabhapondit, A.; Borthakur, A.; Haque, I. Water Soluble Acrylamidomethyl Propane Sulfonate (AMPS) Copolymer as an Enhanced Oil Recovery Chemical. *Energy Fuels* **2003,** *17*, 683-688.

113. Shaughnessy, R. J.; Byeseda, J. J.; Sylvester, N. D. Cationic Polyelectrolyte Flocculation of Oil-Water Emulsions. Effects of Mixing Intensity and Oil Concentration. *Industrial & Engineering Chemistry Product Research and Development* **1983,** *22*, 473-478.

114. Rosen, M. J.; Wang, H. Z.; Shen, P. P.; Zhu, Y. Y. Ultralow Interfacial Tension for Enhanced Oil Recovery at Very Low Surfactant Concentrations. *Langmuir* **2005,** *21*, 3749-3756.

115. West, C. C.; Harwell, J. H. Surfactants and Subsurface Remediation. *Environ. Sci. Technol.* **1992,** *26*, 2324-2330.

116. Harwell, J. H.; Sabatini, D. A.; Knox, R. C. Surfactants for Ground Water Remediation. *Colloids Surf. A* **1999,** *151*, 255-268.

117. Chen, W. T.; Liao, Y. H.; Yu, H.-M.; Cheng, I. H.; Chen, Y. R. Distinct Effects of Zn^{2+}, Cu^{2+}, Fe^{3+}, and Al^{3+} on Amyloid-Beta Stability, Oligomerization, and Aggregation. *J. Biol. Chem.* **2011,** *286*, 9646-9656.

118. Curtain, C. C.; Ali, F. E.; Smith, D. G.; Bush, A. I.; Masters, C. L.; Barnham, K. J. Metal Ions, pH, and Cholesterol Regulate the Interactions of Alzheimer's Disease Amyloid-Beta Peptide with Membrane Lipid. *J. Biol. Chem.* **2003,** *278*, 2977-2982.

119. Dai, B.; Kang, S. G.; Tien, H.; Lei, H.; Castelli, M.; Hu, J.; Zhang, Y.; Zhou, R. Salts Drive Controllable Multilayered Upright Assembly of Amyloid-Like Peptides at Mica/Water Interface. *Proc. Natl. Acad. Sci. U. S. A.* **2013,** *110*, 8543-8548.

120. Hoernke, M.; Koksch, B.; Brezesinski, G. Influence of the Hydrophobic Interface and Transition Metal Ions on the Conformation of Amyloidogenic Model Peptides. *Biophys. Chem.* **2010,** *150*, 64-72.

121. Lau, T. L.; Ambroggio, E. E.; Tew, D. J.; Cappai, R.; Masters, C. L.; Fidelio, G. D.; Barnham, K. J.; Separovic, F. Amyloid-Beta Peptide Disruption of Lipid Membranes and the Effect of Metal Ions. *J. Mol. Biol.* **2006,** *356*, 759-770.

122. Stellato, F.; Menestrina, G.; Dalla Serra, M.; Potrich, C.; Tomazzolli, R.; Meyer-Klaucke, W.; Morante, S. Metal Binding in Amyloid Beta-Peptides Shows Intra- and Inter-Peptide Coordination Modes. *Eur. Biophys. J.* **2006,** *35*, 340-351.

123. Lin-Vien, D., *The Handbook of Infrared and Raman Characteristic Frequencies of Organic Molecules*. Academic Press: 1991.

124. Raczynska, E. D.; Duczmal, K.; Darowska, M. Experimental (FT-IR) and Theoretical (DFT-IR) Studies of Keto-Enol Tautomerism in Pyruvic Acid. *Vib. Spectrosc.* **2005,** *39*, 37-45.

125. Mitsui, K.; Ukaji, T. Infrared Spectra of Some Aqueous Solutions. *Research Reports of Ikutoku Tch. Univ.* **1977,** *B-2*.

126. Babak, V. G.; Desbrieres, J.; Tikhonov, V. E. Dynamic Surface Tension and Dilational Viscoelasticity of Adsorption Layers of a Hydrophobically Modified Chitosan. *Colloids Surf. A* **2005,** *255*, 119-130.

127. Beverung, C. J.; Radke, C. J.; Blanch, H. W. Protein Adsorption at the Oil/Water Interface: Characterization of Adsorption Kinetics by Dynamic Interfacial Tension Measurements. *Biophys. Chem.* **1999,** *81*, 59-80.

128. Chanda, A.; Fokin, V. V. Organic Synthesis "on Water". *Chem. Rev. (Washington, DC, U. S.)* **2009,** *109*, 725-748.

129. Jung, Y.; Marcus, R. A. Protruding Interfacial OH Groups and 'on-Water' Heterogeneous Catalysis. *J. Phys. Condens. Matter* **2010,** *22*.

130. Ovejero, J. M.; Fernandez, R. A.; Dassie, S. A. Ion Transfer across Liquid/Liquid Interface under Forced Hydrodynamic Conditions. I: Digital Simulations. *J. Electroanal. Chem.* **2012,** *666*, 42-51.

131. Kihara, S.; Kasuno, M.; Okugaki, T.; Shirai, O.; Maeda, K. Biomimetic Charge Transfer Reactions at the Aqueous/Organic Solution Interface or through Artificial Membrane. *Electrochemistry* **2012,** *80*, 390-400.

132. Hu, L. F.; Chen, M.; Fang, X. S.; Wu, L. M. Oil-Water Interfacial Self-Assembly: A Novel Strategy for Nanofilm and Nanodevice Fabrication. *Chem. Soc. Rev.* **2012,** *41*, 1350-1362.

133. Niu, Z.; He, J.; Russell, T. P.; Wang, Q. Synthesis of Nano/Microstructures at Fluid Interfaces. *Angew. Chem. Int. Ed.* **2010,** *49*, 10052-10066.

134. Boker, A.; He, J.; Emrick, T.; Russell, T. P. Self-Assembly of Nanoparticles at Interfaces. *Soft Matter* **2007,** *3*, 1231-1248.

135. Fayer, M. D. Dynamics of Water Interacting with Interfaces, Molecules, and Ions. *Acc. Chem. Res.* **2012,** *45*, 3-14.

136. Boucher, J.; Trudel, E.; Methot, M.; Desmeules, P.; Salesse, C. Organization, Structure and Activity of Proteins in Monolayers. *Colloids Surf. B* **2007,** *58*, 73-90.

137. Wang, Y.; Zhang, Y.; Du, W.; Wu, C.; Zhao, J. Intelligent Core-Shell Nanoparticles and Hollow Spheres Based on Gelatin and PAA via Template Polymerization. *J. Colloid Interface Sci.* **2009,** *334*, 153-160.

138. Kwon, H. J.; Gong, J. P. Negatively Charged Polyelectrolyte Gels as Bio-Tissue Model System and for Biomedical Application. *Curr. Opin. Colloid Interface Sci.* **2006,** *11*, 345-350.

139. Ash, P. A.; Bain, C. D.; Matsubara, H. Wetting in Oil/Water/Surfactant Systems. *Curr. Opin. Colloid Interface Sci.* **2012,** *17*, 196-204.

140. Watarai, H.; Teramae, N.; Sawada, T., *Interfacial Nanochemistry: Molecular Science and Engineering at Liquid-Liquid Interfaces*. Kluwer Academic/Plenum Publishers, New York: 2005.

141. Dong, J.; Ozaki, Y.; Nakashima, K. Infrared, Raman, and Near-Infrared Spectroscopic Evidence for the Coexistence of Various Hydrogen-Bond Forms in Poly(Acrylic Acid). *Macromolecules* **1997,** *30*, 1111-1117.

142. Tajiri, T.; Morita, S.; Ozaki, Y. Hydration Mechanism on a Poly(Methacrylic Acid) Film Studied by in Situ Attenuated Total Reflection Infrared Spectroscopy. *Polymer* **2009,** *50*, 5765-5770.

143. Dong, J.; Tsubahara, N.; Fujimoto, Y.; Ozaki, Y.; Nakashima, K. Fourier Transform Infrared Studies of pH- and Temperature-Dependent Conformational Changes of Solid Poly(Methacrylic Acid). *Appl. Spectrosc.* **2001,** *55*, 1603-1609.

144. Vermohlen, K.; Lewandowski, H.; Narres, H. D.; Koglin, E. Adsorption of Polyacrylic Acid on Aluminium Oxide: Drift Spectroscopy and Ab Initio Calculations. *Colloids Surf., A* **2000,** *170*, 181-189.

145. Vermohlen, K.; Lewandowski, H.; Narres, H. D.; Schwuger, M. J. Adsorption of Polyelectrolytes onto Oxides - The Influence of Ionic Strength, Molar Mass, and Ca^{2+} Ions. *Colloids Surf., A* **2000,** *163*, 45-53.

146. Chen, Y. X.; Liu, S. Y.; Wang, G. Y. Kinetics and Adsorption Behavior of Carboxymethyl Starch on Alpha-Alumina in Aqueous Medium. *J. Colloid Interface Sci.* **2006,** *303*, 380-387.

147. Bykov, A. G.; Lin, S.-Y.; Loglio, G.; Miller, R.; Noskov, B. A. Kinetics of Adsorption Layer Formation in Solutions of Polyacid/Surfactant Complexes. *J. Phys. Chem. C* **2009,** *113*, 5664-5671.

148. Stamkulov, N. S.; Mussabekov, K. B.; Aidarova, S. B.; Luckham, P. F. Stabilisation of Emulsions by Using a Combination of an Oil Soluble Ionic Surfactant and Water Soluble Polyelectrolytes. I: Emulsion Stabilisation and Interfacial Tension Measurements. *Colloids Surf. A* **2009,** *335*, 103-106.

149. Paul, H. J.; Corn, R. M. Second-Harmonic Generation Measurements of Electrostatic Biopolymer-Surfactant Coadsorption at the Water/1,2-Dichloroethane Interface. *J. Phys. Chem. B* **1997,** *101*, 4494-4497.

150. Ong, S. W.; Zhao, X. L.; Eisenthal, K. B. Polarization of Water-Molecules at a Charged Interface - 2nd Harmonic Studies of the Silica Water Interface. *Chem. Phys. Lett.* **1992,** *191*, 327-335.

151. Zhang, J.; Pelton, R. The Dynamic Behavior of Poly(N-Isopropylacrylamide) at the Air/Water Interface. *Colloids Surf. A* **1999,** *156*, 111-122.

152. Kawaguchi, S.; Takahashi, T.; Tajima, H.; Hirose, Y.; Ito, K. Preparation, Characterization, and Dissociation Properties of Poly(Acrylic Acid) and Poly(Methacrylic Acid) with Narrow Molecular Weight Distribution. *Polym. J.* **1996,** *28*, 735-741.

153. Garces, J. L.; Koper, G. J. M.; Borkovec, M. Ionization Equilibria and Conformational Transitions in Polyprotic Molecules and Polyelectrolytes. *J. Phys. Chem. B* **2006,** *110*, 10937-10950.

154. Kendrick, M. J., *Metals in Biological Systems*. E. Horwood: 1992.

155. Ghabbour, E. A.; Shaker, M.; El-Toukhy, A.; Abid, I. M.; Davies, G. Thermodynamics of Metal Cation Binding by a Solid Soil Derived Humic Acid. 2. Binding of Mn(II), $Co(NH_3)(3+)(6_{aq})$ and Hg(II). *Chemosphere* **2006,** *64*, 826-833.

156. Ghabbour, E. A.; Shaker, M.; El-Toukhy, A.; Abid, I. M.; Davies, G. Thermodynamics of Metal Cation Binding by a Solid Soil-Derived Humic Acid: Binding of Fe(III), Pb(II), and Cu(II). *Chemosphere* **2006,** *63*, 477-483.

157. Rivas, B. L.; Pereira, E. D.; Robles, P.; Cid, R. Metal Ion Removal from Aqueous Solution by Liquid Phase Polymer-Based Retention Technique. *Macromol. Symp.* **2006,** *235*, 152-160.

158. Bassaid, S.; Chaib, M.; Bouguelia, A.; Trari, M. Elaboration and Characterization of Poly (Acrylic Acid-co-Crotonic Acid) Copolymers: Application to Extraction of Metal Cations Pb(II), Cd(II) and Hg(II) by Complexation in Aqueous Media. *React. Funct. Polym.* **2008,** *68*, 483-491.

159. Gutnick, D. L.; Bach, H. Engineering Bacterial Biopolymers for the Biosorption of Heavy Metals; New Products and Novel Formulations. *Appl. Microbiol. Biotechnol.* **2000,** *54*, 451-460.

160. Rey-Castro, C.; Mongin, S.; Huidobro, C.; David, C.; Salvador, J.; Lluis Garces, J.; Galceran, J.; Mas, F.; Puy, J. Effective Affinity Distribution for the Binding of Metal Ions to a Generic Fulvic Acid in Natural Waters. *Environ. Sci. Technol.* **2009,** *43*, 7184-7191.

161. Palencia, M.; Rivas, B.; Pereira, E. Polymer-Enhanced Ultrafiltration: Counterion Distribution and Its Relation with the Divalent Metal-Ion Retention Properties by Sulfonic Acid Polyelectrolytes. *Polym. Bull. (Berlin)* **2011,** *67*, 1123-1138.

162. Palencia, M.; Rivas, B. L. Metal Ion Retention by Emulsion Liquid Membrane Coupled to Liquid-Phase Polymer-Based Retention. *Colloid. Polym. Sci.* **2011,** *289*, 1695-1709.

163. Porasso, R. D.; Benegas, J. C.; Van Den Hoop, M. G. T.; Paoletti, S. Analysis of Trace Metal Humic Acid Interactions Using Counterion Condensation Theory. *Environ. Sci. Technol.* **2002,** *36*, 3815-3821.

164. Rivas, B. L.; Pereira, E. D.; Moreno-Villoslada, I. Water-Soluble Polymer-Metal Ion Interactions. *Prog. Polym. Sci.* **2003,** *28*, 173-208.

165. Gamboa, C.; Olea, A. F. Association of Cationic Surfactants to Humic Acid - Effect on the Surface Activity. *Colloids Surf. A* **2006,** *278*, 241-245.

166. Chilom, G.; Bruns, A. S.; Rice, J. A. Aggregation of Humic Acid in Solution: Contributions of Different Fractions. *Org. Geochem.* **2009,** *40*, 455-460.

167. Terashima, M.; Fukushima, M.; Tanaka, S. Influence of pH on the Surface Activity of Humic Acid: Micelle-Like Aggregate Formation and Interfacial Adsorption. *Colloids Surf. A* **2004,** *247*, 77-83.

168. Quagliotto, P.; Montoneri, E.; Tambone, F.; Adani, F.; Gobetto, R.; Viscardi, G. Chemicals from Wastes: Compost-Derived Humic Acid-Like Matter as Surfactant. *Environ. Sci. Technol.* **2006,** *40*, 1686-1692.

169. Tamamura, S.; Ohashi, R.; Nagao, S.; Yamamoto, M.; Mizuno, M. Molecular-Size-Distribution-Dependent Aggregation of Humic Substances by Na(I), Ag(I), Ca(II), and Eu(III). *Colloids Surf. A* **2013,** *434*, 9-15.

170. Orsetti, S.; Marco-Brown, J. L.; Andrade, E. M.; Molina, F. V. Pb(II) Binding to Humic Substances: An Equilibrium and Spectroscopic Study. *Environ. Sci. Technol.* **2013,** *47*, 8325-8333.

171. Oosawa, F. Counterion Fluctuation and Dielectric Dispersion in Linear Polyelectrolytes. *Biopolymers* **1970,** *9*, 677.

172. Manning, G. S. Counterion Binding in Polyelectrolyte Theory. *Acc. Chem. Res.* **1979,** *12*, 443-449.

173. Manning, G. S. Limiting Laws and Counterion Condensation in Polyelectrolyte Solutions .4. Approach to Limit and Extraordinary Stability of Charge Fraction. *Biophys. Chem.* **1977,** *7*, 95-102.

174. Manning, G. S. Limiting Laws and Counterion Condensation in Polyelectrolyte Solutions .5. Further Development of Chemical-Model. *Biophys. Chem.* **1978,** *9*, 65-70.

175. Manning, G. S. Simple Model for the Binding of a Polyelectrolyte to an Oppositely Charged Curved Surface. *J. Phys. Chem. B* **2003,** *107*, 11485-11490.

176. Manning, G. S. Limiting Laws and Counterion Condensation in Polyelectrolyte Solutions .I. Colligative Properties. *J. Chem. Phys.* **1969,** *51*, 924.

177. Manning, G. S. Limiting Laws and Counterion Condensation in Polyelectrolyte Solutions .2. Self-Diffusion of Small Ions. *J. Chem. Phys.* **1969,** *51*, 934.

178. Manning, G. S. Limiting Laws and Counterion Condensation in Polyelectrolyte Solutions .3. An Analysis Based on Mayer Ionic Solution Theory. *J. Chem. Phys.* **1969,** *51*, 3249.

179. Manning, G. S. Limiting Laws and Counterion Condensation in Polyelectrolyte Solutions. 7. Electrophoretic Mobility and Conductance. *The Journal of Physical Chemistry* **1981,** *85*, 1506-1515.

180. Manning, G. S. Limiting Laws and Counterion Condensation in Polyelectrolyte Solutions. 6. Theory of the Titration Curve. *J. Phys. Chem.* **1981,** *85*, 870-877.

181. Manning, G. S. Limiting Laws and Counterion Condensation in Polyelectrolyte Solutions. 8. Mixtures of Counterions, Species Selectivity, and Valence Selectivity. *J. Phys. Chem.* **1984,** *88*, 6654-6661.

182. Benegas, J. C.; Cleven, F. M. J.; van den Hoop, M. Potentiometric Titration of Poly(Acrylic Acid) in Mixed Counterion Systems: Chemical Binding of Cd Ions. *Anal. Chim. Acta* **1998,** *369*, 109-114.

183. Porasso, R. D.; Benegas, J. C.; van den Hoop, M. Chemical and Electrostatic Association of Various Metal Ions by Poly(Acrylic Acid) and Poly(Methacrylic Acid) as Studied by Potentiometry. *J. Phys. Chem. B* **1999,** *103*, 2361-2365.

184. Sabbagh, I.; Delsanti, M.; Lesieur, P. Ionic Distribution and Polymer Conformation, Near Phase Separation, in Sodium Polyacrylate/Divalent Cations Mixtures: Small Angle X-Ray and Neutron Scattering. *Eur. Phys. J. B* **1999,** *12*, 253-260.

185. Sabbagh, I.; Delsanti, M. Solubility of Highly Charged Anionic Polyelectrolytes in Presence of Multivalent Cations: Specific Interaction Effect. *Eur. Phys. J. E* **2000,** *1*, 75-86.

186. Schweins, R.; Huber, K. Collapse of Sodium Polyacrylate Chains in Calcium Salt Solutions. *Eur. Phys. J. E* **2001,** *5*, 117-126.

187. Schweins, R.; Lindner, P.; Huber, K. Calcium Induced Shrinking of Napa Chains: A Sans Investigation of Single Chain Behavior. *Macromolecules* **2003,** *36*, 9564-9573.

188. Ikegami, A.; Imai, N. Precipitation of Polyelectrolytes by Salts. *J. Polym. Sci.* **1962,** *56*, 133-152.

189. Ikegami, A. Hydration and Ion Binding of Polyelectrolytes. *J. Polym Sci., Part A: General Papers* **1964,** *2*, 907-921.

190. Michaeli, I. Ion Binding and the Formation of Insoluble Polymethacrylic Salts. *J. Polym. Sci.* **1960,** *48*, 291-299.

191. Ikeda, Y.; Beer, M.; Schmidt, M.; Huber, K. Ca^{2+} and Cu^{2+} Induced Conformational Changes of Sodium Polymethacrylate in Dilute Aqueous Solution. *Macromolecules* **1998,** *31*, 728-733.

192. Tang, C. Y.; Allen, H. C. Ionic Binding of Na^{+} Versus K^{+} to the Carboxylic Acid Headgroup of Palmitic Acid Monolayers Studied by Vibrational Sum Frequency Generation Spectroscopy. *J. Phys. Chem. A* **2009,** *113*, 7383-7393.

193. Tang, C. Y.; Huang, Z.; Allen, H. C. Binding of Mg^{2+} and Ca^{2+} to Palmitic Acid and Deprotonation of the COOH Headgroup Studied by Vibrational Sum Frequency Generation Spectroscopy. *J. Phys. Chem. B* **2010,** *114*, 17068-17076.

194. Tang, C. Y.; Huang, Z.; Allen, H. C. Interfacial Water Structure and Effects of Mg^{2+} and Ca^{2+} Binding to the COOH Headgroup of a Palmitic Acid Monolayer Studied by Sum Frequency Spectroscopy. *J. Phys. Chem. B* **2011,** *115*, 34-40.

195. Simon Kutscher, J.; Gericke, A.; Hühnerfuss, H. Effect of Bivalent Ba, Cu, Ni, and Zn Cations on the Structure of Octadecanoic Acid Monolayers at the Air-Water Interface as Determined by External Infrared Reflection-Absorption Spectroscopy. *Langmuir* **1996,** *12*, 1027-1034.

196. Du, X. Z.; Liang, Y. Q. Roles of Metal Complex and Hydrogen Bond in Molecular Structures and Phase Behaviors of Metal N-Octadecanoyl-L-Alaninate Langmuir-Blodgett Films. *J. Phys. Chem. B* **2000,** *104*, 10047-10052.

197. Gericke, A.; Hühnerfuss, H. The Effect of Cations on the Order of Saturated Fatty-Acid Monolayers at the Air-Water-Interface as Determined by Infrared Reflection-Absorption Spectrometry. *Thin Solid Films* **1994,** *245*, 74-82.

198. Hühnerfuss, H.; Neumann, V.; Stine, K. J. Role of Hydrogen Bond and Metal Complex Formation for Chiral Discrimination in Amino Acid Monolayers Studied by Infrared Reflection - Absorption Spectroscopy. *Langmuir* **1996,** *12*, 2561-2569.

199. Dong, H.; Du, H.; Qian, X. Prediction of pK_a Values for Oligo-Methacrylic Acids Using Combined Classical and Quantum Approaches. *J. Phys. Chem. B* **2009,** *113*, 12857-12859.

200. Konradi, R.; Ruhe, J. Interaction of Poly(Methacrylic Acid) Brushes with Metal Ions: An Infrared Investigation. *Macromolecules* **2004,** *37*, 6954-6961.

201. Konradi, R.; Ruhe, J. Interaction of Poly(Methacrylic Acid) Brushes with Metal Ions: Swelling Properties. *Macromolecules* **2005,** *38*, 4345-4354.

202. Lages, S.; Michels, R.; Huber, K. Coil-Collapse and Coil-Aggregation Due to the Interaction of Cu^{2+} and Ca^{2+} Ions with Anionic Polyacylate Chains in Dilute Solution. *Macromolecules* **2010,** *43*, 3027-3035.

203. Ermoshkin, A. V.; de la Cruz, M. O. Polyelectrolytes in the Presence of Multivalent Ions: Gelation Versus Segregation. *Phys. Rev. Lett.* **2003,** *90*.

204. Reincke, F.; Kegel, W. K.; Zhang, H.; Nolte, M.; Wang, D.; Vanmaekelbergh, D.; Mohwald, H. Understanding the Self-Assembly of Charged Nanoparticles at the Water/Oil Interface. *Phys. Chem. Chem. Phys.* **2006,** *8*, 3828-3835.

205. Wang, D. Y.; Duan, H. W.; Mohwald, H. The Water/Oil Interface: The Emerging Horizon for Self-Assembly of Nanoparticles. *Soft Matter* **2005,** *1*, 412-416.

206. Dai, L. L.; Sharma, R.; Wu, C. Y. Self-Assembled Structure of Nanoparticles at a Liquid-Liquid Interface. *Langmuir* **2005,** *21*, 2641-2643.

207. Robertson, E. J.; Olivier, G. K.; Quan, M.; Proulx, C.; Zuckermann, R. N.; Richmond, G. L. Assembly and Molecular Oroder of Two-Dimensional Peptoid Nanosheets through the Oil-Water Interface. *Submitted to Proc. Natl. Acad. Sci. U. S. A.*

208. Sanii, B.; Kudirka, R.; Cho, A.; Venkateswaran, N.; Olivier, G. K.; Olson, A. M.; Tran, H.; Harada, R. M.; Tan, L.; Zuckermann, R. N. Shaken, Not Stirred: Collapsing a Peptoid Monolayer to Produce Free-Floating, Stable Nanosheets. *J. Am. Chem. Soc.* **2011,** *133*, 20808-20815.

209. Nam, K. T.; Shelby, S. A.; Choi, P. H.; Marciel, A. B.; Chen, R.; Tan, L.; Chu, T. K.; Mesch, R. A.; Lee, B.-C.; Connolly, M. D.; Kisielowski, C.; Zuckermann, R. N. Free-Floating Ultrathin Two-Dimensional Crystals from Sequence-Specific Peptoid Polymers. *Nat. Mater.* **2010,** *9*, 454-460.

210. Olivier, G. K.; Cho, A.; Sanii, B.; Connolly, M. D.; Tran, H.; Zuckermann, R. N. Antibody-Mimetic Peptoid Nanosheets for Molecular Recognition. *ACS Nano* **2013,** *7*, 9276-9286.

211. Murnen, H. K.; Rosales, A. M.; Dobrynin, A. V.; Zuckermann, R. N.; Segalman, R. A. Persistence Length of Polyelectrolytes with Precisely Located Charges. *Soft Matter* **2013,** *9*, 90-98.

212. Hwang, Y. S.; Lenhart, J. J. Adsorption of C4-Dicarboxylic Acids at the Hematite/Water Interface. *Langmuir* **2008,** *24*, 13934-13943.

213. Tucker, I. M.; Petkov, J. T.; Jones, C.; Penfold, J.; Thomas, R. K.; Rogers, S. E.; Terrry, A. E.; Heenan, R. K.; Grillo, I. Adsorption of Polymer-Surfactant Mixtures at the Oil/Water Interface. *Langmuir* **2012,** *28*, 14974-14982.